MODELING THE UNFOLDED PROTEIN RESPONSE AND ITS CONNECTION TO CELLULAR STRESS

A Thesis

Presented to the Faculty of the Graduate School

of Cornell University

in Partial Fulfillment of the Requirements for the Degree of

Master of Science

by

Anirikh Chakrabarti

August 2009

ABSTRACT

The Endoplasmic Reticulum (ER) plays a pivotal role in cellular functioning. Proteins undergo modifications in the ER. The cell monitors protein folding and has a quality control. The incorrectly folded proteins are tagged for degradation or sent back to the refolding cycle. Upon accumulation of incorrectly folded proteins in the cell, due to any alterations in the cellular homeostasis, cellular stress is created. This leads to a cascade of events, termed the Unfolded Protein Response (UPR). Cellular stresses range from hypoxia, nutrient deprivation to external stimulus such as heat or radiation. It is vital to understand the complexities involved in this system, to predict the role of UPR in cancer, diabetes and other diseases associated with misfolded proteins. In the current study, we have created an initial model of the UPR. This model is based on mass action kinetics. We solve this model deterministically, to look at the concentration profiles of the proteins and protein complexes, upon UPR induction. This kind of study, along with the mathematical and statistical tools developed in the Varner lab provide tools to identify fragile elements of the UPR network. These fragile components of the system become targets for intervention by drugs and inform the development of experiments to discover new pharmaceutical treatments.

BIOGRAPHICAL SKETCH

Anirikh Chakrabarti was born in Kolkata, India. His earlier interest in science was fueled by his parents and his brother, and this manifested itself in his winning several scientific competitions and quizzes while in school. He then went on to complete his undergraduate Bachelor of Technology degree in Metallurgy and Material Sciences and Master of Technology degree in Material Sciences from the Indian Institute of Technology (I.I.T) at Mumbai in India. Here he worked on the modeling of cerebrospinal fluid dynamics. Upon graduating from IIT Mumbai, he joined the group of Dr. Jeffrey Varner at Cornell University as a graduate student. Currently he is working on the modeling of the Unfolded Protein Response and its disease relevance towards his PhD.

To my parents and friends, who have always stood by me...

ACKNOWLEDGEMENTS

I would first like to thank Dr. Varner for allowing me to work in the Varner lab and for his continued encouragement and motivation. Dr. Varner has been a true mentor, guide and guardian to me for the last two years. I would also like to thank my committee members Dr. Shuler and Dr. DeLisa. for their words of advice. I would like to thank the Varner lab members for their advice and their ideas. I would like to extend my gratitude towards my friends and family for their support.

TABLE OF CONTENTS

LIST OF TABLES

LIST OF FIGURES

CHAPTER 1

INTRODUCTION

The Endoplasmic Reticulum (ER) plays a key role in cellular functioning, from cell survival to cell death. Some of the key processes for proper functioning of the cell are maintenance of calcium homeostasis, protein synthesis and lipid biosynthesis. The unique environment of the ER holds the key to most of these processes. ER has the highest concentration of Ca^{2+}. It also has a high concentration of Ca^{2+}-dependant molecular chaperones which are required to stabilize protein folding intermediates. The oxidative environment in the ER aids in formation of disulphide bonds, which is essential in the folding of proteins. Besides the ability of the ER to aid in glycosylation and lipidation, it also functions as a signalling organelle by means of releasing Ca^{2+} through the ion channels.

Any alterations to the ER environment is treated as **stress** in the cell. Hypoxia leads to alterations of the cellular redox regulation. This is one form of cellular stress which is common to tumor or cancerous cells. Glucose deprivation, aberration of calcium regulation, viral infection, high fat diet, smoking, neuro-degenerative diseases are some of the instances that have been shown in the literature to induce ER stress. These stresses lead to triggering of an evolutionarily conserved pathway called **Unfolded Protein Response (UPR)**.

Broadly UPR performs three types of functions, adaptation, alarm and apoptosis. Initially the UPR tries to re-establish homeostasis in the cell by inducing transcriptional programs, leading to expression of chaperones that enhance protein folding. Simultaneously, translation of mRNAs is inhibited to reduce the protein load on the ER. If the adaptation step is not sufficient, the UPR in-

duces an *alarm* to the cell. This alarm is representative of the signal transduction events, leading to activation of JNK (Jun N-terminal Kinase), p38 MAPK (mitogen-activated protein kinase), and NF-κB (transcription factor nuclear factor - κB). These signaling events activate downstream proteins involved in cellular immunity and defense. If all these adaptive motions fail to compensate for the ER stress, cellular death (apoptosis) is induced. Apoptosis could be either caspase-dependent or caspase-independent. ER stress is also seen to initiate autophagy.

The target of this project was to identify the governing interactions in the UPR network from the literature and to model these interactions using a deterministic approach. A fully functional model of the UPR could in fact provide us a closer look at the key elements of this network. The aim of this study is to identify these key aspects of the network. This information shall help us to prioritize new experiments and to obtain key targets for drug development.

This information could be gained by doing a sensitivity analysis of the network and by edge-coupling studies which would function as a knockout study in the experimental sense. One key challenge faced in this kind of study is to identify the rate constants for the interactions which are not available in the literature. To target this issue, we are using a multiple objective thermal annealing scheme, in addition to hand-fitting the model to certain experimental observations made in the literature.

Using these techniques we have been able to generate a family of models that best describe, qualitatively, the Unfolded Protein Response.

CHAPTER 2

UNDERLYING BIOLOGY OF THE UNFOLDED PROTEIN RESPONSE AND ITS DOWNSTREAM EFFECTS

Throughout the lifetime of a cell, it is subjected to varied sources of stress. Radiation, hypoxia, nutrient deprivation, free radicals accumulation, toxins and microbial pathogens are a few sources of ER stress. These could either be mitigated by the cells' protective machinery or could lead to cell death and irrevocable damage. To manage these exogenous forms of stress, the cell has developed specific pathways to counteract its effects.

One of the key locations for cellular stresses to manifest themselves is in the ER. The primary source of stress in the ER is the accumulation of unfolded proteins. Newly synthesized proteins enter the ER through the SEC61 channel in the ER membrane. Upon entering, the protein attains a three dimensional conformation followed by post translational modifications. Some of the key modifications include disulphide bond formation and N-linked glycosylation. After these modifications, a protein can be labeled as being correctly folded, if it has attained its native conformation. In case the environment in the cell is not right for folding, there is an accumulation of unfolded proteins in the cell. The phenomenon initiated by the accumulation of unfolded proteins is known as the Unfolded Protein Response (UPR).

UPR was initially studied extensively in yeast cells. In yeast, it is primarily controlled by one pathway. Higher organisms have a highly evolved three-pronged signal transduction pathway for UPR. In normal cells, the cell has a Quality Control, which ensures the correctly folded state of the proteins. Incorrectly folded proteins are removed from the ER by means of ER Associated

Degradation (ERAD). In case there is an overload of unfolded proteins, UPR is initiated to induce translation attenuation and selective transcription of certain proteins (e.g. molecular chaperones). In case the overload is not resolved, apoptosis or autophagy is induced to destroy the cell. The following chapter details the underlying biology in the above mentioned aspects of the cellular functioning.

2.1 Protein Folding and Quality Control in the cell

It is vital for a cell's proper functionality to have the proteins in the correctly folded state. The process by which the quality of the proteins in a cell is maintained is termed as Quality Control (QC)[41].

Proteins are synthesized and mature in the ER. The molecular chaperones and the folding factors in the ER plays a major role in the QC [41]. Some of the vital chaperones playing a role in the folding process are enlisted in table 2.1. Certain cotranslational and post-translational modifications take place in the ER. Cotranslational modifications occur as the protein enters the ER through the proteinaceous channel known as the translocon complex. This is followed by the post-translational modifications taking place in the ER lumen. Some of these modifications include disulphide-bond formation, signal-peptide cleavage and N-linked glycosylation. Finally, oligomeric assembly takes place for these modified proteins. The delicate balance of the folded and unfolded state of the protein is depicted in figure 2.1.

The QC, ensures that a premature exit of the proteins in the unfolded state is restricted. In general, QC occurs in two phases. In primary QC, all the pro-

Table 2.1: The key chaperones of the endoplasmic reticulum

Chaperone Family	Detials
HSP70s	BiP and GRP170 are the members of this family. BiP plays a key role in the binding and assists the folding of nascent proteins. It also plays a central role in ERAD and UPR.
HSP40s	ERdj1-5 are the members of this family. They stimulate BiP ATPase activity *invitro*
HSP90	GRP94 is the only known member of this family. Its role in UPR is still not substantiated.
Calnexin and Calreticulin	These proteins are instrumental in the folding of proteins that have monoglucosylated N-linked glycans.
Thiol-disulphide oxidoreductases	Protein disulphide isomerase is a member of this group. It catalyses and leads to oxidation, isomerization and reduction of the disulphide bonds.

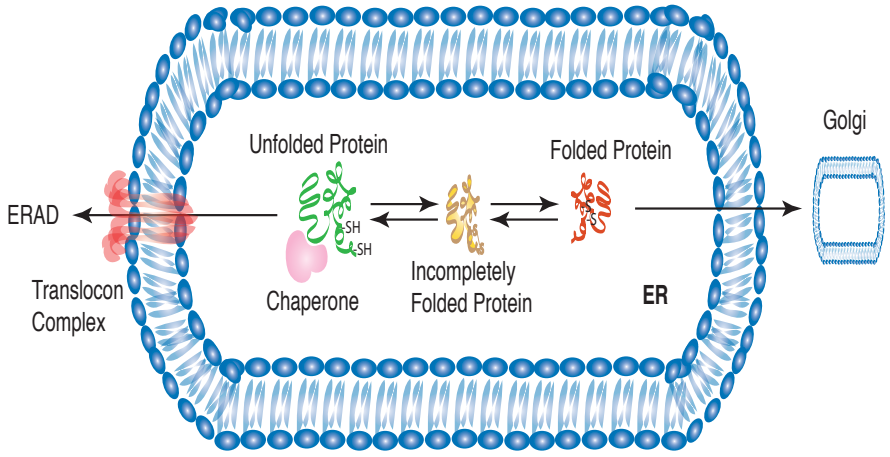

Figure 2.1: Effect of the ER environment in Protein Folding: Chaperones play a key role in the equilibrium between the correctly folded and unfolded proteins in the ER. Chaperones bind to the incorrectly folded proteins and inhibit aggregation, thereby promoting folding. They also play a role in targeting unfolded proteins for degradation (ERAD).

teins are checked for their folded state [42]. The closeness to the native structure, could be used as a measure for protein folding. The presence of exposed hydrophobic regions, unpaired cysteine residues, and the ability to aggregate could be some of the markers to measure the deviation from the native state of the protein. This deviation is sensed by chaperones such as: BiP, calnexin, calreticulin, glucose-regulated protein (GRP 94), thiol-disulphide oxidoreductases, protein disulphide isomerase (PDI) and ERp57. These chaperones bind to the proteins that have not folded correctly [46, 66, 67]. This binding increases the time the protein spends in the ER lumen, giving it a chance to fold correctly. This process is depicted in the figure 2.2 for the case of glycoproteins.

There are some exceptions to this proposed system [55, 124]. As these pro-

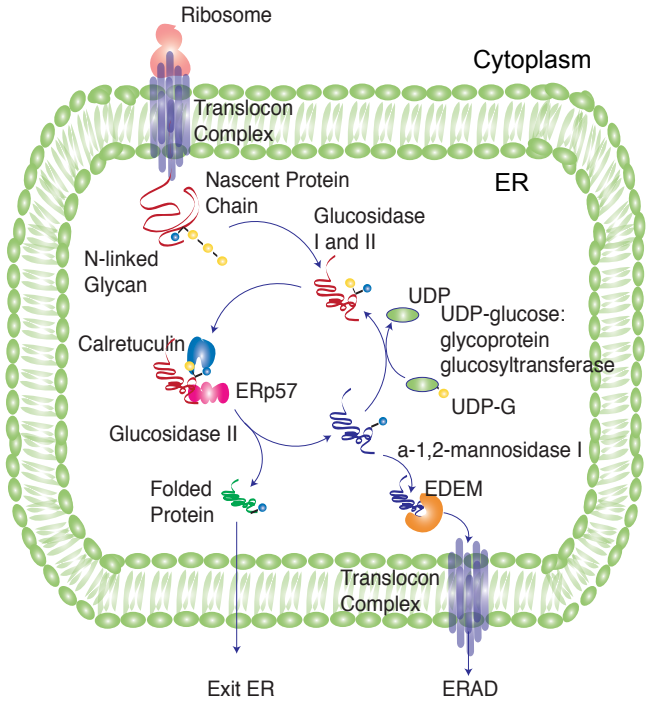

Figure 2.2: Importance of calnexin/calreticulin in the protein folding cycle. Yellow circles attached to the protein denote Glucose groups and blue circles denote Mannose group. After entering the ER lumen, glucosidase I and II remove two glucose groups. The monoglucosylated glycoprotein, then interacts with calnexin/calreticulin. These chaperones interact with the thiol-disulphide oxidoreductase ERp57. Cleavage of the last glucose residue by glucosidase II, leads to the release of the chaperones. At this time, the protein could have either folded and left the ER or it could have attained an incorrectly folded state. The incorrectly folded proteins are then the substrates of UDP glucose:glycoprotein glucosyltransferase, which puts a glucose residue back to the incorrectly folded protein. This step enables the protein to spend some more time in the ER to fold correctly. If the protein fails to fold in a repeated number of cycles, the mannose residue is removed by α-1,2-mannosidase I. This enables the protein to be recognized by ER-degradation-enhancing 1,2-mannosidase-like protein (EDEM). This targets the unfolded proteins for ER-associated degradation (ERAD).

teins are bound to the chaperones, they go through the calnexin/calreticulin cycle. Calnexin and calreticulin bind specifically to monoglucosylated glycan (Glc1Man7-9GlcNAc2) (Glu - Glucose, Man - Mannose, GlcNAc - N-acetylglucosamine) [212, 110, 65, 169]. ERp57 binds to the calnexin complex [140, 26]. Glucosidase II leads to breaking up of the complex, by hydrolysis of the glucose from the monoglucosylated core glycan. UDP-glucose: glycoprotein glucosyltransferase (GT) reglycosylates the processed protein which allows reattachment with calnexin/calreticulin [149]. This is selective and only occurs when there is an improper folding of the protein.

In this way the cycle of glycosylation and deglycosylation leads to the proteins spending sufficient time in the ER to fold correctly. Failure of the above mentioned cycle leads to targeting of the proteins for ERAD[119].

2.2 ER associated degradation (ERAD)

The major components of ERAD are: recognizing the correct unfolded protein, targeting the protein for degradation, retro-translocation, ubiquitylation and proteasomal degradation [205].

There could be many folding aspects that the cell might use to recognize an incorrectly folded protein. One of these features include the exposure of hydrophobic patches, which are generally hidden in correctly folded proteins. Molecular chaperones like HSP70, recognize these exposed patches and bind to the proteins. This mode of ATP-dependent binding and release of HSP70 ensures that the incorrectly folded proteins do not exit the ER. Co-chaperones and nucleotide-exchange factor (NEFs) also play a key role as seen in figure

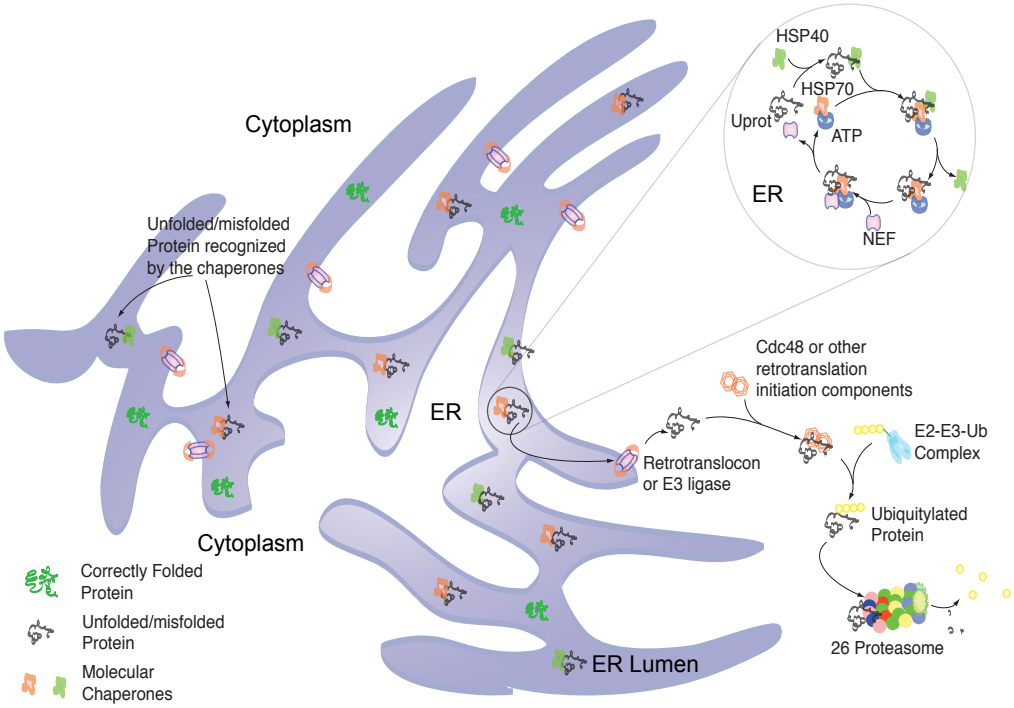

Figure 2.3: Molecular chaperones like HSP70 recognize the unfolded proteins and allow them to spend some time in the ER to undergo refolding cycles. In case these proteins fail to fold correctly they are translocated out of the ER where they are tagged by Ubiquitin and ultimately degraded by the 26S Proteasome.

2.3. N-linked glycans and/or di-sulphide bonds are features that are used for targeting the proteins for ERAD [205].

Once the proteins have been selected, they are retro-translocated into the cytoplasm. This is where the they are ubiquitylated.

Ubiquitin (Ub) is activated by an E1 Ub-activating enzyme. This step is followed by the transfer of the Ub from the E1 to the E2 through the formation of a thioesters linkage. Now in the presence of E3 Ub ligases this Ub-E2 system can transfer the Ub to improperly folded proteins. The ubiquitylated proteins are

now targeted to the 26S proteasome and degraded [205] as seen in figure 2.3.

During ER Stress, QC and ERAD fail to manage the high loads of protein and this leads to accumulation of unfolded proteins in the ER. This condition initiates UPR. Owing to accumulation of the unfolded proteins in the cell, the ER resident chaperone (BiP) break free from the ER stress transducers. These ER stress transducers are located in the ER membrane, with their N-terminals in the ER and their C-terminals in the cytosol. The chaperones released from these transducers are now employed in protein folding. There are competing theories about the activation of these transducers. Some say that the release of the chaperones lead to the activation of these transducers, while other believe its direct activation by unfolded proteins. Some of these theories are discussed in the following sections. PRKR-like ER kinase (PERK), inositol-requiring kinase 1 (IRE1) and activating transcription factor 6 (ATF6) are the key ER stress transducers.

2.3 Inositol-requiring kinase 1 (IRE1) branch of UPR

IRE1 is a type I transmembrane protein serine/threonine present in the ER membrane. This 100 kDa protein has an endoribonuclease domain along with a Ser/Thr kinase domain. IRE1 exists as two homologues: IRE1α and IRE1β. IRE1α is expressed ubiquitously [195]. IRE1β is found in the intestinal epithelia [195, 209]. The N-terminal of IRE1 located in the ER lumen is the key in sensing the overload of unfolded proteins [25, 171, 182].

IRE1 is activated by the homooligomerization or homodimerization [171, 214]. This activation is mediated by the luminal domains in the ER. Cytosolic

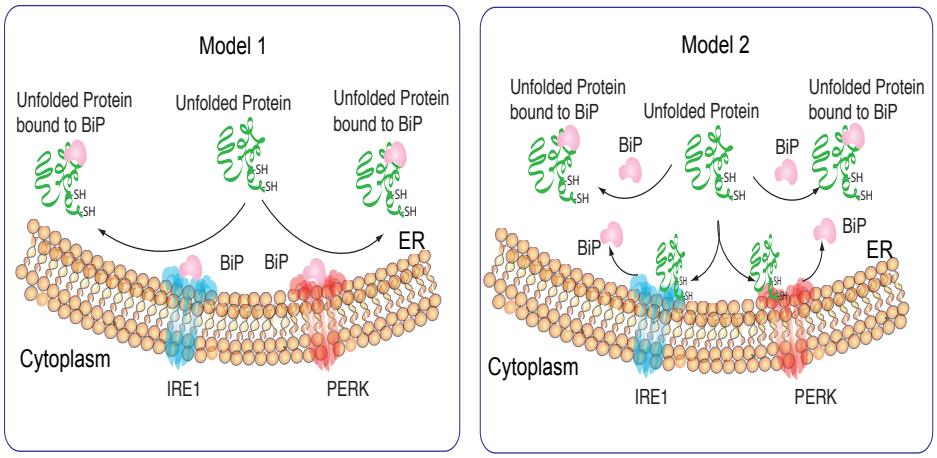

Figure 2.4: Two competing models for the activation of IRE1 and PERK are known. In Model 1, release of BiP from the ER transducers by competitive binding to the unfolded proteins lead to activation of the ER stress transducers. In Model 2, unfolded proteins directly lead to the activation of the ER stress transducers. In the current study, we are using model 1.

parts of the IRE1 also facilitates the activation [214].

Two models have been presented for activation of IRE1 and PERK as in figure 2.4. According the the first model, upon UPR induction, BiP is sequestered away from the luminal domain of IRE1 and PERK [87]. In unstressed cells, BiP forms a complex with the luminal domain of IRE1 and PERK [9, 139, 109] which undergoes dissociation upon ER stress [9, 139]. It was also shown that overexpression of BiP would lead to reduced activation of IRE1 and PERK [9, 88].

The second model states that IRE1 can directly sense the amount of folded proteins. This argument is based on the presence of the peptide binding domain in the IRE1 which leads to interaction with unfolded proteins [109, 108].

UPR induction leads to activation of the IRE1 by autophosphorylation of the kinase domain [171, 214, 213, 146]. This activation enables the endoribonuclease

domain to cleave the XBP1-mRNA [176, 227, 102]. This cleavage occurs both at the exon-intron junctions in the XBP1-mRNA. The spliced XBP1-mRNA is translated to produce a 41 kDa XBP1 protein (XBP1s) as seen in figure 2.5. Upon UPR activation we find that there is rapid proteasomal degradation of the XBP1 that has not been cleaved [99, 229]. Homodimerization of XBP1s with NF-Y leads to binding of this complex with several UPR genes [113, 158]. IRE1α directly plays a key role along with XBP1 in cleaving several proteins to balance the role of proteins in the ER [72].

Phosphorylated IRE1α is dephosphorylated by protein phosphatase two C 2 protein (Ptc2P) [195]. A proper feedback control loop for the IRE1 pathway has yet to be defined.

IRE1 also functions as a protein kinase. IRE1 binds the tumor necrosis factor(TNF) receptor associated factor 2 (TRAF2) as seen in figure 2.5. This has been shown to play a major role in the JNK activation [203, 134]. JNK activation leads to activation of pro-apoptotic BIM [103, 154] and inhibiting Bcl2 [220]. BIM in normal cells is sequestered in motor complexes interacting with the cytoskeleton [103]. Upon JNK activation BIM is detached from the motor complexes and this leads to BAX/BAK dependant apoptosis as seen in figure 2.6.

It has been found that IRE1 directly interacts with caspase 12 [223] which has a key role in UPR induced apoptosis. Humans do not show the presence of caspase 12. It has been argued that caspase 4, which a close counterpart to caspase 12 play a role in ER stress induced apoptosis [71]. It was also shown that caspase-4 activation was affected by Bcl2 overexpression. The results stated that caspase-4 activation takes place due to ER-stress but the relation with the effector caspases has not been established [71]. This claim has partially been sub-

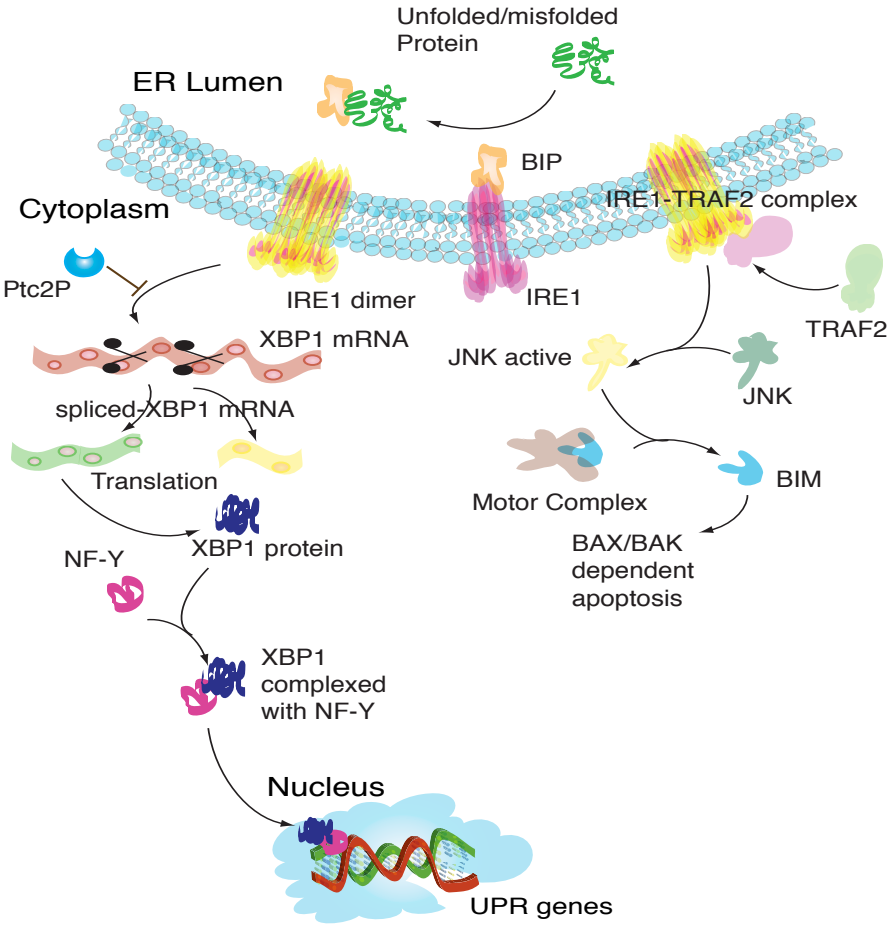

Figure 2.5: Upon UPR induction, IRE1 is activated. This leads of cleavage of the XBP1-mRNA, leading to production of a 41kDa XBP1 proteins (XBP1s). XBP1s along with NF-Y binds with several UPR genes. Activated IRE1 also binds with tumor necrosis factor(TNF) receptor associated factor 2 (TRAF2) leading to activation of JNK downstream. This step is instrumental in initiating apoptosis downstream.

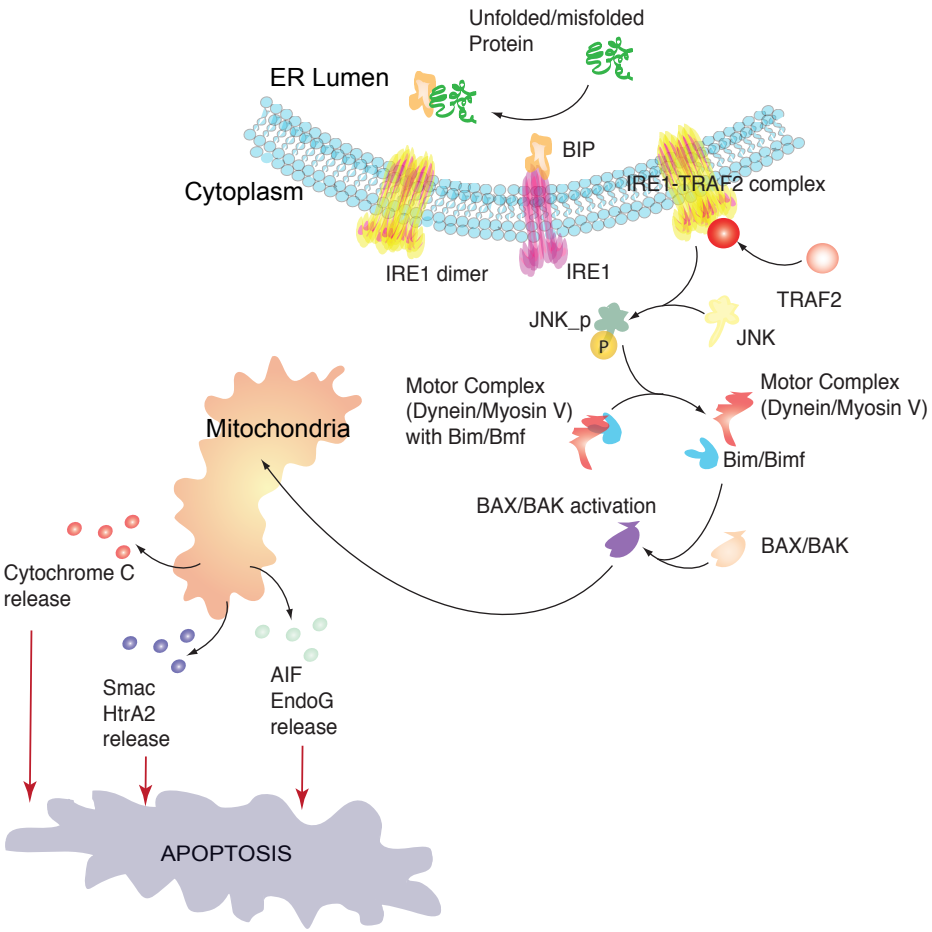

Figure 2.6: This schematic represents JNK-dependant apoptosis signaling pathway. IRE1 branch leads downstream to the phosphorylation of the Bim and Bmf by JNK. JNK phosphorylation leads to the release of Bim, Bmf from the dyenin and myosin V motor complexes. The activated Bim, Bmf could directly lead to the activation of the Bax/Bak or by indirectly binding to Bcl2 lead to the activation of Bax/Bak. This downstream leads to the mitochondria mediated apoptosis.

stantiated in a few of cell types [40]. IRE1 directly plays a role in the apoptotic pathway downstream by interacting with BAX and BAK [69].

2.4 PRKR-like ER kinase (PERK) Pathway

PERK is a type I transmembrane protein, consisting of a ER luminal stress sensing domain and a cytosolic protein kinase domain. The C-terminal protein kinase domain shares homology to the EIF2α kinases, PKR, GCN2 and HRI [63, 179, 178]. Activation of PERK follows the same models as discussed in the activation of IRE1. This activation leads to the phosphorylation leading to activation of the kinase domains. This downstream leads to the phosphorylation of the eukaryotic translation initiation factor 2α (eIF2α) as seen in figure 2.7.

Phosphorylation of eIF2α plays a three-fold role downstream. The first effect is reduction in general translation. This is followed by an increase in the clearance of the accumulated proteins in the ER by ERAD. Selective translation of mRNAs takes place, for example, mRNA for the bZIP transcription factor ATF4 [111]. ATF4 targets the genes that encode for GRP78 and GRP94 [64]. The role of this branch is to degrade the accumulated proteins and improve protein folding. It has been shown that PERK $-/-$ cells are extremely sensitive to ER stress [62, 168].

The role of PERK in apoptosis has not been clearly defined. It has been shown that it can induce autophagy [92, 49]. There is evidence to support that PERK delays the onset of the apoptotic branch of UPR. It has been demonstrated that the PERK branch of apoptosis leads to the induction of cellular inhibitor of apoptosis (cIAPs) [58]. This evidence goes a long way in establishing a pro-

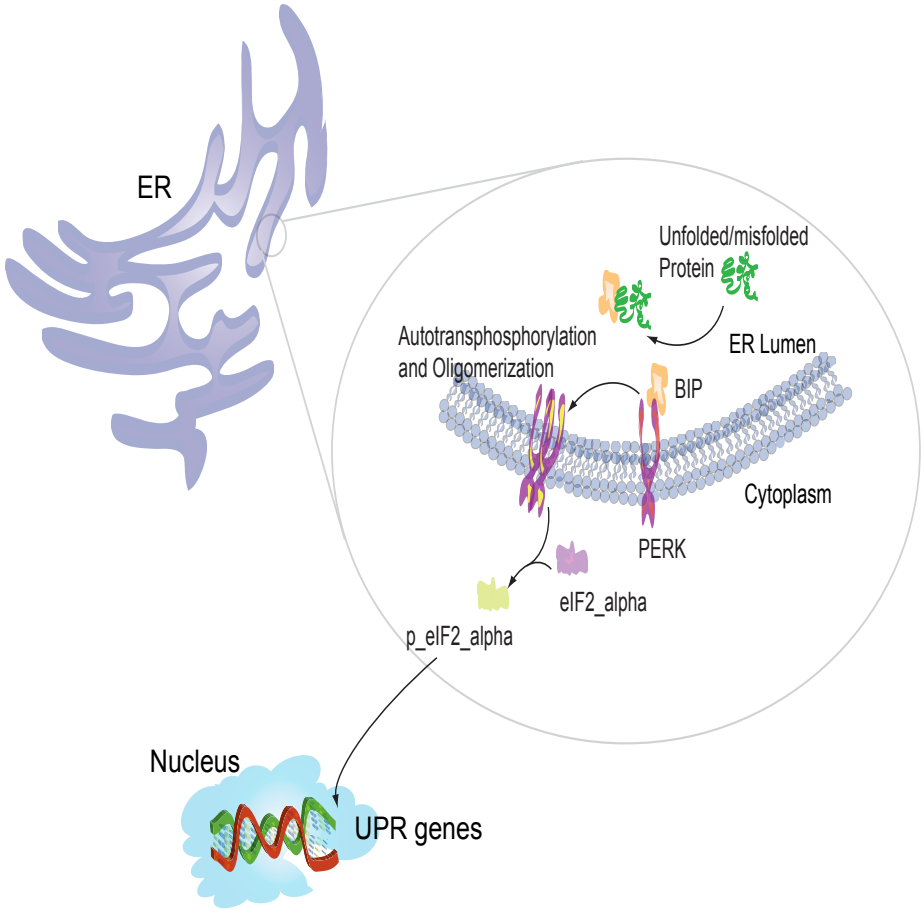

Figure 2.7: Upon UPR induction, PERK is activated which leads to phosphorylation of eIF2α. This step has a three fold effect downstream, which leads to reduced translation, increased ERAD and selective translation of certain proteins like ATF4.

survival role of the PERK branch. The exact mechanism has not been understood, though the phosphorylation of AKT has been suggested to play a role [58]. It shall be interesting to note the relation between apoptosis the PERK branch of UPR.

2.5 Activating transcription factor 6 (ATF6) branch of UPR

ATF6, is a type II ER transmembrane protein that is normally located on the ER membrane. This positioning is enabled by the ER-targeting hydrophobic sequences. The cytosolic component of the protein encodes a bZIP transcription factor [183]. ATF6 (90 kDa) is synthesized in the ER in two homologous forms: ATF6α [183, 56] and ATF6β [123, 85, 96]. Upon ER stress the actions of ATF6 are broadly different from the IRE1 and PERK branches of UPR. ER stress leads to the release of the GRP78 (BiP) from ATF6. Following this, ATF6 is translocated to the Golgi Complex [20] as in figure 2.8. In the golgi, it is cleaved in the luminal domain by serine protease site-1 protease (S1P) [183]. This is further followed by a cleavage by the metalloprotease site-2 protease (S2P) [183, 222, 174] as in figure 2.8. This cleavage phenomenon is called Regulated Intramembrane Proteolysis (RIP). This cleavage at the juxtamembrane site allows the transcriptional domain of ATF6 to be released to the cytosol. The domain (50kDa) comprizing of the bZIP region of ATF6, migrates to the nucleus leading to regulation of gene expression [222]. Some of the known binding sites for the cleaved ATF6 domains are ATF/cAMP response element (CRE) [211] and the ER stress response elements (ERSE) I and II [226, 89]. This binding action is controlled by the nuclear factor Y (NF-Y) [89, 228].

ATF6β has been reported to be heterodimerized upon BiP control [194]. There have been reports of ATF6β to play roles of transcriptional activation [96] but weaker in strength compared to ATF6α. This might have a role in the control of activation of ATF6α [221, 192]. The mechanism of the BiP interaction with ATF6 is still on shaky grounds. Golgi localization sequences (GLS1 and GLS2) seem to be instrumental in playing a key role in the BiP action on ATF6. It was

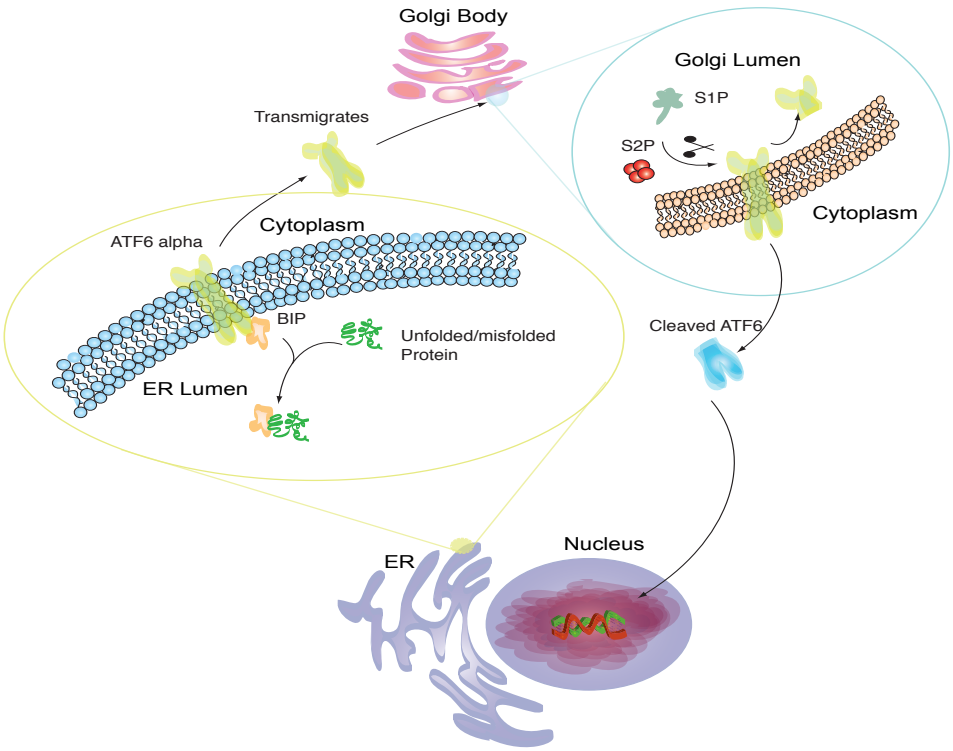

Figure 2.8: Upon UPR induction ATF6 transmigrates to the golgi body, where it is cleaved by S1P and S2P protease. The cleaved ATF6 part moves to the nucleus, where it binds to the ER stress response elements (ERSE) I and II.

noted that BiP binding to GLS1 was the reason for the retention of ATF6 in the ER [173]. Upon release of BiP in case of ER stress, the GLS2 domain targeted the movement of the ATF6 to the Golgi body [173]. Recently, it has been shown that ER stress leads to the restarting of the BiP ATPase cycle. This leads to the dissociation of BiP from ATF6 [175]. CRT, a lectin, also might have a role in keeping the ATF6 in the ER [73]. There are still many unanswered questions in the exact mechanism for ATF6 transport from the membrane to the Golgi body.

The cleaved ATF6 stimulates ER stress genes by homodimerization or heterodimerization with other bZIP transcription factors. Some of the target genes

for cleaved ATF6 domains are GRP78, PDI and ER degradation-enhancing alpha-mannosidase-like protein 1 (EDEM1). These actions lead to an increase in the chaperone activity and degradation of unfolded proteins [221, 215].

Downstream effect of ATF6α also includes a cytoprotective response, including the regulation of regulator of calcineurin 1 (RCAN1) [6]. Calcineurin is a calcium activated protein-phosphotase B. It plays a role in the control of the Bcl2 proteins and Bcl2-antagonist of cell death (BAD). Calcineurin dephosphorylates BAD, allowing it to dimerize with Bcl2 [208]. This set of actions is proapoptotic. The role of RCAN1 is to act as an endogenous inhibitor of calcineurin [6].

ATF6 family of transcription factors includes CREG3L2, CREB-H, LUMAN (CREB3) and OASIS [52]. The role of these family members in ER stress is yet to be documented.

2.6 UPR mediated CHOP Induction

Growth-arrest and DNA-damage-inducible gene 153 (GADD153) is normally present in low numbers in the mammalian cells [165]. GADD153 also known as CHOP is a 29kDa protein consisting of 169 amino acids in humans. The GADD genes are induced generally during genotoxic stress signals and growth arrest signals. Perturbations in the ER homeostasis leads to induction of CHOP and accumulation in the nucleus. CHOP protein comprises of an N-terminal transcriptional activation domain and a C-terminal basic-leucine zipper (bZIP) domain. The bZIP domain plays a key role in the homodimerization of the protein [117, 118]. CHOP is phosphorylated by the p38 MAPPP kinase family of proteins [210, 118]. MAPKKK ASK1 is required for JNK activation in the IRE1

branch of UPR [134, 196]. This can lead to the activation of the p38 MAP kinase [134]. ASK1 null cells do not show ER-stress induced apoptosis [134].

CHOP is shown to be one of the highest inducible genes during ER stress [177]. The idea is that CHOP plays a key role downstream of all the 3 pathways that are initiated by the ER stress. CHOP promoter region in humans has two ERSE motifs and one AARE motif [228, 201, 17]. ATF4, which is induced by the PERK branch of UPR, binds to the AARE domains of the CHOP gene. PERK null cells show almost zero induction of CHOP and ATF4 [168, 60], suggesting the dominance of the action of ATF4 and CHOP genes. On the other hand, we see weak interaction between the ATF6 and IRE1 branches and the CHOP gene.

Studies related to CHOP overexpression have revealed that it leads to reduced Bcl2 protein concentrations. Similarly, overexpression of Bcl2 prevents apoptosis induced by CHOP [117, 120]. It has been shown that CHOP protein is instrumental in translocation of BAX from the cytosol to the mitochondrion [54]. The direct role of CHOP protein with Bcl2 has not yet been established.

2.7 ER Stress and Autophagy

Studies indicate that the ER stress triggers autophagy [137, 224, 7, 82, 74, 92, 49]. PERK, IRE1 and excess of free cytosolic Ca^{2+} play key roles in initiating autophagy in ER stressed cells [137, 74, 92, 49].

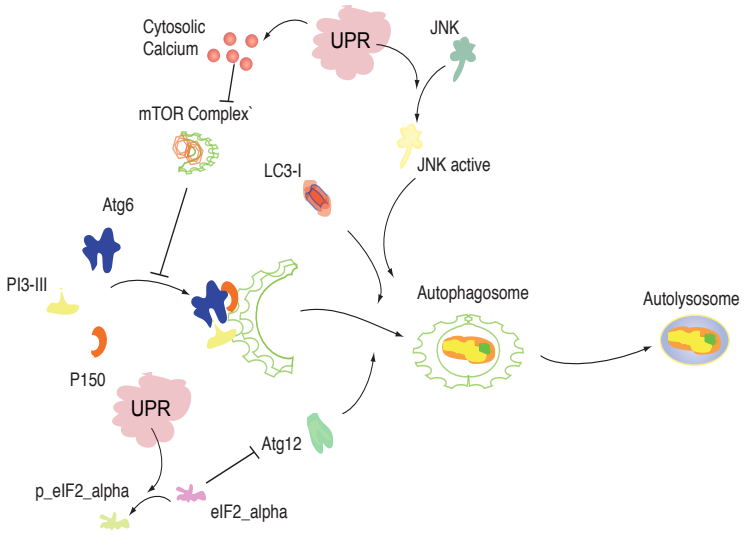

Figure 2.9: Upon ER stress, a part of the cytosol, organelles or both are engulfed in a double membrane. This structure is called Autophagosome. This leads to the formation of an autolysosome, which is degraded to complete the cycle of autophagy.

2.7.1 General machinery of Autophagy

Autophagy, in the classical sense, is the method by which a cell recycles its macromolecules and its organelles. This process is initiated by the formation of an autophagosome. Autophagosome comprises of a part of the cytosol or cellular organs or both, bound by a double membrane [104, 93, 22] as in figure 2.9. This autophagosome then binds to the endolysosomal vesicles leading to the creation of the autolysosome. This autolysosome is then degraded, completing the cycle of autophagy.

The key proteins playing a role are class III phospha-tidylinositol 3-kinase (PI3K), p150 myristylated protein kinase and beclin 1 (atg6). These proteins are involved in the nucleation and formation of the autophagosomal membrane.

This is followed by the elongation of this membrane by two-ubiquitin-like conjugation systems. This step is marked by the conversion of the free form of the microtubule-associated protein 1 light chain 3 (LC3 also called atg8), LC3-I to membrane-bound form LC3-II. LC3-II serves as the marker for the initiation of autophagy.

The autophagy branch in eukaryotic cells is inhibited by the mammalian target of rapamycin complex 1 (mTORC1) protein complex [136, 121]. This complex consists of mammalian target of rapamycin (mTOR), regulatory associated partner of mTOR (raptor) and mLST8 [22, 167, 23].

2.8 UPR mediated apoptosis

Apoptosis is a type of cell death program that maintains tissue homeostasis in multicellular organisms and regulates immune response. Mutations that impair apoptosis often lead to diseases such as autoimmune disorders and cancer. Apoptosis is characterized by nuclear and cytoplasmic condensation, blebbing of the plasma membrane and DNA fragmentation [84]. The dying cell eventually disintegrates into membrane-enclosed apoptotic bodies. These apoptotic bodies are quickly destroyed by phagocytes or the neighboring cells. This is in contrast to Necrosis, which is a pathological dying process involving the unnatural death of cells and tissue. Apoptosis does not induce the inflammatory process or cause tissue scarring, which is a hallmark of necrosis. Apoptosis, thereby, serves as an ideal process for cell elimination in embryogenesis and tissue homeostasis.

A common biomarker for apoptosis includes the activation of the aspartate-

specific proteases collectively known as caspases [2]. There are a total of 14 members of the caspase family [191]. Each of them shares the basic structural homology with the Caenorhabditis elegans cell death protein CED-3. Caspases contain the conserved pentapeptide active site QACXG(X can be R, Q or D). Caspases are activated from their zymogens (procaspases), in response to various death cues. TRAIL (TNF-related apoptosis-inducing ligand), Fas, TNFa and extrinsic stress factors such as UV and chemical-agents are some of the death cues. Caspase function by rapidly dismantling the key cell cycle, cytoskeletal and organelle proteins by proteolytic cleavage. This makes the dying cell unable to initiate or maintain normal cellular functions.

The core of the cell-death program consists of three major components: the Bcl-2 family of proteins, the caspases and the Apaf-1/CED-4 protein. Activation of these components is vital in the morphological changes observed during apoptosis.

2.8.1 Critical Role of Caspases

A total of 14 caspases (cysteinyl aspartate-specific proteases) have been identified in mammals. They can be classified into 3 groups: initiators of apoptosis (group I), effectors (group II) and inflammatory caspases (group III) 2.2. Caspases exist as inactive enzymes analogous to zymogens. Caspases in this zymogen form are called procaspase and this control is necessary to prevent unnecessary cell death. Procaspases consist of an N-terminal prodomain structure, a large 20kDa (p20) subunit and another 10kDa subunit (p10). The p20 and p10 subunits are connected by a linker region in many caspases. Typically,

Table 2.2: Types of Caspases

Subfamily	Role	Members
I	Apoptosis Initiator	Caspase 2, 8, 9, 10
II	Apoptosis Executioner	Caspase 3, 6, 7
III	Inflammatory Mediator	Caspase 1, 4, 5

the inflammatory and initiator caspases have large prodomain regions of 100 residues. It has also been noted that effector caspases have small prodomains of 20-30 amino acids [98]. Active caspase is generated by proteolytic processing of the proenzyme and subsequent release of the prodomain.

2.8.2 Convergence of the apoptotic pathways

Death cues result in the activation of caspases by proteolytic processing of procaspases. In the sequence of events, initiator caspases are activated before the executioner caspases. The initiator caspases, caspase-8 and caspase-9, can self-activate themselves upon formation of dimers in response to death cues [126]. The executioner caspases, such as caspase-6, caspase-3 and caspase-7, are activated by the initiator caspases. Activated executioner caspases can initiate the activation or inactivation of a number of substrates to facilitate the cell death process. In addition, executioner caspases can also activate initiator caspases to form a positive feedback. There are 2 pathways that result in activation of caspases in response to apoptotic signals, as seen in figure 2.10. They are the death-receptor mediated and the stress mediated pathways.

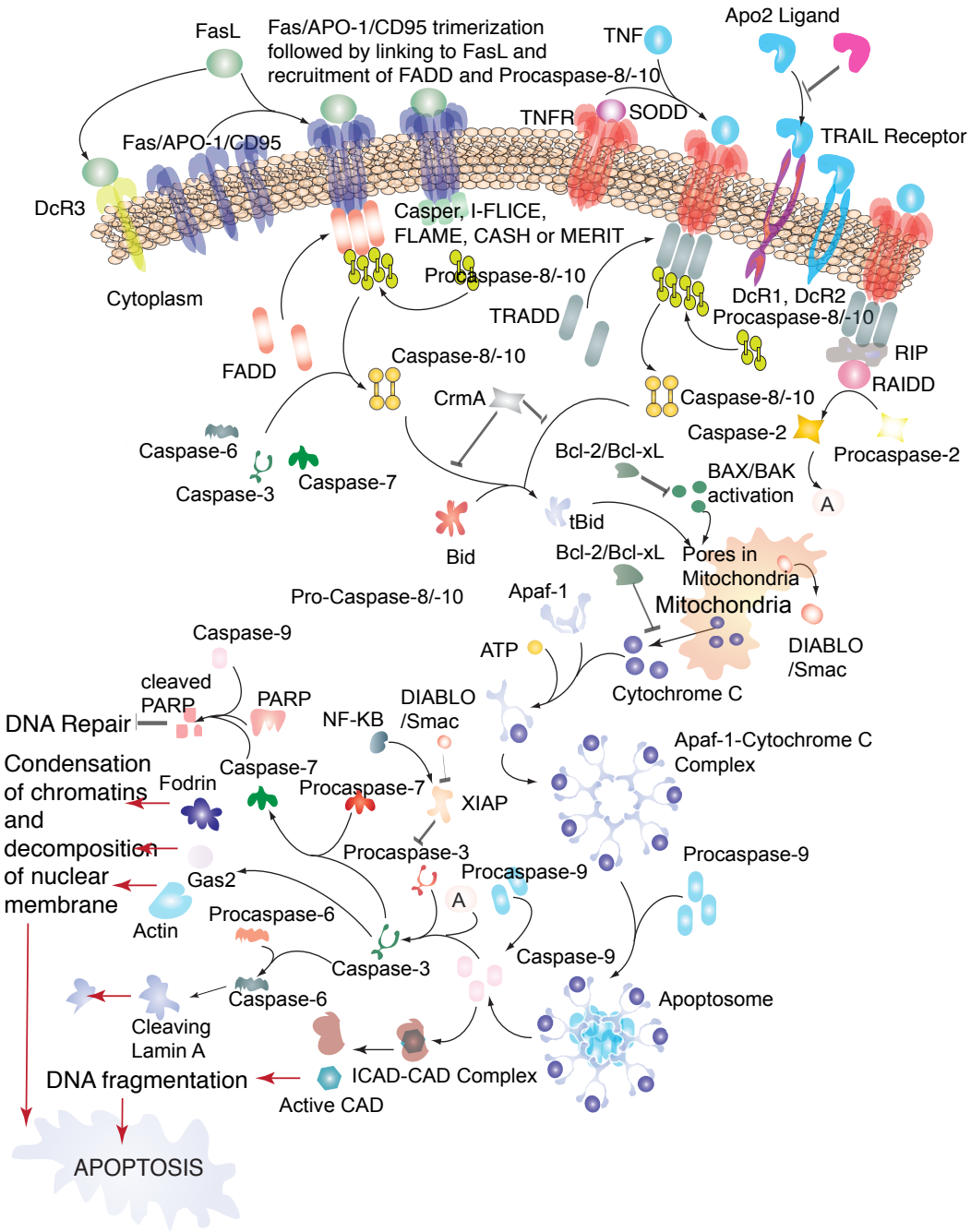

Figure 2.10: Apoptotic pathway in a cell is either Death-receptor mediated or stress-mediated. Both the pathways converge onto the mitochondria where they finally lead to activation of Caspase 9 and release of DNA damage inducible agents from the Mitochondria.

Death-receptor Mediated Pathway

The first pathway is initiated by ligand-mediated activation of death receptors on the plasma membrane. These death receptors belong to the tumor necrosis receptor (TNFR) family. They include Fas receptors (CD95 or APO-1), TNFR1, TRAIL-R1 (TNF-related apoptosis-inducing receptor-1), TRAIL-R2, DR3, DR4 and DR5 [127, 1, 5]. Fas/CD95 ligand (FasL) binds to Fas. TNF binds to TNFR1. Apo3 ligand (Apo3L) binds to DR3. Apo2 ligand (Apo2L or TRAIL) binds to DR4 and DR5 [5]. Binding of the ligand to the receptor generates intracellular signals, leading to caspase activation.

There are three distinct steps involved in the process. In the first step, ligand-induced receptor trimerization takes place, as seen in figure 2.10. This is followed by the recruitment of adaptor proteins to activate the receptors. Receptor activation recruits adaptor proteins like FADD (Fas-associated death domain) and TRADD (TNFR1 death domain associated protein). Other adaptor proteins like RIP (Receptor interacting protein), RAIDD and MADD have also been identified. The adaptor proteins contain DEDs which facilitate interactions between adaptors and activated death receptors. The exposed DED of the procaspase-8 interacts with the DED of the FADD leading to oligomerization of procaspase-8 [14, 126]. This leads to formation of a massive molecule complex called DISC (death inducing signal complex). Caspase-8 and caspase-10 both react with FADD in the ligand-mediated activation of death receptors. They have different apoptosis substrates and thereby function differently. Dimerization of procaspase-8 results in the formation of active caspase-8 and caspase-10. Caspase-8/10 cleaves the BH3 (Bcl2-homology domain) protein, Bid, resulting in a truncated version called tBid. This tBid binds to the survival protein, Bcl2.

This binding releases multidomain pro-apoptotic proteins belonging to the Bax subclass: Bak and Bax. Bax and Bak oligomerize and facilitate the process of cell-death by permeabilizing the mitochondrial membrane.

Stress-Mediated Pathway

The second pathway that activates caspases is the stress pathway. Stress signals include chemicals, UV irradiation, nutritional deprivation and overexpression of pro-apoptotic proteins such as Bax. Endoplasmic reticulum (ER) stress results in accumulation of unfolded or malfolded proteins. ER stress may also lead to perturbation of Ca^{2+} homeostasis. Stress signals cause oligomerization of pro-apoptotic proteins, such as Bax and Bak, downstream, as seen in figure 2.11. These proteins are normally sequestered at the mitochondrial outer membrane by the survival protein Bcl2, under non-apoptotic conditions.

2.8.3 Convergence and downstream effects of the core apoptotic pathways

Once Bax and Bak oligomerize, they insert into the mitochondrial membrane and breach membrane integrity. This results in a net efflux of cytochrome C from the mitochondria to the cytosol as in figure 2.11. Apaf-1 binds to and hydrolyzes ATP/dATP to ADP/dADP. Cytosolic cytochrome C binds to Apaf-1 and induces a conformational change in Apaf-1. Cytochrome C binds to Apaf-1 in the absence of ATP, but the complex is unstable. Cytochrome C and Apaf-1 form a multimeric complex. This initiates the formation of the apoptosome by Apaf-1-

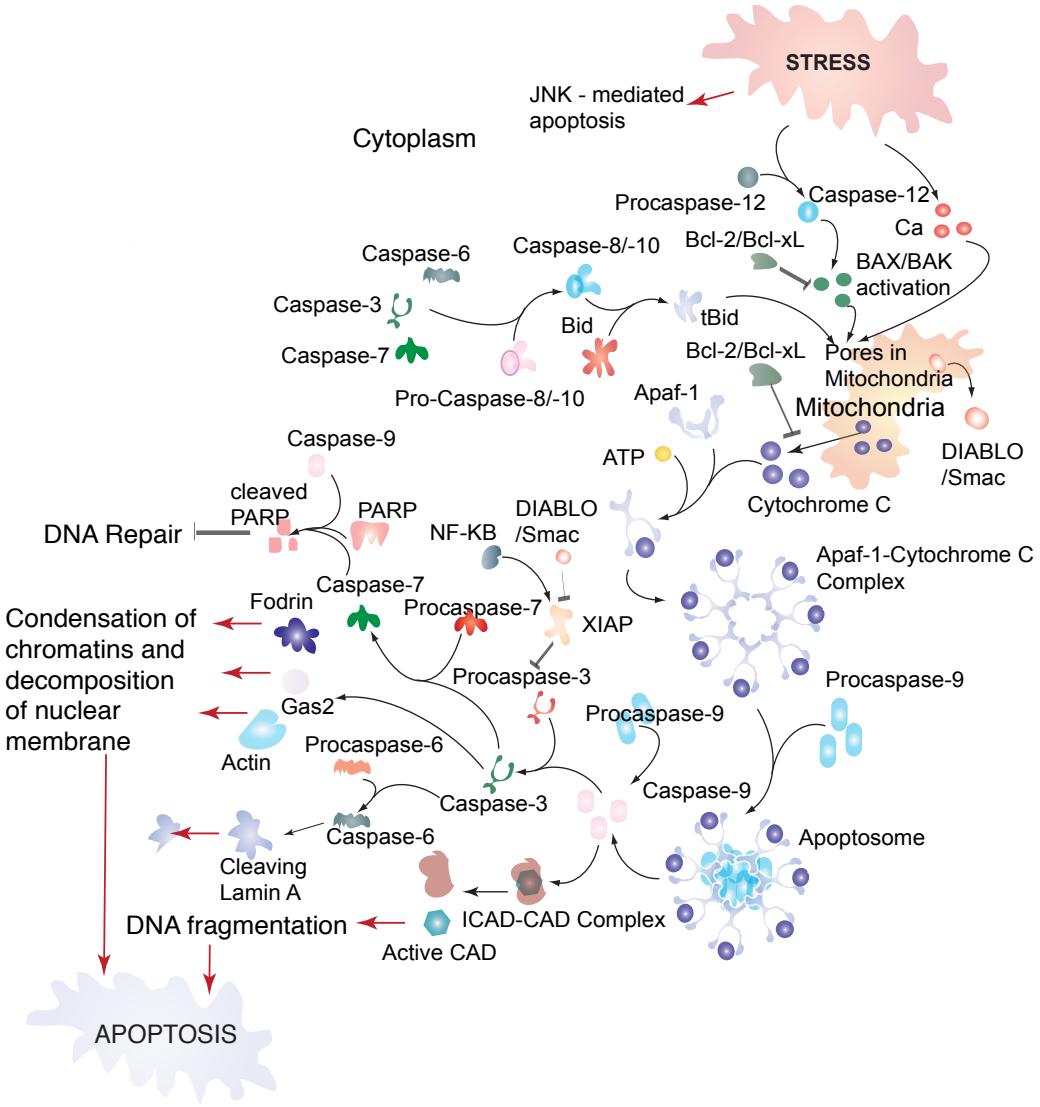

Figure 2.11: UPR mediated apoptosis is controlled by the activation of BAX/BAK. This mediates the formation of PTP on the mitochondrial membrane, thereby releasing cytochrome C and other DNA damage inducible products from the mitochondria. Activation of Procaspase 9 takes place, leading to further activation of the executioner caspases.

mediated recruitment of procapase-9 via homologous CARD motifs, as seen in figure 2.11. The N-terminal of Apaf-1 and the prodomain of procaspase-9 have complementary shapes and opposite charges. The apoptosome is a 1MDa heptamer that consists of 7 cytochrome C, 7 Apaf-1 and 7 procapase-9 molecules. This complex brings the procaspase molecules into close proximity and permits autocatalysis [235]. The activated caspase-9, in turn, activates procaspase-3 and procaspase-7. The activated caspase-3 goes back to activate caspase-9. This forms a positive feedback loop as seen in figure 2.11. Not surprisingly, the mice deficient in Apaf-1 exhibit a phenotype similar to that of caspase-3-deficient mice [57, 19]. These mice die soon after birth and exhibit enlarged brains. This observation, however, does not mean that Apaf-1 is indispensable at the cellular level. The activated executioner caspases cleave cellular proteins like PARP [poly (ADP-ribose) polymerase], lamin, fodrin and Bcl2, as in figure 2.11. This leads to morphological changes in these proteins.

2.8.4 The Calcium Connection with UPR

Recent evidence indicates that there is a crosstalk between the ER and mitochondria during apoptosis, which might initiate mitochondrial apoptotic events [33].

This crosstalk may be facilitated via the release of Ca^{2+} ions from the ER into the cytosol, in response to ER stress. Increased cytosolic Ca^{2+} leads to mitochondrial uptake of Ca^{2+} as in figure 2.13.

Increased Ca^{2+} uptake initiates mitochondrial membrane fission and caspase activation via a mechanism which is yet unknown. The details of ER Ca^{2+} release are yet to be elucidated. Ca^{2+} concentration in the ER determines the cells

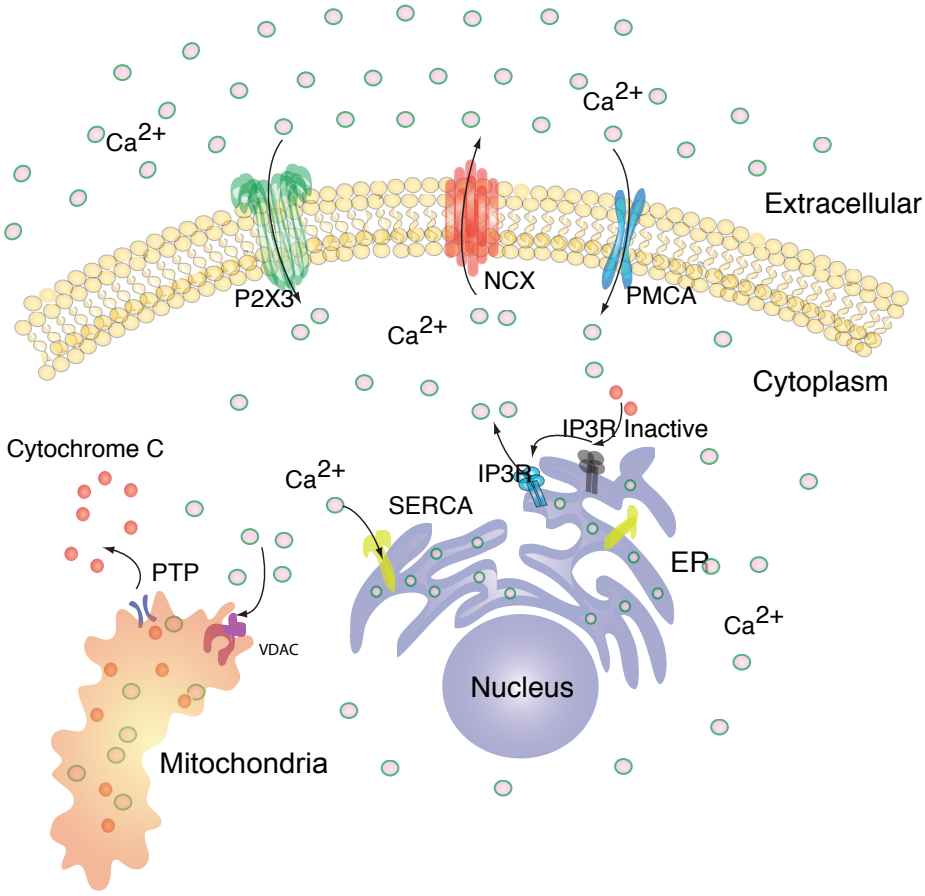

Figure 2.12: Release of Ca^{2+} into the cytoplasm leads to activation of the IP3R channels, leading to further increase in cytosolic Ca^{2+}. Excess cytosolic Ca^{2+} is taken in by the mitochondria. This leads to release of cytochrome C from the mitochondria leading to apoptosis.

sensitivity to apoptotic stress. Genetic ablation of the ER Ca^{2+} buffering protein calreticulin, or overexpression of plasma membrane Ca^{2+} ATPases protect cell from apoptosis [128, 153]. Overexpression of SERCA or Calreticulin sensitizes cells to apoptosis [153, 4]. A few key drivers of the process of ER Ca^{2+} release in response to stress signals have been identified. Fas-mediated caspase-8 activation leads to cleavage of the membrane-bound ER protein, Bap31 . Although

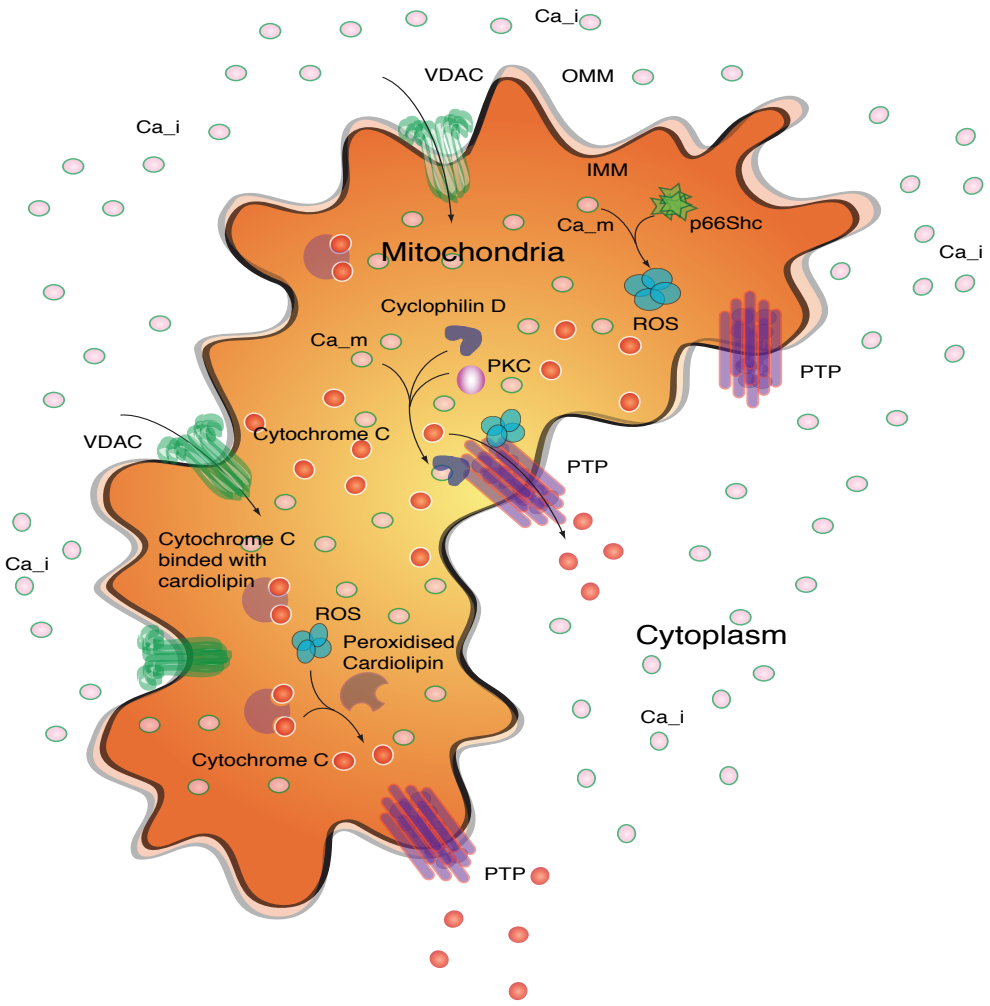

Figure 2.13: Mitochondria intake of Ca^{2+} leads to formation of ROS in the mitochondria and formation of PTP pores on the mitochondrial membrane. This leads to the release of cytochrome C and other apoptotic agents form the mitochondria into the cytoplasm.

Bap31 is membrane-bound, its caspase-recognition sequence faces the cytosol, and therefore is accessible for cleavage by caspase-8. The truncated product, Bap20, is believed to promote the release of ER Ca^{2+}. Bcl2 is also located on the ER membrane and the disruption of Bcl2 leads to increased release of ER Ca^{2+} [38, 190, 33]. It is assumed that ER-based Bcl2 protein is likely to function in a manner akin to that of mitochondrial Bcl2 [1]. Ca^{2+} release via inactivation of Bcl2 also results in the activation of ER-specific caspases-4 and 12. These caspases, in turn, are able to activate the executioner caspases-3, -6 and -7. Bad is the pro-apoptotic protein that bores holes into the mitochondrial membrane by self-oligomerization. Interestingly, Bad is regulated by the Ca^{2+}-binding protein phosphatase, called calcineurin. Calcineurin is activated by binding to active calmodulin protein, also a Ca^{2+}-binding protein, and four Ca^{2+} ions. Under normal conditions, Bad is kept sequestered in the cytosol by the cytoplasmic anchor, 14-3-3sigma. The activity of Bad is inhibited by the addition of a phosphate group by Akt, a serine-threonine protein kinase. Upon induction of apoptosis, 14-3-3sigma is cleaved by caspase-3, thus releasing Bad. The activity of Bad is further enhanced by calcineurin-mediated dephosphorylation of the inhibitory phosphate group (added by Akt). Once active, Bad can translocate to the mitochondrial membrane and initiate membrane permeabilization.

Thapsigargin induces the release of Ca^{2+} from the ER, leading to increase of cytosolic Ca^{2+} [170]. This acts as an irreversible inhibitor of SERCA pump [97]. Ca^{2+} has been shown to modulate the apoptotic signals [132]. The key role of the Ca^{2+} which enters the mitochondria is to modulate the permeability transition (PT) pore (PTP) [8]. PTP has been shown to modulate the apoptotic signals [32].

2.8.5 Other aspects of apoptosis mediated by stress

IRE1α, ATF6 and PERK are transmembrane protein kinases which play a key role as ER stress sensors. The oligomerized protein kinases then activate the p38MAPK and JNK stress pathways and also inhibit the translation factor, eIF2. These stress pathways can lead to the activation of DNA damage response proteins such as p53. p53 indirectly facilitates caspase activation by enhancing the transcription of pro-apoptotic proteins such as Bad. Caspase-12 plays a major role in apoptosis during stress-mediated UPR. JNK activation occurs using TRAF2 and ASK1, as in2.6. CHOP mediates in the apoptosis such that overexpression of CHOP induces cell cycle arrest [86]. Heterodimerization of ATF4 and C/EBP induces the expression of GADD153 [43]. This leads to the control of various genes including Bcl2 family of proteins. Dimerization of GADD153 and CREB suppresses the expression of Bcl2 [120]. Overall stress induced apoptosis occurs through mitochondria-dependant, mitochondria independent, and caspase-12 pathways.

2.9 Critical role of GRP78 in UPR

Elevated glucose metabolism is seen in Cancer cells along with increased glycolytic activity. Tumor cells grow faster than they get blood supply. These conditions lead to a microenvironment that is deprived of glucose and hypoxic. A direct consequence of this fact is the accumulation of underglycosylated and incorrectly folded proteins. These lead to the initiation of UPR.

GRP78 belongs to the HSP70 family of proteins. Under normal conditions,

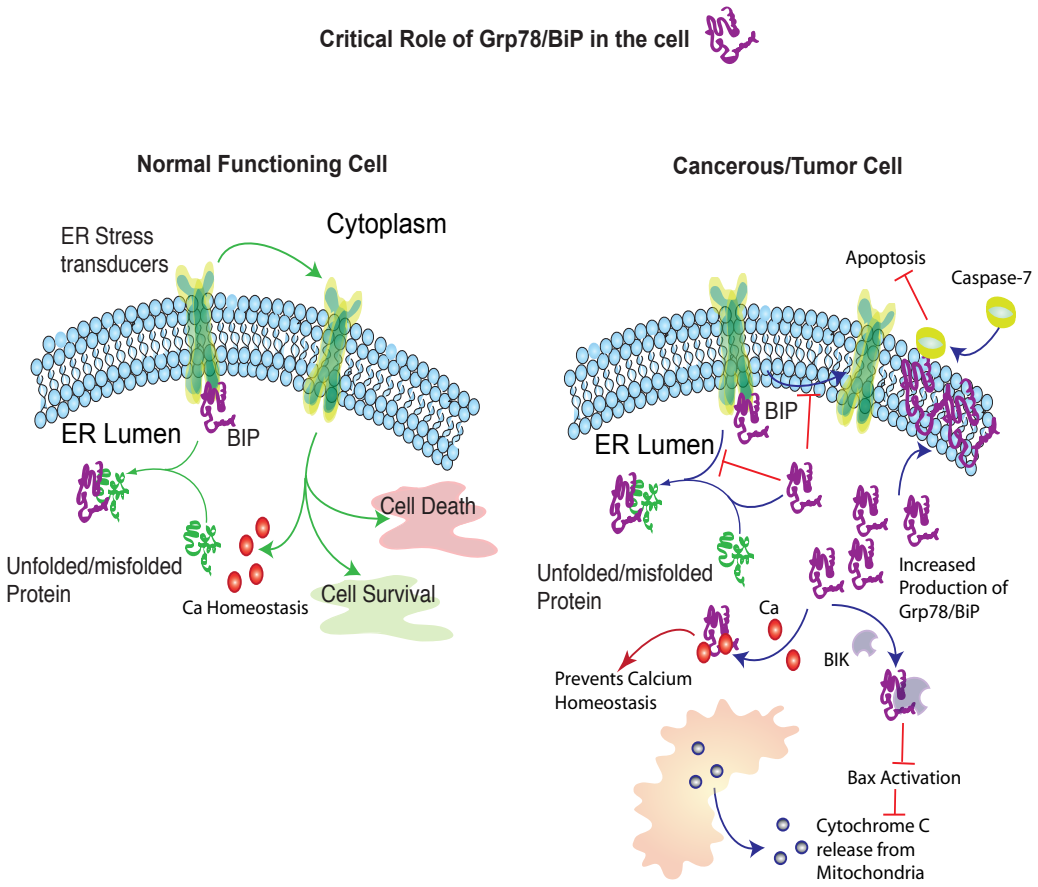

Figure 2.14: In a normal cell, GRP78 leads to alteration of Ca^{2+} homeostasis, cell death or cell survival in case of cellular stress. In a cancer or tumor cell, GRP78 binds to Ca^{2+} thereby preventing alterations of Ca^{2+} homeostasis. GRP78 binds to BIK leading to prevention of BAX mediated apoptosis. So the normal functionality of a stressed cell is altered due to the role of GRP78.

GRP78/BiP resides in the ER. BiP is involved in facilitating proper protein folding, preventing protein aggregation and targeting proteins for degradation. BiP also plays a role in binding ER Ca^{2+}, thereby acting as an ER stress regulator [101, 68]. Normally it is attached to ER stress transducers and, on initiation of UPR, is detached from the transducers.

Higher amounts of BiP is seen to be expressed in tumors [106, 39]. It has also been seen that BiP is detected on the surface of highly metastatic prostate cancer cells [125]. Higher production of BiP prevents the formation of misfolded proteins. Due to binding of the BiP to Ca^{2+}, it preserves ER Ca^{2+} homeostasis. Some amount of BiP is also located on the ER membrane [160]. ER membrane localization could lead to binding and inhibition of caspase-7. This prevents apoptosis induced by ER stress and genotoxic drugs [105, 160, 29]. This also leads to resistance to chemotherapeutic agents, as noted in lung, bladder, stomach, breast tumors and epidermoid carcinoma [105]. BiP also binds and prevents activation of BIK, which prevents the activation of BAX [157, 47]. This prevents release of cytochrome C from the mitochondria, thus preventing apoptosis.

CHAPTER 3

MODEL FORMULATION AND MODEL ANALYSIS OF UNFOLDED PROTEIN RESPONSE

3.1 Materials and Methods

The interactions of the proteins in Unfolded Protein Response, were modeled using a set of differential equations. This model was solved deterministically to obtain concentration profiles of proteins. These profiles were compared to the experimental observations found in the literature.

Once we obtained a qualitatively correct representation of the system, we studied the robustness of the system using sensitivity analysis and coupling studies. This cycle of model formulation and analysis presents provides the opportunity improve the model in every trial. This full circle approach has been shown to work in other studies in the Varner lab. The mathematical tools employed in the formulation and analysis of this model is presented in the current chapter.

3.1.1 Formulation and solution of the model equations

The unfolded protein response model was formulated as a set of coupled Ordinary Differential Equations (ODEs):

$$\frac{d\mathbf{x}}{dt} = \mathbf{S} \cdot \mathbf{r}(\mathbf{x}, \mathbf{p}) \qquad \mathbf{x}(t_o) = \mathbf{x}_o \tag{3.1}$$

The symbol $\mathbf{S}$ denotes the stoichiometric matrix (521×964). The quantity $\mathbf{x}$ denotes the concentration vector of proteins or protein complexes (521×1). The

term $\mathbf{r}(\mathbf{x}, \mathbf{p})$ denotes the vector of reaction rates (964×1). Each row in $\mathbf{S}$ described a protein while each column described the stoichiometry of network interactions. Thus, the (i, j) element of $\mathbf{S}$, denoted by σ_{ij}, described how protein i was involved in rate j. If $\sigma_{ij} < 0$, then protein i was consumed in r_j. Conversely, if $\sigma_{ij} > 0$, protein i was produced by r_j. Lastly, if $\sigma_{ij} = 0$, there was no protein i in rate j. All of these interactions were obtained from the literature.

We assumed mass-action kinetics for each interaction in the network. The rate expression for protein-protein interaction or catalytic reaction q:

$$\sum_{j \in \{\mathbf{R}_q\}} \sigma_{jq} x_j \rightarrow \sum_{p \in \{\mathbf{P}_q\}} \sigma_{pq} x_p \tag{3.2}$$

was given by:

$$r_q\left(\mathbf{x}, k_q\right) = k_q \prod_{j \in \{\mathbf{R}_q\}} x_j^{\sigma_{jq}} \tag{3.3}$$

The set $\left\{\mathbf{R}_q\right\}$ denotes reactants for reaction q. The quantity $\left\{\mathbf{P}_q\right\}$ denotes the set of products for reaction q. The k_q term denotes the rate constant governing the qth interaction. Lastly, σ_{jq}, σ_{pq} denote stoichiometric coefficients (elements of the matrix $\mathbf{S}$). We treated every interaction in the model as non-negative. All reversible interactions were split into two irreversible steps. The mass-action formulation, while expanding the dimension of the initiation model, regularized the mathematical structure. The regular structure allowed automatic generation of the model equations. In addition, an analytical Jacobian ($\mathbf{A}$) and matrix of partial derivatives of the mass balances with respect to the model parameters ($\mathbf{B}$) were also generated. Mass-action kinetics also regularized the model parameters. Unknown model parameters were one of only three types, association, dissociation or catalytic rate constants. Thus, although mass-action kinetics increased the number of parameters and species, they reduced the complexity of model analysis. In this study intracellular concentration gradients of the pro-

teins is simplified as having different species for each compartment. All these equations are solved using the LSODE routine in OCTAVE (v 2.9) on Apple machines.

3.1.2 Creation of the ensemble of models

Once the basic architecture of the model was set, it was important to obtain the rate constants (964 unknowns) for the interactions. These rate constants were not available in the literature. So the initial formulation of the model, involved the guessing of the rate constants and further improving of the guess based on literature data. These self-improving iterations were carried out untill we got the best resemblance to the data available.

Eight experimental constraints were used to formulate the rate constants of the model along with the understanding of the remaining network as seen in the literature. These experimental constraints are in fact western blot data of certain proteins in the UPR pathway measured at certain time points. The western blot data is quantified using GelEval 1.22 (FrogDance Software). GelEval allows us to measure the densities of the gel bands. To reduce inconsistency in the reading, multiple readings were obtained for the mean and standard deviation. A tabulation of the measured data along with the specific species are presented in tables 3.1-3.8.

These measurements give us a measure of the density of the bands. Owing to the differences in the protocol undertaken by different labs, different blots could have different implications. So the key here is to treat the data so as to normalize them to obtain some consistency in the data. This we do by normalizing the

Table 3.1: Geleval measurements of BiP Wester blots [9]

Time (mins)	Avg. Intensity ± Std. Dev.
0	0.4035 ± 0.1737
10	0.3280 ± 0.1778
20	0.14 ± 0.0445

Table 3.2: Geleval measurements of Caspase 3 Western blots [159]

Time (hrs)	Avg. Intensity ± Std. Dev.
0	0.2795 ± 0.0007
12	0.2670 ± 0.0005
24	0.2570 ± 0.0028
36	0.3135 ± 0.0134

Table 3.3: Geleval measurements of Caspase 7 Western blots [159]

Time (hrs)	Avg. Intensity ± Std. Dev.
0	0.3 ± 0.0001
12	0.29 ± 0.0014
24	0.3503 ± 0.0021
36	0.2385 ± 0.0021

Table 3.4: Geleval measurements of Cleaved Parp Western blots [159]

Time (hrs)	Avg. Intensity ± Std. Dev.
0	0.28 ± 0.0042
12	0.31 ± 0.0056
24	0.5255 ± 0.0091
36	0.6155 ± 0.0275

Table 3.5: Geleval measurements of PERK Western blots [9]

Time (mins)	Avg. Intensity ± Std. Dev.
0	0.811 ± 0.0791
10	0.6085 ± 0.1350
20	0.056 ± 0.0028

Table 3.6: Geleval measurements of Phosphorylated PERK Western blots [9]

Time (mins)	Avg. Intensity ± Std. Dev.
0	0.064 ± 0.0028
10	0.6385 ± 0.0813
20	0.835 ± 0.0565

Table 3.7: Geleval measurements of Pro-caspase 7 Western blots [159]

Time (hrs)	Avg. Intensity ± Std. Dev.
0	0.571 ± 0.0353
12	0.446 ± 0.0155
24	0.325 ± 0.0155

Table 3.8: Geleval measurements of Pro-caspase 12 Western blots [159]

Time (hrs)	Avg. Intensity ± Std. Dev.
0	0.551 ± 0.0098
12	0.4125 ± 0.0035
24	0.235 ± 0.0020

above mentioned data presented in tables 3.1-3.8.

Say we have the experimental data for species x_i for time $\{t_1, t_2, .., t_n\}$ as:

$$ex_i = \{ex_{i,t_1}, ex_{i,t_2}, ..., ex_{i,t_n}\} \tag{3.4}$$

Given this set of data we normalize the data as:

$$\hat{ex}_i = \frac{ex_{i,t_1} - min\{ex_i\}}{max\{ex_i\} - min\{ex_i\}} \tag{3.5}$$

This normalizing is done with every data set to obtain consistency. Once we have the normalized data, the next step is to obtain a best parameter set by hand. Initially a best guess estimate of the parameters is done by hand fitting so as to obtain the best set of parameters which we shall call as the *nominal set*. In order to compare the result with the experimental values, we pick out the simulation values for the species x_i for the entire time period $\{t_1, ..., t_n\}$ as:

$$sx_i = \{sx_{i,t_1}, sx_{i,t_2}, ..., sx_{i,t_n}\} \tag{3.6}$$

We normalize the simulation data in the same scheme as 3.5 to maintain consistency.

$$\hat{sx}_i = \frac{sx_{i,t_1} - min\{sx_i\}}{max\{sx_i\} - min\{sx_i\}} \tag{3.7}$$

Scaling the simulation results similar to the experimental results, allows us to compare the qualitative profiles of the proteins. The basic idea behind this approach is to consider the western blots as representative of a function limiting

its values to 0 and 1. So the darkest plot is equal to 1 and the lightest blot is equal to 0.

Once we have obtained the best possible nominal set, the question arises whether this is the best possible representation of the system of equations involved in UPR. There could be multiple combinations of rate constants that could represent the system qualitatively. This problem is pertinent to such a system, owing to the larger number of unknowns and limited number of constraints. This issue was addressed by formulating a family of models, that behave qualitatively similar to the nominal model set. The family of models was generated using the Multi-Objective thermal annealing scheme.

3.2 Multi-Objective Simulated Annealing Scheme

After obtaining the nominal set of parameters, the search of ensemble of parameters posed a challenge. Several uses of multi-objective schemes have been used in literature [184, 147]. These schemes use Pareto-Fronts to dictate selection of ensemble of parameters.

We treat the data set of each protein as one objective function. As a result, the eight objective functions we formulate, form the objective function space, wherein we are looking for the global minimum. The objective functions were defined as minimizing the error between the current evaluation of the simulation with the native set of parameters and the experimental results obtained from the literature. So the error or the i^{th} objective function value is formulated as:

$$error_i = \sum_t \{\frac{s\hat{x}_{i,t} - e\hat{x}_{i,t}}{0.5 * e\hat{x}_{i,t}}\}^2 \tag{3.8}$$

The aim of the optimization scheme is to minimize $error_i$ as stated in equation 3.8. Any optimization scheme to be used to minimize an 8-dimensional objective space, must address the trade-off between each objective function. Using the concept of Pareto-Fronts based optimization targets this issue justly. The concept of Pareto-Fronts combined with Simulated Annealing presents a suitable scheme, to obtain an ensemble of parameters.

Getting into the depth of the scheme, the energy function E(x) is defined as the scalar measure of $error_i$. Imposing the condition of Pareto-Fronts, we obtain certain optimum solutions which are a set of non-dominant solutions. These optimum solutions are a trade-off of the multiple objective functions. On the other hand, a single objective minimization scheme uses one objective function, using all the errors. In this type of algorithm, we do not have the option to control the errors in each data point. In our system, it is imperative to give weighted importance to all the objective functions. Pareto-Front based optimization schemes allows simultaneous minimization of all the objective functions.

In our model, a Pareto-optimal based energy function is used which uses the rank-based fitness assignment [44]. If we have kV_i as the the solution (set of rate constants) and it is dominated by p members, then based on the archive of the solutions the rank of the current solution is given by

$$rank(kV_i|\mathbf{F}_{archive}) = p \tag{3.9}$$

In simple sense the rank of the solution is equal to the number of solutions

that are dominating it. This dominance is measured based on the values of the objective values. So the basic non-dominant solutions are ranked '0'. The acceptance probability of the solution kV_i is based on the rank value,

$$P_{accept}(kV_i) = \exp -rank(kV_i|\mathbf{F}_{archive})/T \tag{3.10}$$

Here T is the computational annealing temperature. So the solutions with higher energy have a chance of being accepted only at higher temperatures. Accordingly at lower temperatures, the solutions come closer to a global minimum. The algorithm is outlined in table 3.9.

The updating scheme of the parameters include, generating a new parameter set based on randomly perturbing the parameters by upto ±50. The solution is now accepted based on the probability as stated in equation 3.10.

So the key features of this algorithm are: the initial temperature, the annealing scheme and the perturbation method. The effect of the initial temperature was tested and finally we settled with the temperature as dependent on n, which is equal to the dimension of the objective space. So the initial temperature is set as $n/log(2)$. This allows initially half of the proposals with rank value n to be accepted. This also means that initially parameters with rank less than n have a higher probability than of being accepted. In our case the value of n is 8, as we are using 8 objective functions or in other words 8 experimental sets to match our data.

Now according to the annealing scheme, the temperature is adjusted as we are coming close to the global minimum. The temperature is updated according to $T_k = \beta^k T_o$. Here β is chosen based on the final temperature and the epoch k is

Table 3.9: Algorithm for Multi-objective Thermal Annealing

kV : parameter vector
C(**kV**) : multi-objective cost function vector
$(C(kV) = (error_1(kV), error_2(kV), ..., error_8(kV)))$
F : an archive of the current estimate of the ensemble
R(**C**(**kV**)|**F**) : a Pareto-optimal rank based dominance measure
$\mathbf{kV} = \mathbf{kV_{init}}$: the starting point of parameters
$\mathbf{T} = \mathbf{T_0}$: initial annealing temperature
Repeat
kV_{new} = perturb (kV_{old})
Generate the new parameter set by randomly perturbing the previous parameter set
Calculate $C(kV_{new})$ and $R(C(kV_{knew})\|F)$
$P_{accept}(kV_{new}, kV_{old}) \equiv exp\{-R(C(kV_{new})\|F)/T\}$
if $P_{accept}(kV_{new}, kV_{old})$ > rand(0,1)
Move to kV_{new}
Update the archive F
endif
T = annealing(T)
EndRepeat(Until the termination condition is satisfied)

updated every 100 iterations as ($k = 1, ..., 10$).

The third key feature of the algorithm is the perturbation scheme. There are certain options in the way we perturb the parameters. It is possible to perturb parameters one at a time, but this proves to be computationally very expensive. On the contrary, the other possibility is to perturb all the parameters together. This poses the requirement of a long time to find an acceptable solution. This is the scheme that has been used in perturbing the rate constants in our model. A better methodology which can be employed in the future models is to divide the parameters into subgroups and use weighted perturbation schemes.

Once we obtained a family of parameters, we study the robustness of the system, using sensitivity analysis and coupling studies.

3.2.1 Sensitivity analysis of the UPR network

Overall State Sensitivity Coefficients (OSSC) were used to estimate which structural elements of the UPR network were sensitive [185]. OSSC values were determined by first calculating the first-order sensitivity coefficients at time t_k:

$$s_{ij}(t_k) = \left.\frac{\partial x_i}{\partial p_j}\right|_{t_k} \tag{3.11}$$

First-order sensitivity coefficients were computed by solving the matrix differential equation:

$$\frac{d\mathbf{s}_j}{dt} = \mathbf{A}(t)\,\mathbf{s}_j + \mathbf{b}_j(t) \qquad j = 1, 2, \ldots, P \tag{3.12}$$

subject to the initial condition $\mathbf{s}_j(t_0) = \mathbf{0}$. In equation 3.12, j denotes the parameter index, P denotes the number of parameters in the model, $\mathbf{A}$ denotes the Jacobian matrix, and $\mathbf{b}_j$ denotes the jth column of the matrix of first-derivatives

of the mass balances with respect to the parameter values (denoted by **B**). An analytical Jacobian and matrix of first-derivatives of the mass balances w.r.t the parameters:

$$\mathbf{A} = \left.\frac{\partial \mathbf{f_x}}{\partial \mathbf{x}}\right|_{(\mathbf{x}^*,\mathbf{p}^*)} \qquad \mathbf{B} = \left.\frac{\partial \mathbf{f_x}}{\partial \mathbf{p}}\right|_{(\mathbf{x}^*,\mathbf{p}^*)} \tag{3.13}$$

were generated from the model equations. The quantity $\mathbf{f_x} = \mathbf{S} \cdot \mathbf{r}(\mathbf{x}, \mathbf{p})$ and $(\mathbf{x}^*, \mathbf{p}^*)$ denotes a point along the unperturbed model solution. The sensitivity equations required that we solve the model equations to evaluate the **A** and **B** matrices. Thus, we formulated the sensitivity problem as an extended kinetic-sensitivity system of equations [37]:

$$\begin{pmatrix} \dot{\mathbf{x}} \\ \dot{\mathbf{s}}_j \end{pmatrix} = \begin{bmatrix} \mathbf{S} \cdot \mathbf{r}(\mathbf{x}, \mathbf{p}) \\ \mathbf{A}(t)\,\mathbf{s}_j + \mathbf{b}_j(t) \end{bmatrix} \qquad j = 1, 2, \ldots, P \tag{3.14}$$

where $\dot{\mathbf{x}} = d\mathbf{x}/dt$ and $\dot{\mathbf{s}}_j = d\mathbf{s}_j/dt$. We solved the kinetic-sensitivity system for multiple parameters in a single calculation using the LSODE routine of OCTAVE (www.octave.org). The first-order sensitivity coefficients were then used to calculate the OSSC value for parameter j:

$$OSSC_j(t) = \frac{p_j}{N_s}\left(\sum_{k=1}^{N_T}\sum_{i=1}^{N_s}\left[\frac{1}{x_i}\left.\frac{\partial x_i}{\partial p_j}\right|_{t_k}\right]^2\right)^{1/2} \tag{3.15}$$

The terms N_T, N_s denote the number of time points considered and the state dimension of the model, respectively. This sensitivity was calculated on the nominal set. The scaled parameter ranking was calculated based upon the magnitude of the OSSC value:

$$\theta_{sj} = \frac{N_P - R_{sj}}{N_P} \tag{3.16}$$

N_P denotes the number of kinetic parameters and R_{sj} denotes the ranking of parameter j calculated using parameter set s. We estimated the fragility of each protein or protein-complex in the network according to the relationship:

$$\mathcal{F}_s = |\mathbf{S}|\,\Theta_s \tag{3.17}$$

$|\mathbf{S}|$ denotes the absolute value of the stoichiometric matrix. Θ_s denotes the vector of scaled parameter rankings calculated using parameter set s.

Another methodology employed in the calculation of the sensitivities was by normalizing the sensitivity coefficients using the nominal parameter and state values:

$$N_{ij} = s_{ij}(t_k)\frac{p_j}{x_i} \tag{3.18}$$

The normalized sensitivities are then time-averaged by integration using Simpson's rule:

$$NSS_{ij} \equiv \frac{1}{T}\int_0^T dt \cdot |N_{ij}(t)| \tag{3.19}$$

The normalized sensitivities NSS_{ij} can be interpreted as the approximate fractional change of the state variables x_i for a small change in the parameter p_j. This sensitivity values were analyzed using the method of Hearne to estimate the best combination of parameters to obtain the best result.

3.2.2 Monte-carlo coupling analysis of the UPR architecture.

Coupling coefficients of the form:

$$\alpha\left(i, j, t_o, t_f\right) = \left(\int_{t_o}^{t_f} x_i\left(t\right) dt\right)^{-1} \left(\int_{t_o}^{t_f} x_i^{(j)}\left(t\right) dt\right) \tag{3.20}$$

were calculated to understand the robustness of the UPR network. Here t_0 and t_f denote the initial and final simulation time respectively. i and j denote the

indices for the reference species and the perturbed species respectively. The coupling coefficient $\alpha\left(i, j, t_o, t_f\right)$ is the ratio of the integrated concentration of a network output in the presence (numerator) and absence (denominator) of structural or operational perturbation. If $\alpha\left(i, j, t_o, t_f\right) > 1$, then the perturbation *increases* the output concentration. Conversely, if $\alpha\left(i, j, t_o, t_f\right) \ll 1$ the perturbation *decreases* the output concentration. Lastly, if $\alpha\left(i, j, t_o, t_f\right) \sim 1$ the perturbation does not influence the output concentration. In this study, we simulated edge coupling which induces the removal of a particular reaction to understand the change of all the protein concentrations based on the reaction removal. This scheme also has inbuilt the option to do protein knockouts.

CHAPTER 4

RESULTS AND DISCUSSION

The primary approach employed in this study, is to mimic a complex biological system by constructing an equivalent mathematical model. We have used the 'system of systems' approach, to model the UPR machinery of the cell. The fully functional model describe, qualitatively, the trends observed for some of the species (proteins) in literature. It is not just the model but even the tools that was used to generate this model, that is of interest in this study.

4.1 Parameter ensemble creation results

Multi-objective thermal annealing scheme was used to generate the parameter sets as stated in table 3.9. There could be many developed strategies for selection and perturbation of the parameters. Owing to the complexity of the system, we purturbed all the parameters simultaneously.

The scheme for perturbation employed in this study is:

$$kV_{new} = kV_{old} * (1 + (2 * rand(N, 1) - 1) * G) \tag{4.1}$$

Here N is the number of unknown rate constants (964). G is a constant which determines the maximum and minimum variation of the rate constants (G=0.5 denotes ± 50% variation of the rate constants). This perturbation scheme, is employed into the multi-objective Pareto-Frontiers algorithm stated in table 3.9.

Every perturbation is accepted provided they meet two conditions:

Criterion 1: They have met the rank criterion $Rank(kV_{new}) \leq 2$

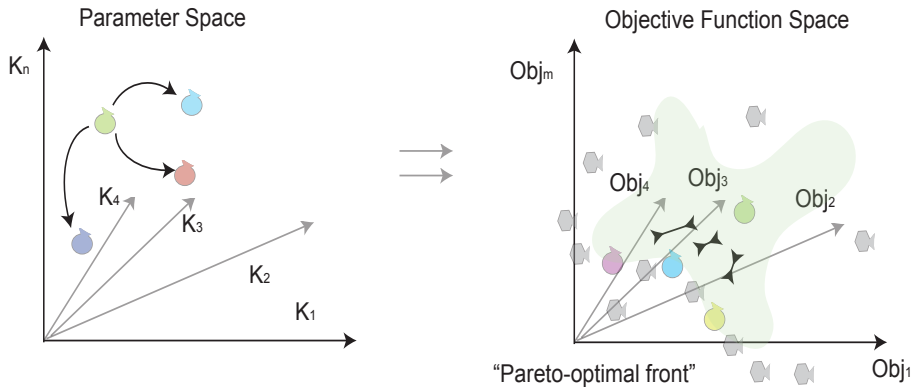

Figure 4.1: Low Diversity search of the parameter space: This enables us to obtain parameters sets that best describe the local minimum around the nominal set. The perturbation scheme involves perturbing the nominal set every time.

Criterion 2: Maximum value of the objective value should be less than three times the objective value of the nominal set. Lower limit of the objective value gives a lower acceptance rate of parameters and vice versa for higher limits.

Besides the perturbation scheme and the acceptance criterion, the search of the parameter space is also significant. To target this issue, two different searching strategies were used. The first approach was meant to search the parameter space around the nominal set as in figure 4.1. This is representative of the local minimum in the parameter space.

We represent the ensemble of parameters as EOP and the individual elements as EOP_i. The plot of the Coefficient of Variation (CV) of the EOP for the low diversity case is show in figure 4.2. CV is measured as the ratio of the standard deviation to the mean. This gives an idea of the normalized measure of dispersion of EOP. In the low diversity case the CV values ranges from 0.273-

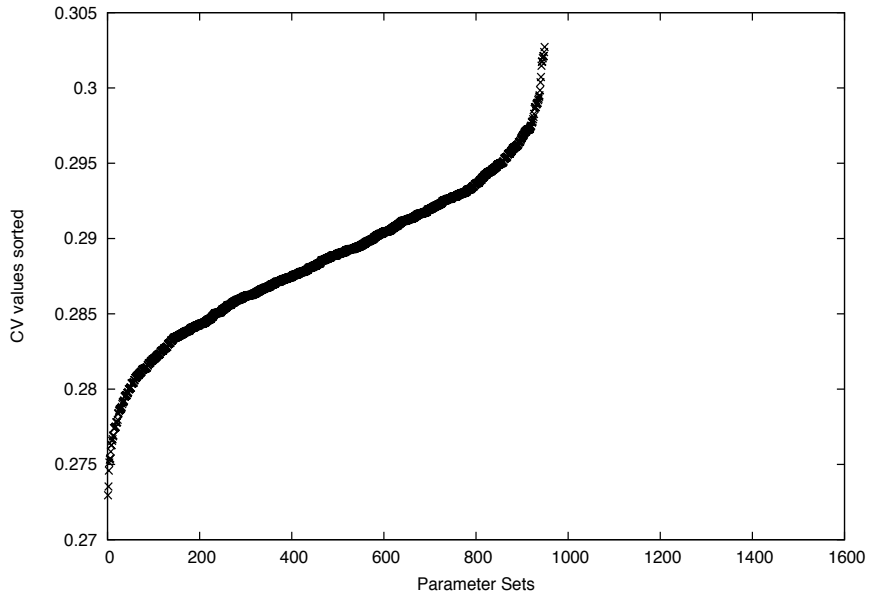

Figure 4.2: CV plot of the low diversity ensemble of parameters: This plot is representative of the low diversity of the ensemble with the CV centered around 0.29.

0.305. These values represent the lack of diversity in the parameters. It can also be seen as representing the local minima in and around the nominal parameter set.

The spread of the ensemble around the parameter space can be studied using the 2^{nd} norm of the EOP_i. The histogram of the 2^{nd} norm values is plotted in 4.3. This shows a clear bell shaped curve centered around 0.3. The standard deviation of the distribution is the required spread parameter.

This kind of study, as just described, does not encapture the possible high diversity in the parameters. We utilize a different approach to address this

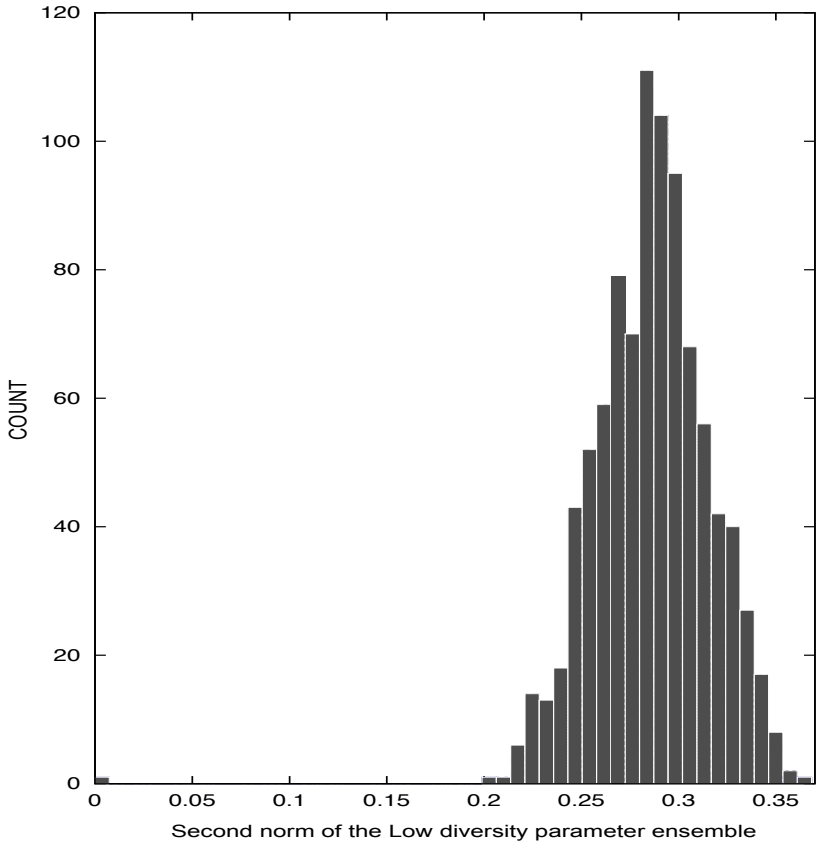

Figure 4.3: Histogram of the 2^{nd} norm of the low diversity ensemble of parameters: This shows how the ensemble of parameters is spread around a mean CV of 0.29.

drawback. In this modified approach, each perturbation was based on the previous accepted perturbation. The perturbation scheme and the acceptance criterion was similar to the low diversity ensemble creation scheme. This scheme is shown in the figure 4.4.

In this case we moved around a great deal in the parameter space. This is represented by the cv plot and the histogram plots.

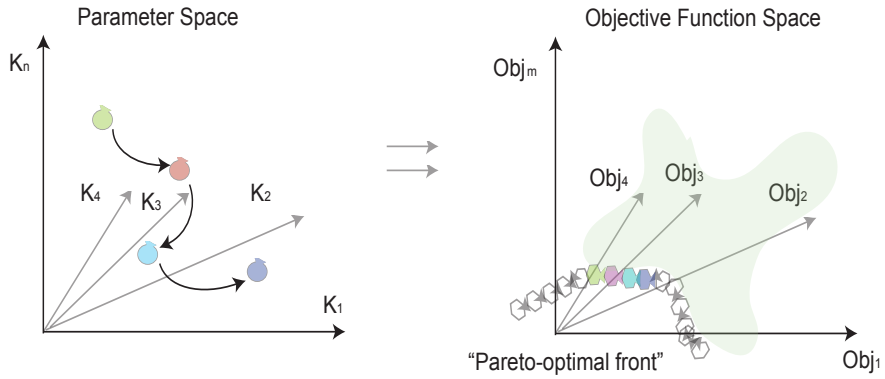

Figure 4.4: High Diversity search of the parameter space: This strategy is targeted to obtain diverse parameter sets well beyond the local minimum of the nominal set. This search strategy could indeed lead us to the global minimum of the parameter space. In this scheme every perturbation of the parameters is based on the previous accepted perturbation.

In comparison to the low diversity case we see that in the high diversity case we have higer CV (in the range of 10). To compare the diversity of the ensemble of parameters we look of the 2^{nd} norm of the values as in figure 4.6. The values of the 2^{nd} norm range from 0 – 146 in the high diversity case, in comparison to 0 – 0.35 for the case of low diversity ensemble. This ensures that the spread of the parameters from the nominal set is quite diverse. Having ensured that we have the correct strategy employed in searching the parameter space we look into how the model is behaving.

The scheme employed to search the parameter space along with the optimizing scheme of pareto frontiers is in contrast to the approach where a single objective function is optimized. We have classifed the experimental data into 8 objective funcitions. The optimizing scheme finds a trade-off to reach the global minima in the parameter space. We took a look at the evaluations of these ob-

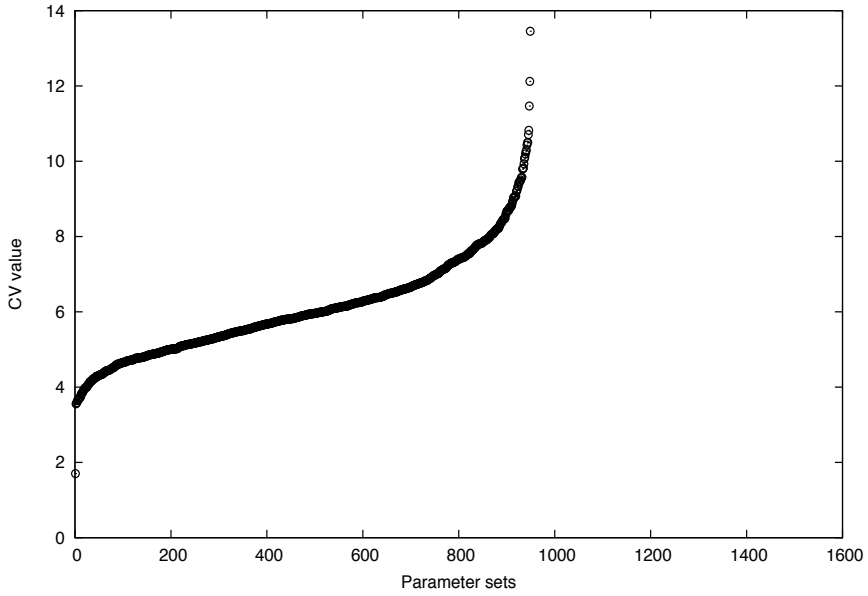

Figure 4.5: CV plot of the high diversity ensemble of parameters: This plot shows the high diversity of the parameter sets obtained as compared to the low CV of 0.29 obtained in the low-diversity case.

jective values to see how well the fronts were formed. This gives an idea as to which parameter set is more important than the other.

In figure 4.7 and 4.8, the objective values are evaluated for the all the parameter sets and plotted against each other. For the low diversity case as in figure 4.7 we see that (top left part of the quadrant) the objective values are not well constrained. This suggests that these functions were not the controlling functions during parameter search. On the contrary we see well defined pareto fronts on the lower right quadrant. This tells us that objective function 6 and 7 are of prime importance for parameter selection. The approach of having a tradeoff in terms of objective values for multiple objective functions is clearly

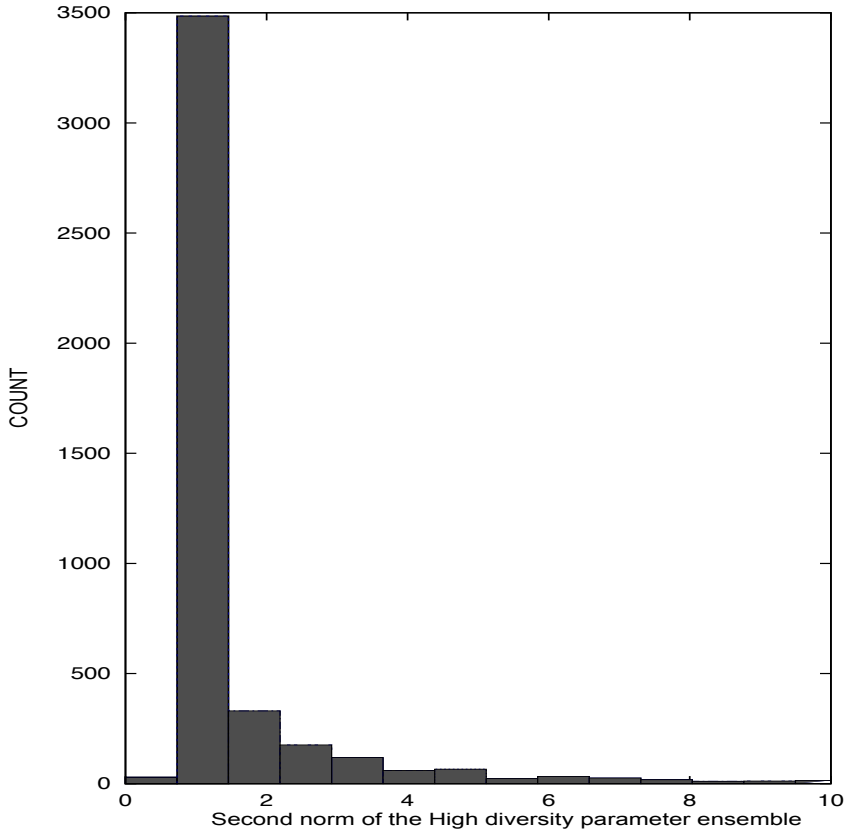

Figure 4.6: Histogram of the 2^{nd} norm of the high diversity ensemble of parameters: This shows the wide range of CV of the parameter space that is explored. In this scheme, we see that we have reached a global minimum centered around the CV of 1.

demonstrated in the figure 4.7.

When we look at the high diversity case in figure 4.8, we find well defined pareto fronts on the lower part of the figure. This observation is consistent in saying that objective function 6, 7 and 8 are of prime importance. This corresponds to the tradeoff between the error values of Caspase 3, Caspase 7 and Cleaved Parp. One interesting thing to note that there are two parrallel fronts

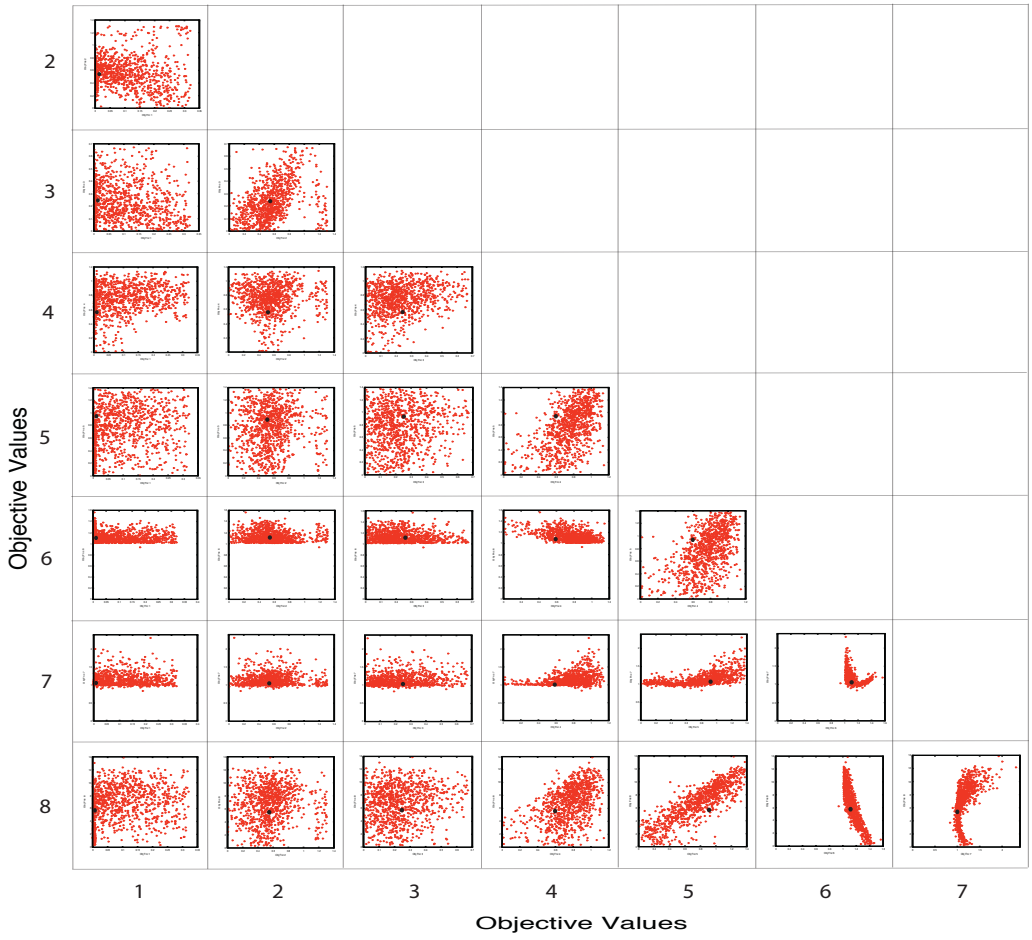

Figure 4.7: Combined grid of objective value plot for the Low diversity: This is a combination of 2-dimensional plots of each objective function with the other. The black dot in each of the plots indicate the objective value of the nominal set. We find that some objective functions are tightly constrained, like objective functions 6,7. The scheme has been successful in obtaining a trade-off between these functions, as shown in the lower right quadrant. Other objective functions do not have that much variation over the parameter space that has been explored. So we have some scattered plots towards the upper left quadrant of the figure.

being created in the top left corner. This could denote bifurcation in the system. It could also imply the presence of two local minimas in the parameter space which have the same objective function evaluations. This area of the model is yet to be studied. This kind of study could be used to identify the significant objective functions and to improve optimization techniques.

4.2 Model Validation

Once we obtained the parameter sets using both the schemes, we look at how the model is behaving with respect to the training and prediction sets. The choice of the training and prediction sets was purely at random. Some upstream and some downstream data sets were selected at random and divided into two groups. One group was used for training the data and the other to test the predictions of the model.

The interaction of BiP with PERK and IRE1 has been studied [9]. The authors stated that ER stress induced by Thapsigargin (Tg) leads to the dissociation of the BiP-PERK complex. This study was conducted in AR42J cells. These cells were treated with Tg or dithiothreitol (DTT) for certain time periods. The treated cells were then immunoprecipitated with the corresponding antisera. The individual components were then resolved by SDS-PAGE. This set of data is used for training the model. The performance of the model with respect to this data is shown in figure 4.9.

In another study, Sak2 cells were treated with 0.5 μM thapsigargin to induce ER stress [159]. Cytosolic extracts from these cells were extracted and analyzed by western blots. Caspase-12, caspase-9, caspase-7, caspase-3 and PARP were

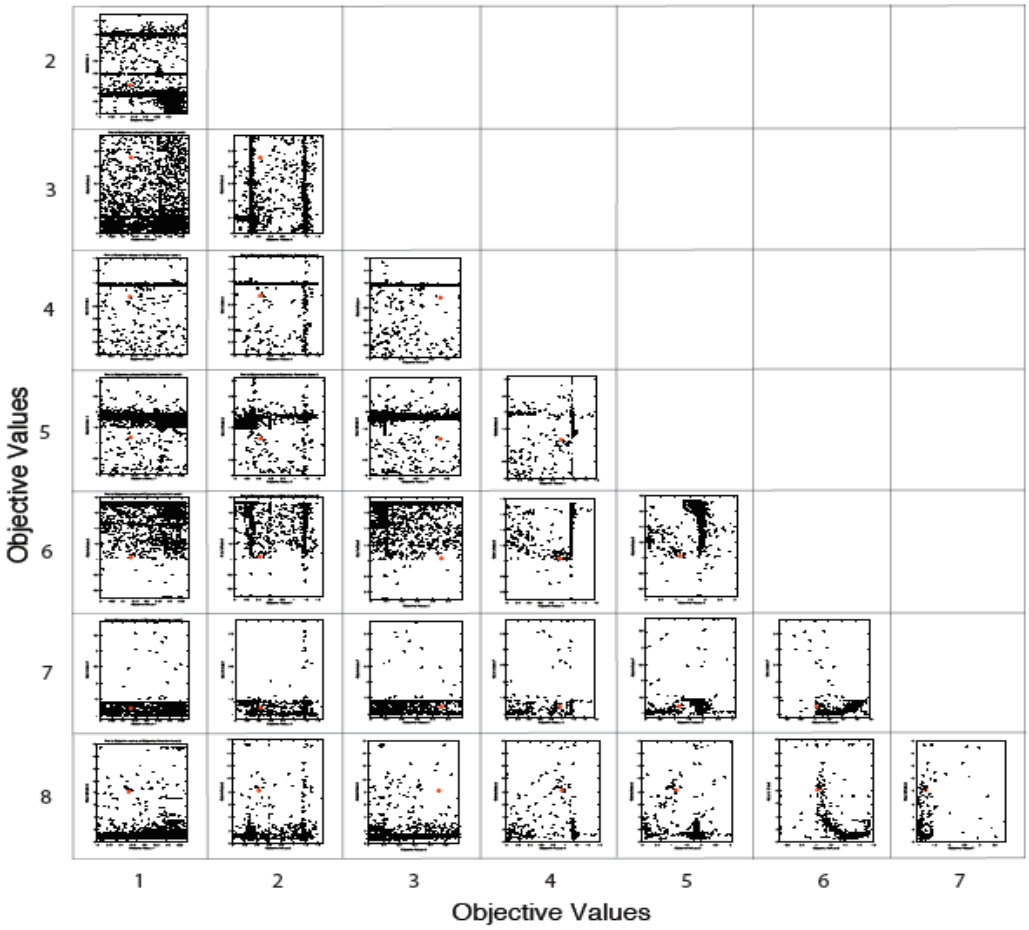

Figure 4.8: Combined objective plot for the high diversity: This is a combination of 2-dimensional plots of each objective function with the other. We find that some objective functions are tightly constrained, like objective functions 6,7. The scheme has been successful in obtaining a tradeoff between these functions, as shown in the lower right quadrant. On the contrary we find multiple fronts towards the upper left quadrant. These fronts could be representative of bifurcation in the system. It could also be representation of local minima in the parameter space. This are of the model is yet unexplored in the study.

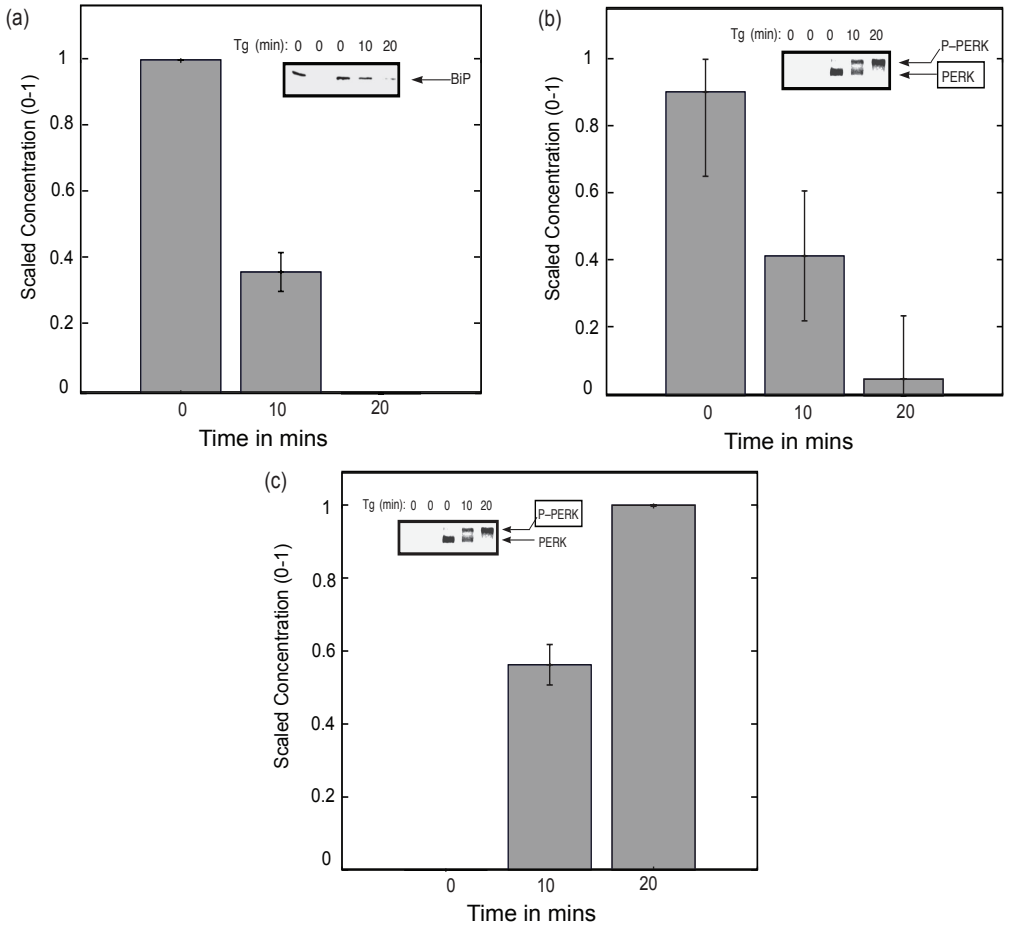

Figure 4.9: Plot of model output against training data for the low diversity case. Simulation results are plotted as the grey bar graphs with one standard deviation as the error bar. Experimental data taken from [9]. In the experiments AR42J cells were treated with thapsigargin (Tg) or dithiothreitol (DTT) for the indicated time periods, and immunoprecipitated with the indicated antisera. (a) Upon UPR induction BiP is seen to vary consistently to the experimental data (b) Shows the trends observed for PERK upon UPR induction (c) Phosphorylated PERK profile upon UPR induction. We see that the right trend is followed in the model as seen in the data.

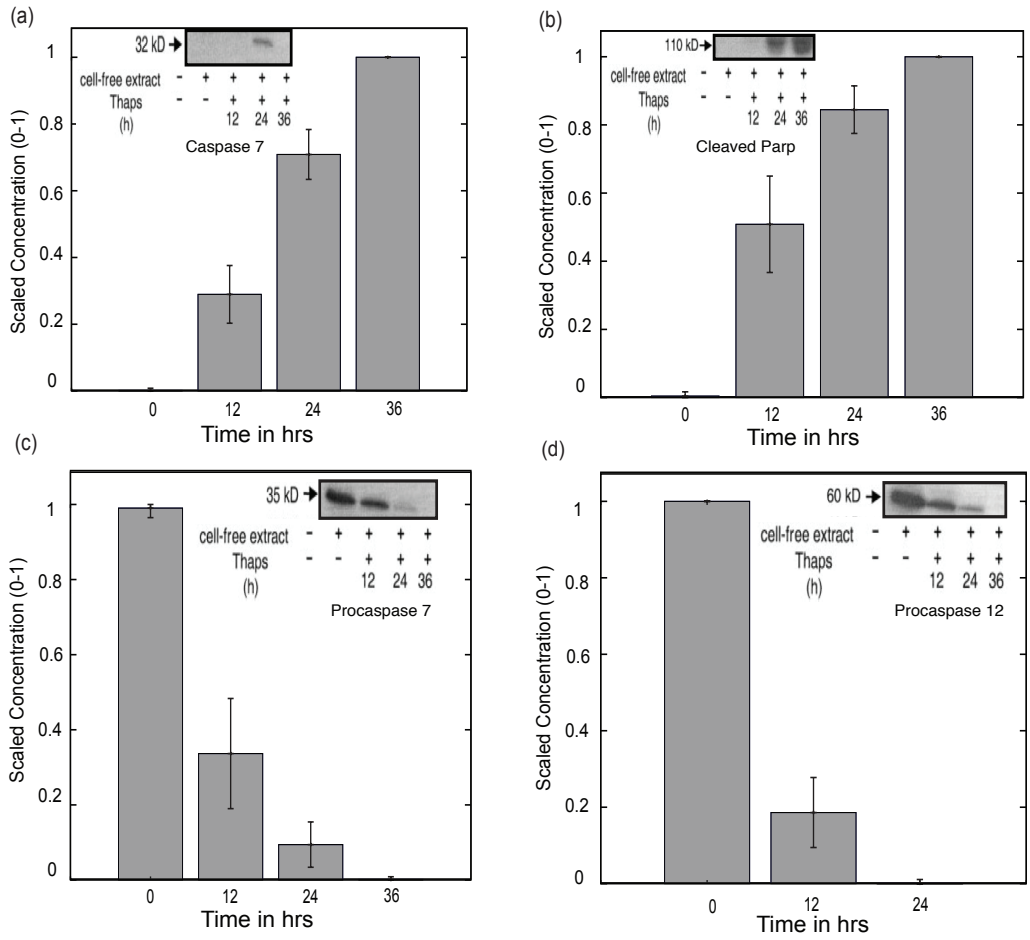

Figure 4.10: Plot of model output against training data for the low diversity case. Simulation results are plotted as the grey bar graphs with one standard deviation as the error bar. Experimental data taken from [159]. In this experiment Sak2 cells were treated with 0.5 μM thapsigargin for the indicated times. Cell-free cytosolic extracts from thapsigargin treated cells were prepared and analyzed by Western blot analysis. (a) Caspase 7 profile (b) Cleaved Parp profile (c) Procaspase 7 profile (d) Procaspase 12 profile upon UPR induction is shown. We see that the model is behaving consistent to the experimental data.

some of the key components that were studied. Some of the data presented in this study were used as the training sets for our UPR model. Low diversity ensemble, shows clearly to be following the trends as seen in the experimental observation.

Similarly we look at the performance of the model with the high diversity in the parameters as in figure 4.11.

We see that qualitatively similar results and closeness to training data for both the low and the high diversity ensemble of parameters. Again, the aim is to mimic the real system observations. As an additional note, increasing the number of data sets for training will further constrain the system. This could provide further improvement in the model performance.

4.3 Model Predictions

Having seen that the model behaves correctly according to the training data sets, it now remains to see how well the model predicts the species that it has not been trained for. This ability of the model was tested for a few species across different stages of the pathway with some other western blots data available in the literature.

In one study [64], MEF's were treated with Thapsigargin (Tg, 0.4 μ M). Immunoblots of the ATF4 from the nuclear fractions were compared to the simulation results. The high diversity and the low diversity models makes correct predictions for the formation of ATF4 upon UPR induction as seen in figure 4.12(a) and 4.13(a).

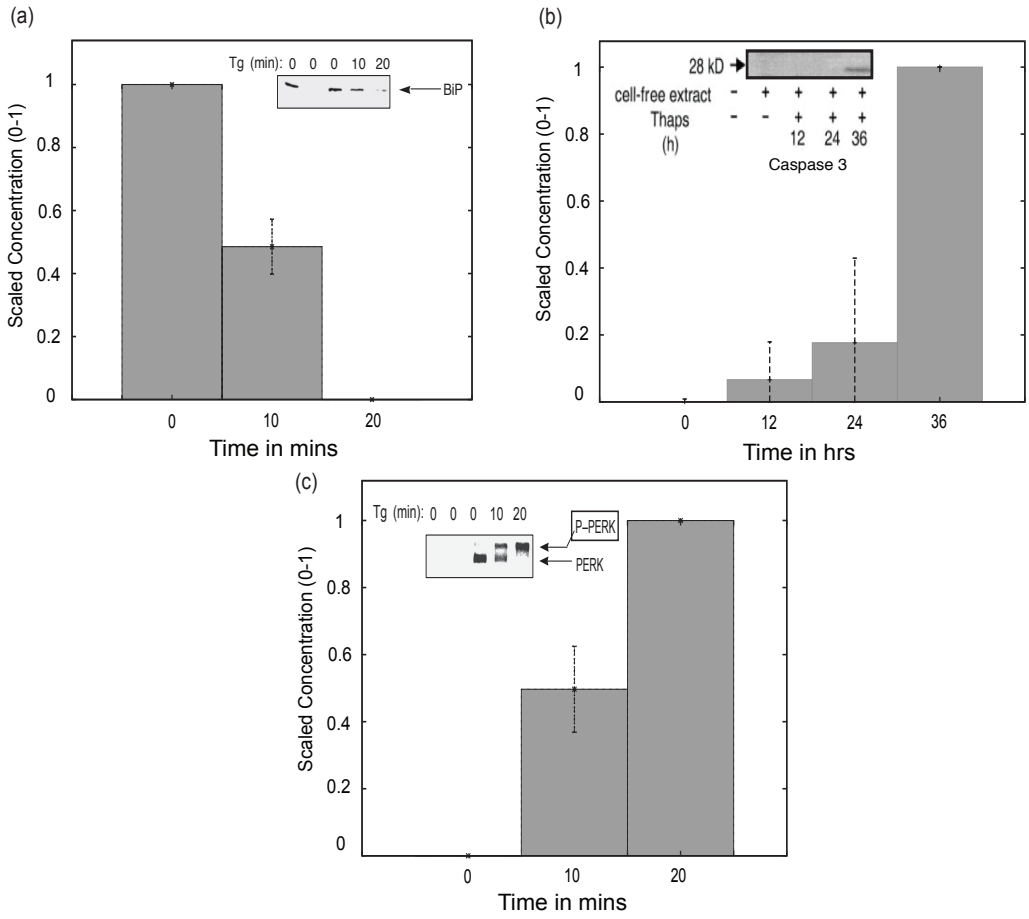

Figure 4.11: Plot of model output against training data for the high diversity case. Simulation results are plotted as the grey bar graphs with one standard deviation as the error bar. Experimental data taken from [9, 159]. (a) and (c) Data taken from [9]. In the experiments AR42J cells were treated with thapsigargin (Tg) for the indicated time periods, and immunoprecipitated with the indicated antisera. Profile of BiP and phosphorylated PERK are shown as matching the experimental data. (b) Data taken from [159]. In this experiment Sak2 cells were treated with 0.5 μM thapsigargin for the indicated times. Cell-free cytosolic extracts from thapsigargin treated cells were prepared and analyzed by Western blot analysis. Comparison of Caspase 3 profile upon UPR induction is shown with respect to the experimental evidence.

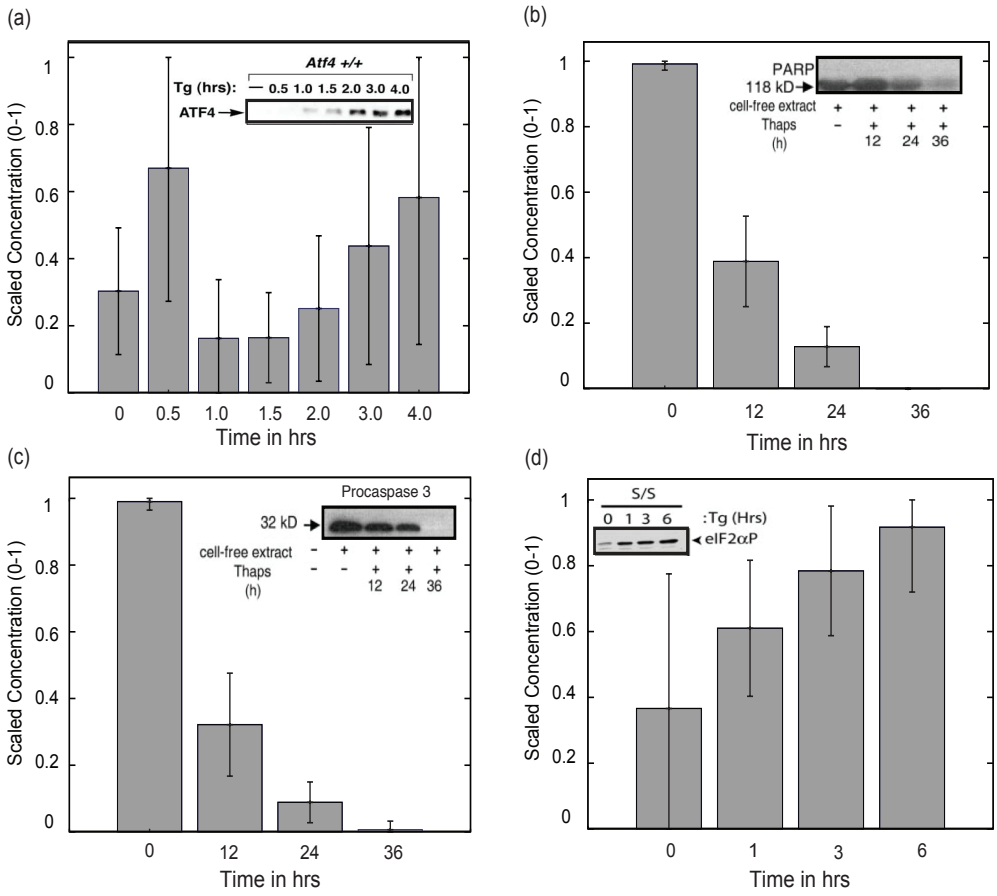

Figure 4.12: Plot of model output against prediction data for the Low diversity case. Simulation results are plotted as the grey bar graphs with one standard deviation as the error bar. Experimental data taken from [64, 159, 204]. (a) Data obtained from [64]. Immunoblots of ATF4 from the nucleur fraction of the untreated and thapsigargin-treated (Tg, 0.4μM) in mouse fibroblasts are compared to the simulation data. (b) and (c) Data obtained from [159]. Cell-free cytosolic extracts from thapsigargin treated Sak2 cells, treated with 0.5 μM thapsigargin are analyzed. In (b) the western blot of Whole PARP is compared with the simulation result. In (c) the western blot of Procaspase 3 is compared with the simulation result. (d) Data taken from [204]. Phosphorylation of eIF2α, in wild type (S/S) MEF cells, treated with 1.0 μM Tg is compared with the simulation results of our model. We show consistent performance of the model, according to the experimental observations.

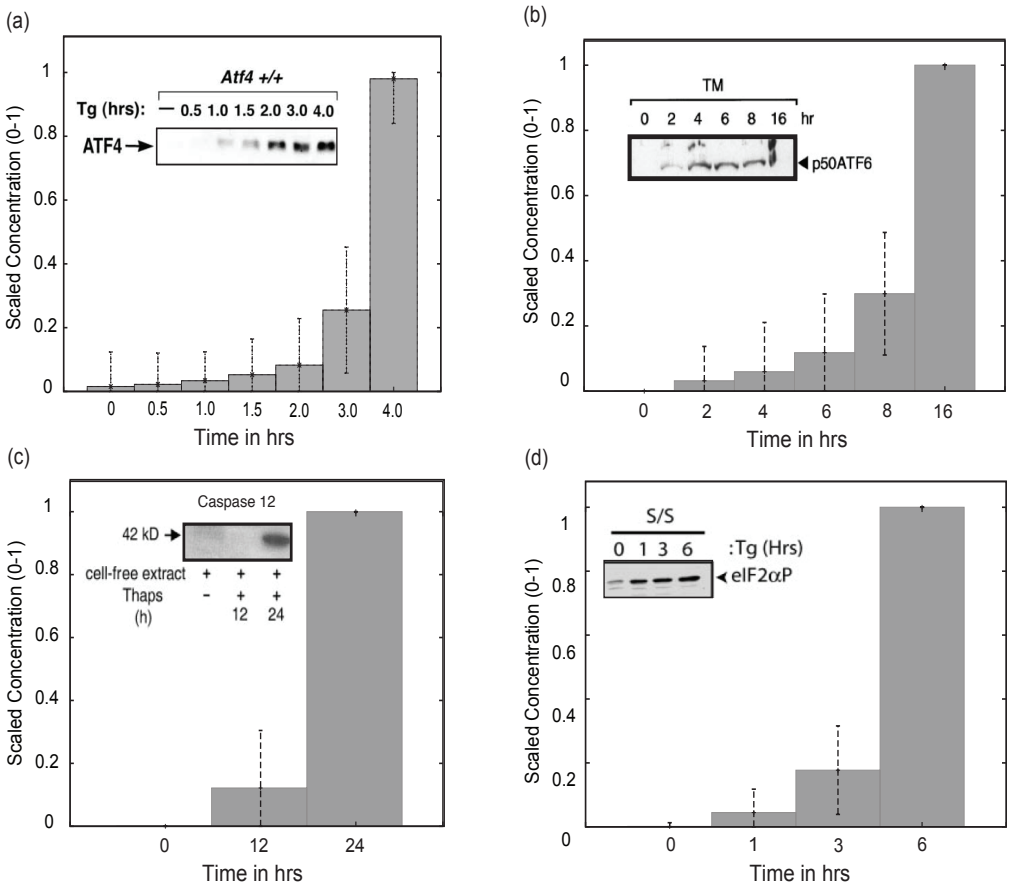

Figure 4.13: Plot of model output against prediction data for the high diversity case. Simulation results are plotted as the grey bar graphs with one standard deviation as the error bar. Experimental data taken from [64, 183, 159, 204]. (a) Data obtained from [64]. Immunoblots of ATF4 from the nucleur fraction of the untreated and thapsigargin-treated (Tg, 0.4μM) in mouse fibroblasts are compared to the simulation data. (b) Data obtained from [183]. Western blot of cleaved ATF6 in tunicamycin-treated HeLa cells is compared with the simulation result. (c) Data obtained from [159]. Western blots of Caspase 12 in Sak2 cells, treated with 0.5 μM thapsigargin is compared with the simulation result. (d) Data taken from [204]. Phosphorylation of eIF2α, in wild type (S/S) MEF cells, treated with 1.0 μM Tg is compared with the simulation results of our model. We see consistent predictions of the the species from the model at hand.

In [159] Sak2 cells were treated with 0.5 μM thapsigargin for certain time periods. Cell-free cytosolic extracts from thapsigargin treated cells were prepared and analyzed by Western blot analysis. We compared the simulation results of Procaspase 3 and whole PARP to the western blot data presented in this paper. We found that the model is representing the correct trend as seen from the experimental results, shown in figure 4.12(b) and (c).

In [204], wild type (S/S) MEF cells were treated with 1.0 μM Tg for the indicated number of hours. Phosphorylation of eIF2α was measured by immunoblot by using Ab that specifically recognizes eIF2α phosphorylated at Ser-51. This result is compared with the simulation results of our model. We see consistent correct predictions in high and low diversity ensembles, as seen in figure 4.12(d) and 4.13(d).

The model as a whole, is behaving in the correct manner as seen by the prediction sets. We can employ more data sets to test this system. Now that we are convinced that the model work, we go on to test the fragility of the system.

4.4 Sensitivity Analysis of the UPR Model

Once we obtained the fully functional model which match the training data, we look into the fragility of the system. Sensitivity analysis reveals the fragile components of the system. Given the constraint of computational effort involved, the sensitivity calculations have been run on the system with and without UPR induction for the nominal set of parameters only.

In figure 4.14 we see the plot of the OSSC values for the UPR model. In fig-

ure 4.14(a) we have the plot of the OSSC values with UPR induction. In figure 4.14(b) we have the OSSC values without UPR induction. We find that the same species are consistently sensitive, with and without UPR induction. This idea is presented in figure 4.14(c). The x axis denotes the OSSC values with UPR induction and the y axis without UPR induction. It is amply clear that the sensitive species are not preferentially sensitive upon UPR activation.

Due to the large number of species in the plot, we do not get a clearer idea of the important species. So we subdivided the system to its key components: UPR initiation, ERAD, apoptosis and translational machinery of the proteins. We took a deeper look into these subdivisions of the model. Breaking up of the ATF6-BiP complex is seen to be the most sensitive step in the UPR initiation part of UPR. Similarly the cleavage of the BiP and ER stress transducers complexes have high OSSC's. The binding of the unfolded protein to the chaperone HSP40 is also relatively important as seen in figure 4.15(a). In the apoptotis group of reactions of the model, we find that increased translation of BiP is of prime importance, along with the nuclear migration of AIF as seen in figure 4.15(b). Translation of chaperones and the ER stress transducers are in general more sensitive as seen in figure 4.15(c). In the ERAD component of the UPR network, activation of the Ubiquitin by reacting with ATP is seen to be the most sensitive reaction as seen in figure 4.15(d).

Another alternate approach was used to calculate the sensitivities, as discussed in the chapter 3.2.1. Once we have the NSS values, we go on further to rank these parameters. We carry out the singular value decomposition of the NSS matrix. The V matrix obtained thereby, contains the basis vector direction of the NSS matrix. We sort these parameters and rank them in a scale of 1-100.

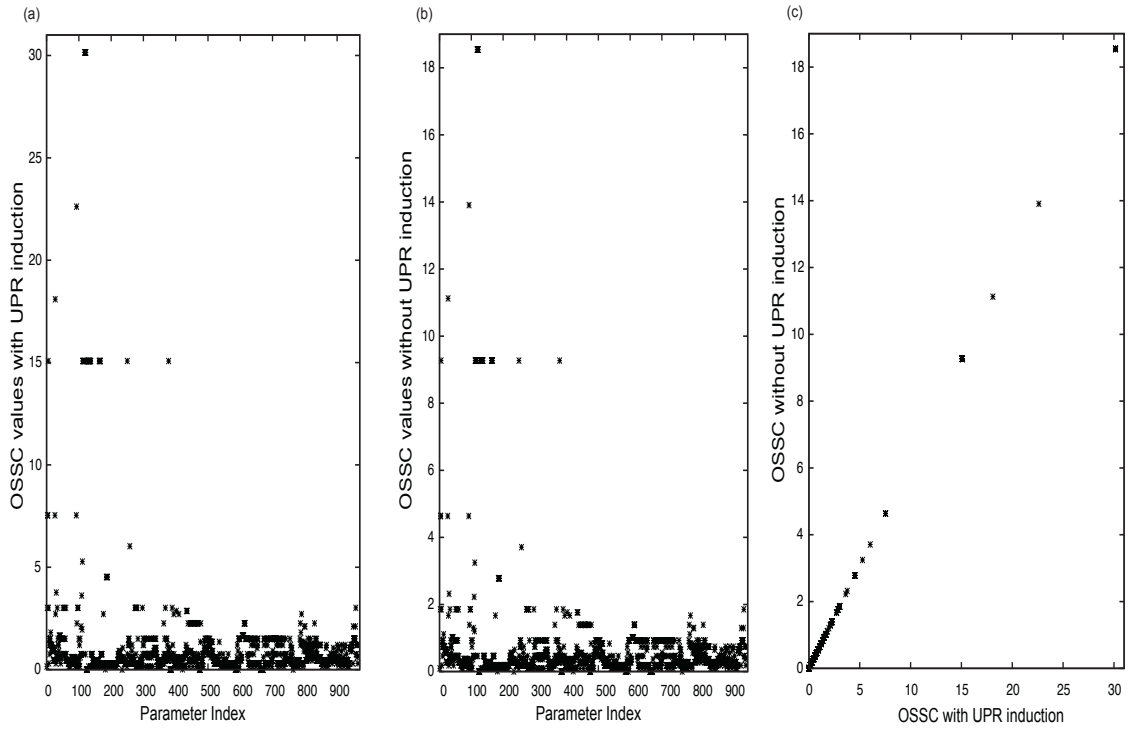

Figure 4.14: Plot of the OSSC for the UPR model. (a) This plot shows the OSSC values with UPR induction. (b) This plot shows the OSSC values with no UPR induction (c) Combined plot of the OSSC values with UPR induction on the X axis and without UPR induction in the Y axis. These plots show the highly fragile components of the model and also show that these components remain fragile in the stressed and the unstressed cell.

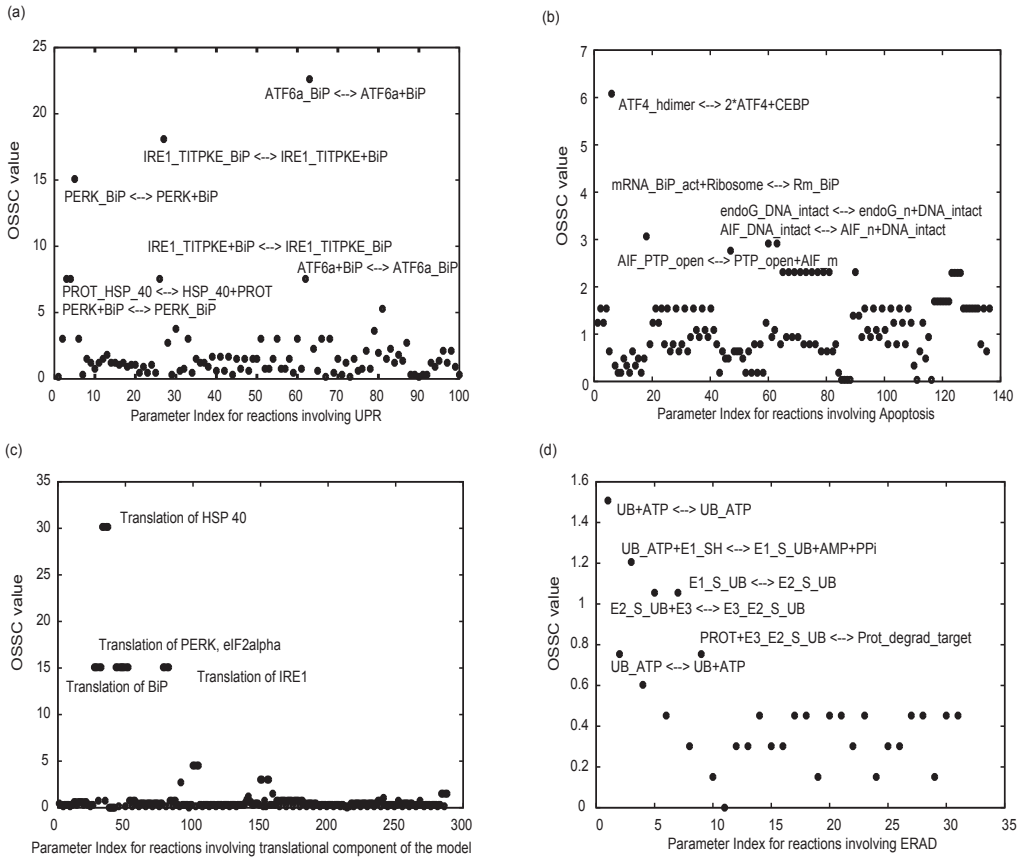

Figure 4.15: Modular plot of the UPR model: (a) Breaking of the ER stress transducers and BiP complex are relatively the most fragile part of the UPR branches. (b) In the apoptosis module, breaking up of the homo-dimer of ATF4 is seen to be the most sensitive reaction. Increase in the amount of BiP being produced is rightly seen as a highly sensitive reaction. (c) In the translation module of the network, the translation of HSP40, which is required to sense the unfolded protein, is of high importance closely followed by PERK, IRE1, eIF2α and BiP translation. (d) In the ERAD component of the model, it is seen that the presence of ATP and the reaction of the same with Ubiquitin is the key step.

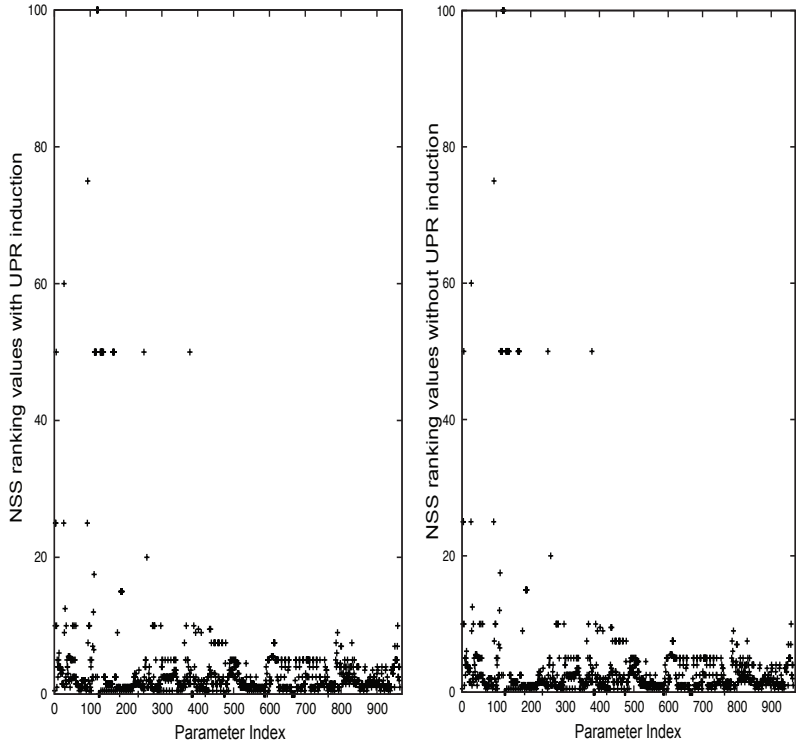

Figure 4.16: Plot of the NSS value ranking for the UPR model. (a) This plot shows the NSS ranking for the parameters with UPR induction. (b) This plot shows the NSS ranking with no UPR induction. These plots show the highly fragile components of the model and also show that these components remain fragile in the stressed and the unstressed cell. Similar results are also seen by using the OSSC scheme of sensitivity analysis.

These ranked parameters are shown in the figure 4.16. The output is consistent with the OSSC results.

It is seen that both the methodologies give the same results, in terms of demarcating the most sensitive parameters. These highly sensitive parameters can

Table 4.1: Highly sensitive reactions as clustered by the k-means algorithm

Rn. ID	Reaction	OSSC with UPR	OSSC without UPR
5	PERK+BiP → PERK_BiP	15.077	9.2714
27	IRE1_TITPKE_BiP → IRE1_TITPKE+BiP	18.092	11.1256
93	[] → ATP	22.615	13.9070
112	[] → mRNA_BiP	15.077	9.2714
113	mRNA_BiP+Ribosome → Rm_BiP	15.077	9.2714
114	Rm_BiP → mRNA_BiP+Ribosome	15.077	9.2714
116	Rm_BiP → Ar_BiP	15.077	9.2714
117	Ar_BiP → BiP+Ribosome	15.077	9.2714
118	[] → mRNA_HSP_40	30.153	18.5427
119	mRNA_HSP_40+Ribosome → Rm_HSP_40	30.153	18.5427
121	Rm_HSP_40 → Ar_HSP_40	30.153	18.5427
122	Ar_HSP_40 → HSP_40+Ribosome	30.153	18.5427
128	[] → mRNA_PERK	15.077	9.2714
129	mRNA_PERK+Ribosome → Rm_PERK	15.077	9.2714
131	Rm_PERK → Ar_PERK	15.077	9.2714
132	Ar_PERK → PERK+Ribosome	15.077	9.2714
133	[] → mRNA_eIF2a	15.077	9.2714
134	mRNA_eIF2a+Ribosome → Rm_eIF2a	15.077	9.2714
136	Rm_eIF2a → Ar_eIF2a	15.077	9.2714
137	Ar_eIF2a → eIF2a+Ribosome	15.077	9.2714
163	[] → mRNA_IRE1_TITPKE	15.077	9.2714
164	mRNA_IRE1_TITPKE+Ribosome → Rm_IRE1_TITPKE	15.077	9.2714
166	Rm_IRE1_TITPKE → Ar_IRE1_TITPKE	15.077	9.2714
167	Ar_IRE1_TITPKE → IRE1_TITPKE+Ribosome	15.077	9.2714
250	[] → Ribosome	15.077	9.2714
378	Bcl2+Bak → Bcl2_Bak	15.077	9.2714

be further clustered using k-means clustering, to find the most sensitive parameters. These highly sensitive reactions are enlisted below in table 4.4.

4.5 Edge Coupling Study

Edge coupling study was done on the network according to the scheme defined in chapter 3.2.2. Most of the proteins in the model, have a translational component built in the model along with a degradation component. The approach is to remove one reaction at a time and see how its effect is felt by the other species in the system. In the current model with 964 reactions, all of these reactions were

removed, one at a time, and the effect on the components was observed. The effect could be either upregulation or downregulation of a species or no effect at all. This gives us a computational equivalent of the knockout studies done in the wet experiments.

We sorted out the most important reactions, by using the most sensitive reactions according to the data of the sensitivity study. The approach used here was to cluster the values using k-means clustering. K-means clustering was done to divide the sensitivity values to 2 clusters. The cluster with the higher mean was picked and the elements of this cluster as tabulated in 4.4, was the subject of study for the coupling studies.

The figure 4.17 denotes the coupling studies of the 26 highly sensitive nodes of the UPR network. The color coding of the graph is binary, where green is upregulated and blue is downregulated. We find that all of these sensitive knockouts, leads to the upregulation of certain species (5 -BiP,11-eIF2α,51-Bim,54-Bcl2,72-ATF6,76-S1P and 78-S2P). Edge removal of reaction 112 (Formation of ATP) and 250 (Formation of the Ribosome) leads to the widespread effect over all the species. Reaction 250 removal leads to overall downregulation of the species. These results are consistent with our current understanding of the system.

Bcl2 is upregulated to counteract the effect of UPR. This is seen in the form of upregulation of species 54, in the coupling studies. If the formation of ATP is hindered, there is a breakdown of the ERAD machinery of UPR. This clearly has a widespread effect over the entire UPR functioning. This is correctly predicted by the coupling studies. It is interesting to note that amongst the entire apoptotic machinery, only the Bcl2 and Bim are points of concern. Further studies on

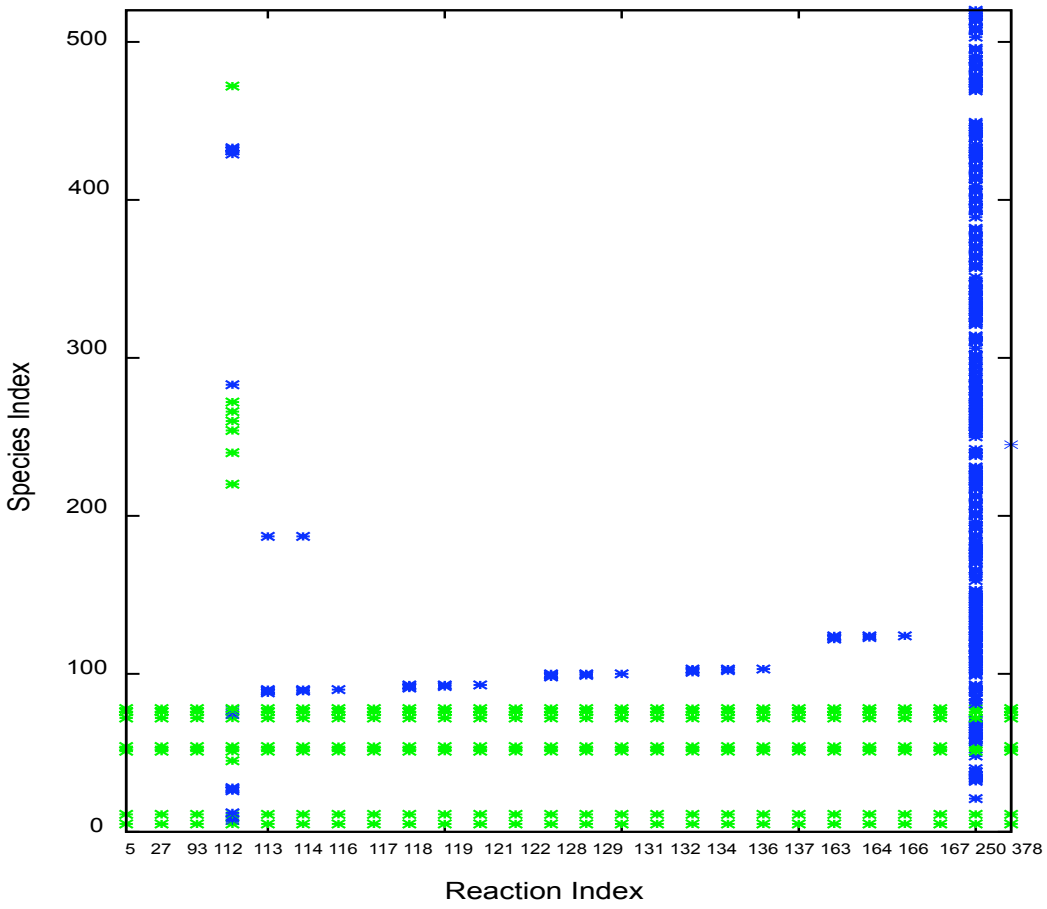

Figure 4.17: This figure shows the results of coupling studies for the 26 highly sensitive reactions as obtained from the sensitivity studies. Blue color denotes downregulation while green indicates upregulation of the species indicated on the y axis. An interesting result here shows that knockout of reaction 250 (production of the ribosome) leads to widespread downregulation of all the species involved in the UPR network.

this model might explain this better.

We have been successful, in modeling the UPR network to some extent. It is providing the right trends of the species as seen in literature. It is encouraging to find that sensitivity studies and coupling studies are providing the anticipated outcomes. It shall be interesting to couple this network with other models, like that of Hypoxia and Inflammatory response of a cell.

CHAPTER 5

SUMMARY AND FUTURE DIRECTIONS

Overall we have developed an ensemble of models that is qualitatively representative of the unfolded protein response. There are 964 reactions and 521 species in the model. Most of the data that was used to formulate the model, were from different cell lines. The canonical ensemble of models, presents us with a family of models that describe qualitatively the process over the diverse data-sets.

However, this model does not include the survival aspects of UPR. There are several anti-apoptotic pathways, including the NF-κB pathway, mTOR pathway and the role of autophagy that is not included in the model. The connection of translation to caspases is also not present in the model.

Two strategies were used to address the diversity of the models. The low diversity or the localized search around the nominal set provided an ensemle of models with 968 parameter sets. This case has an average Cv of 0.3. The high diversity or the wide area search of the parameter space provided an ensemble with 4200 parameters and an average Cv of 1.0. These ensembles are dependent on the optimization scheme. This gives us the opportunity to test the effect of temperature and weighted use of the objective functions in the future work.

Analysis of the models revealed results that were consistent with the literature as well as some new information. Sensitivity analysis revealed the importance of HSP40 in the UPR. Initiation of UPR by dissociation of BiP is relatively important. This gives us motivation to test the other alternative source of activation of UPR. However the current analysis was based on the nominal set. A

deeper analysis could be obtained by looking over the ensemble of models.

Coupling studies puts light on the importance of translation in the model. However in the current model, translation is in a simplified form. We need to incorporate the translation aspects into the model. The key role of ATP dependent steps in the model. This study is done on the nominal set and needs to be done over the entire ensemble.

So at the current state we prioritize our work into two broad areas. Our first task is to include surivival aspects of UPR along with other related pathways. Once we have a functionally complete model, we shall employ this model to study Hypoxia, wherein UPR plays a major role.

5.1 Completing the UPR model: Inclusion of survival aspects

In the step towards having a complete model of UPR, we need to incorporate some major pathways including NF-κB pathway, mTOR pathway and the AKT pathway. Currently in our group we have a functioning model of the AKT and mTOR activation which has been studied in the translation model. We shall begin with incorporating this aspect into the UPR network and build on it, to include the other downstream effects of AKT. Some other key areas that we have identified to include into the model are listed in the following sub sections.

5.1.1 Inflammatory response and UPR

UPR and the inflammatory response are connected through several modalities. UPR marks the increase in Reactive Oxygen Species (ROS), the increase in the

release of Ca^{2+} from the ER, activation of transcription factor nuclear factor - κB (NF-κB) and the mitogen-activated protein kinase, JUN N-terminal kinase (JNK) [233].

Oxidative Stress

Oxidative stress is marked by the accumulation of Reactive oxygen species (ROS). ROS are small molecules that are highly reactive due to the presence of unpaired electrons. Protein folding requires energy and oxygen for the formation of intramolecular and intermolecular disulphide bonds [200]. During disulphide bond formation, protein disulphide isomerase (PDI) and ER oxidoreductin 1 (ERO1) play a key role as seen in figure 5.1. PDI accepts electrons leading to the formation of disulphide bonds. ERO1 is involved in removal of the electrons from the PDI to the molecular oxygen. Use of oxygen as the terminal recipient of electrons lead to the generation of ROS [199]. Increase in load of protein folding leads directly to the increase in ROS.

Cells mediate the accumulation of ROS in the cells using the UPR pathways. The PERK pathway of UPR leads downstream to the phosphorylation of NRF2 (nulcear-factor-erythroid-derived 2 (NF-E2)-related factor 2) [64, 28]. Phosphorylated NRF2 translocates to the nucleus and leads to the transcription of antioxidant and oxidant-detoxifying enzymes like NAD(P)H-quinone oxidoreductase, haem-oxygenase 1 and glutathione S-transferase [115, 231]. It also leads to the increase in transcription of glutathione which aids in maintaining the redox state of the cell [64, 28, 27]. PERK−/− cells lead to the accumulation of ROS in comparison to PERK+/+ cells [64, 27]. ROS mediate inflammation [156].

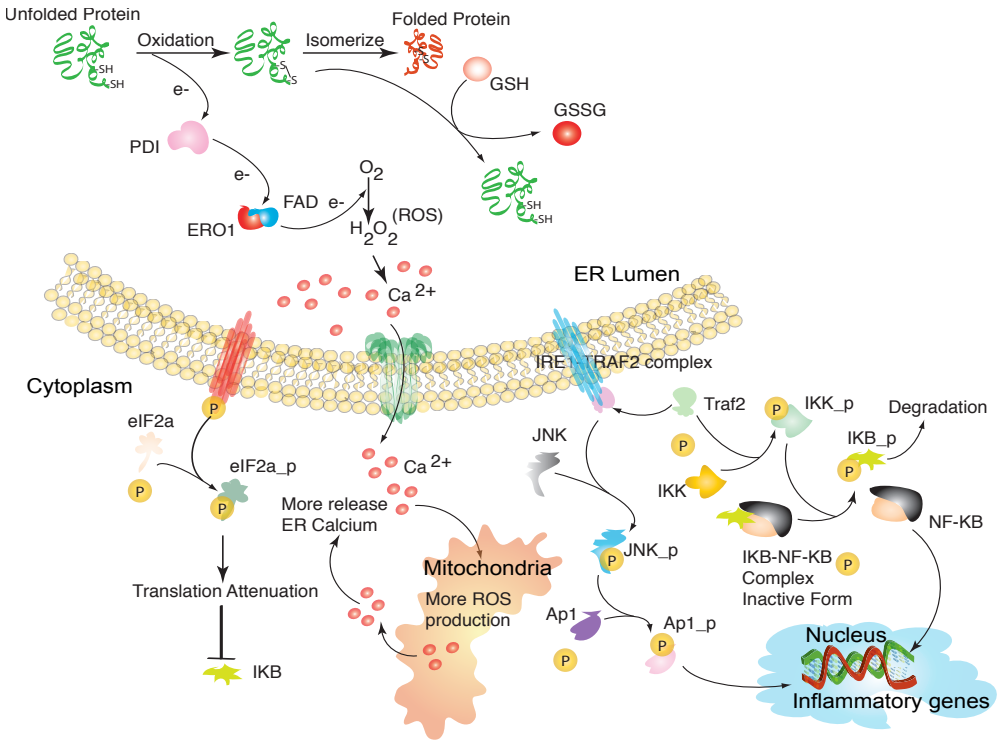

Figure 5.1: UPR and Inflammatory response: Formation of disulphide bonds is a key step in the folding of the protein correctly in the ER. The enzyme PDI accepts electrons from the folding proteins leading to the oxidation of the thiol (SH) groups. This step mediates the formation of the disulphide bonds. ERO1 in association with FAD transfers electrons from the PDI to molecular Oxygen. This results in the formation of the hydrogen peroxide (ROS). Upon UPR induction, PERK downstream leads to translation attenuation which leads to lower concentration of IκB. Simultaneously the IRE1 branch of UPR leads to phosphorylation of IκB which leads to release of NF-κB. Phosphorylated IκB is targeted for degradation and free NF-κB goes to the nuclei where it activates the inflammatory genes. IRE1 also leads to the activation of the JNK pathway which leads to the activation of AP1 which goes to the nuclei to activate the inflammatory genes. The ROS produced during UPR leads to the release of Ca^{2+} from the ER through the ER-based Ca^{2+} channels. This excess of Ca^{2+} in the ER migrates to the mitochondria where it further leads to the production of ROS. This alteration in ER Ca^{2+} homeostasis leads to further ER stress.

NF-κB and PERK crossover

NF-κB plays a central role in inflammation [163]. Normally NF-κB is present in the inactive state stably bound to the inhibitor of NF-κB (IκB). UPR leads to phosphorylation and subsequent degradation of IκB. This allows the activation of NF-κB and subsequent transport to the nucleus and transcription of several inflammatory genes. There is evidence to suggest that release of calcium into the cytosol during UPR might have a role in the activation of NF-κB [35]. There could be a direct role of PERK branch of UPR by attenuating translation of inhibitors of NF-κB [34].

Role of IRE1α and NF-κB and JNK

The IRE1α-TRAF2 complex leads to the phosphorylation of IκB and thereby the nuclear translocation of NF-κB [75] as seen in figure 5.1. The IRE1α-TRAF2 complex also leads to the activation of protein kinase JNK. Activated JNK leads to the phosphorylation of transcription factor activator protein 1 (AP1) which leads to the expression of inflammatory genes [30]. The exact machinery involved in the inflammatory response is yet not well understood.

All of this information is from a varied set of experiments that have been over a diverse set of cell lines. Our next step is to conduct laboratory experiments to test the validity of the interactions in the mammalian cancer cell lines like HL-60 or LNCaP.

5.2 Study the role of UPR in Hypoxia

Once we have a functioning model of UPR with the survival aspects incorporated in it, we shall study the role of UPR in Hypoxia. ER not only acts as the center for maturation of proteins, but also a center for oxygen sensing and signaling. This enables a critical role of the ER in Hypoxic cell conditions. Deprivation of O_2 has recently been shown to be an initiator of UPR.

It has been seen that Hypoxia leads to PERK activation and downstream phosphorylation of eIF2α [91]. This effect is seen to occur in time scale of minutes, in case of anoxic conditions. Under moderate hypoxia conditions i.e. (1%) O_2, we see that this response is a bit slower [90]. It is interesting to note that eIF2α shows a transient response [90, 91, 112]. The importance of PERK pathway was demonstrated in PERK−/− MEF's. PERK knockout mice show increased occurrence of apoptosis in contrast to their wild-type counterparts [91, 10].

Hypoxia is associated with growing tumors. This gives the idea that in case of tumors we see glucose deprivation, amino acid deprivation and oxidative stress along with oxygen shortage which lead to ER stress and UPR [232]. It has also been noted that XBP1 splicing takes place, which gives reason to believe that IRE1 branch of UPR is activated as well [164]. These evidence do not provide a mechanism connecting UPR and Hypoxia, but does provide evidence of initiation and importance of UPR in apoptosis. This presents an unique opportunity to investigate the critical role of UPR in a tumor cell. It is also noted that UPR and mTOR play a critical role in controlling the UPR signal in case of tumors and cancer cells.

Our hypothesis is that UPR and translation plays a key role in the Hypoxic cell. We shall test this hypothesis in a bone derived cell line. We plan to investigate the activation of mTOR and AKT activation unpon induction of Hypoxia. To test the importance of translation, we shall test the phosphorylation status of 4E-BP1 and eIF4E. We shall test the link of translation to a hypoxic cell. For testing we shall conduct transcription factor arrays to track gene expression shifts. The changes in mRNA shall be validated by qRT-PCR. Alterations in protein concentrations shall be tested by western blot studies.

Besides Hypoxia, UPR is seen to be relevant in many other diseases. Some of the key relations are discussed in the following sections.

5.3 Relevance of UPR in other diseases

ER stress plays a key role in diseases ranging from neurodegenration, cardiac diseases, cancer, diabetes, hypoxia to muscle degeneration. Some of the key diseases having a role of ER stress is demarcated in 5.2. Proper understanding of the mechanisms involved in the above mentioned diseases presents an unique opportunity for targets of potential drug discovery 5.3. We shall take a deeper look at some of these disorders and see the currently understood role of UPR and UPR-mediated apoptosis in these diseases.

5.3.1 Cardiac ailments

Recently diseases like myocardial ischaemia, cardiac hypertrophy, atherosclerosis and heart failure have are shown to have a defining role of UPR [52]. ER

Table 5.1: ER stress-related diseases

Disease	Relevance of ER Stress	Protein of interest
Alzheimer's disease (AD)	AD-induced Presenilin 1 induces ER stress with suppressed protective UPR signaling	Presenilin, PERK-eIF2α [202, 83, 189, 122, 135]
Parkinson's disease (PD)	Suppressed ER-stress-induced apoptosis, parkin expression controlled by ER stress	Parkin, α-synuclein [31, 187, 76, 151, 166]
Amyotrophic lateral sclerosis	Interference of ERAD machinery, activation of ASK1	SOD, ASK1 [133]
Stroke	ER stress induction in neurons activating UPR and apoptosis associated with CHOP induction and ASK1 activation	PERK-eIF2α , ASK1 [188, 217, 206, 216, 95, 150, 186]
Bipolar Disorder	Medications induce UPR	XBP1 polymorphisms [81, 21, 80]
Heart Disease	UPR leads to degeneration of cardiac myocytes, transaortic constriction and myocardial infarction induces UPR	ASK1 [53, 138, 193, 180, 145, 207]

Table 5.2: ER stress-related diseases

Disease	Relevance of ER Stress	Protein of interest
Atherosclerosis	ER stress induced in vascular cells	IRE1 pathway [50, 107, 230, 100, 61, 100]
Type 1 diabetes	Impaired PERK pathway leads to type 1 diabetes	PERK-eIF2α [168, 3, 45, 218, 77, 143, 142]
Type 2 diabetes	Obesity leads to ER stress leading to Insulin resistance	XBP1 and JNK [144]
Cancer	Protective branches of UPR are upregulated	GRP78, XBP1, PERK [181, 48, 79, 164, 11]
Autoimmune disease	UPR leads to autoantigen production	GRP78, HLA-B27 [197, 13, 24]

stress in cardiac hypertrophy models have shown consistent occurance [138]. Expression of XBP1, GRP78 and PDI is shown consistently in these models [**?**]. It has been argued that induction of GRP78 leads to the preconditioning of the heart which provides subsequent protection from further challenges [180, 207]. It has been shown that ASK1 activity increases in mice after aortic constriction and during myocardial infarction [219]. So the ASK1 has a significant role in the myocardiocyte cell death [116].

PUMA [131] gene studies, which also leads to pro-apoptotic signaling shows significant roles in cardioprotection [198]. An interesting thing to note here is the

role of p53 as it is shown to induce the activity of PUMA involving a key role of p73 which is a related transcription factor (ramadan,terrinoni,melino).

ATF6α has been shown to be cardioprotective [114]. The cells that have high expression of ATF6α have better functional recovery and also less apoptotic and necrotic death [114]. ER stress is initiated in vascular cells due to Hypercholesterolaemia and elevated triglycerides. This leads to cytokines production downstream as shown in the endothelial cells [50]. CHOP plays a vital role in expression of cytokines, thus showing a significant role of atherosclerosis [107]. Vascular endothelial cells lead to induction of ER stress due to high-protein diets which create a by-product called Homocysteine [230]. XBP1 has been shown to regulate lipogenesis and leads to activation of ER stress and dyslipidaemias [100]. Overall ER stress has significant role to play in atherosclerosis.

5.3.2 Diabetes

In type I diabetes, the pancreatic β cells secrete large amounts of insulin and glycoproteins. It has been shown that PERK deficient mice are more prone to diabetes and progressive hyperglycemia [61]. Pancreatic β cells have shown that the NO-induced apoptosis is CHOP dependent [143].

Type II diabetes is caused due to insulin resistance. PERK phosphorylation, EIF2α phosphorylation and upregulation of GRP78 have been noted in high-fat diet studies of mice liver and adipose tissue. JNK activation, which occurs downstream of the ER stress pathway plays a major role in insulin resistance. The course which we might choose to target is to reduce the JNK activation. We could also try to increase the chemical chaperones in the cytoplasm to increase

the sensitivity to insulin [144].

5.3.3 Cancer

ER stress and role of UPR and UPR-mediated apoptosis seem to be gaining grounds in being important in tumors and cancer. GRP78 and XBP1 are seen to be overexpressed in tumors in vivo and in hypoxic cancer cells [181, 48]. Generally in hypoxic regions of tumor cells and cancerous cells, UPR functions as a protective mechanism. Less tumorigenic activity has been noted in GRP78-deficient fibrosarcoma cells and XBP1-deficient and PERK-deficient mouse fibroblasts [79, 164, 11].

PERK and IRE1 thus present themselves as ideal targets in cancer therapy. Versipelostatin, a compound that controls the rise of GRP78 protein has been shown to produce antitumor activity in tumor xenograft models [148]. Interleukin 24 (IL24), a cytokine that binds with GRP78 is another possible target for antitumor activity [36]. Another aspect of UPR, proteasome inhibition plays a key role in tumor-related apoptosis. Antitumor acivity has been seen in pancreatic cancers in the preclinical studies of bortezomib (Velcade; Millennium/Janssen-Cilag) [129, **?**]. Nelfavir (Viracept; Pfizer) and atazanavir (Reyataz; Bristol-Myers Squibb) have been shown to induce UPR markers like GRP78 and CHOP in malignant gliomas. This leads to the triggering of apoptosis [155]. HIV protease inhibitors lead to inhibition of the proteasome leading to ER stress. p-53 independant apoptosis is seen to be induced by the induction of GRP78, CHOP due to the action of Brefeldin A [18].

5.3.4 Immune disorders

Plasma cells rely heavily on the role of UPR which is seen in XBP1 defficient mice which alters their homeostasis [162]. Bortezomib plays a key role here as it leads to depletion of the plasma cells by inducing ER stress. XBP1 deficiency leads to drastic reductions in the amount of dendritic cell numbers in mice [78]. Unfolded protein accumulation and UPR-induction has been noted in autoimmune diseases like rheumatoid arthritis, imflammatory bowel diseases and multiple sclerosis. UPR has a key role to play in autoimmunity.

It has been shown that B-cells and other cells of the immune system rely on an intact UPR [197]. CREBH, an ER-membrane bound transcription factor is structurally similar to ATF6 [141]. Upon ER stress CREBH transmigrates to the Golgi and undergoes cleavage by S1 and S2 proteases. This cleavage releases an N-terminal fragment that migrates to the nucleus [234]. It is seen that upon knockdown of the CREBH in hepatocytes, there is reduction in the mRNA encoding C-reactive protein and serum amyloid P-component. Both of these proteins are associated with innate immune response [234]. It is also seen that UPR and CREBH are induced by pro-inflammatory cytokines like IL-6 and IL-1β [234].

UPR and autoimmunity may work together using the following schemes:

- Recognition of misfolded proteins by autoreactive immune cells.
- Release of neo-autoanitgens and UPR related autoantigens by cells under ER stress.
- Cells under UPR lead to perturbation of immune-tolerance mechanisms leading to further autoimmunity.

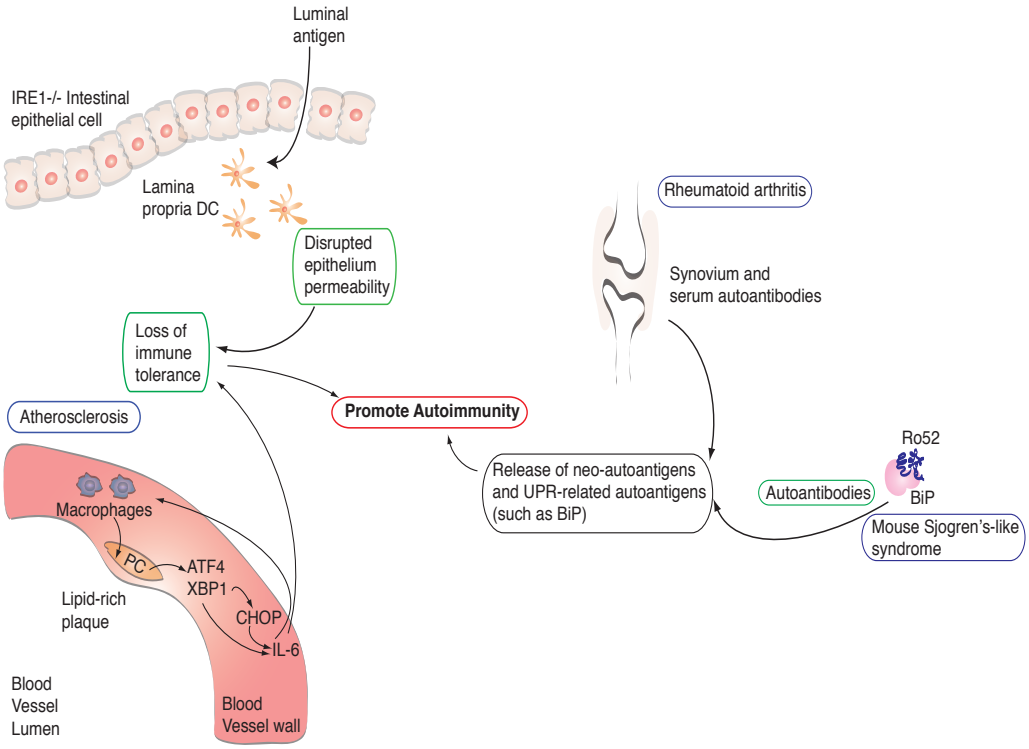

Figure 5.2: UPR and its role in autoimmunity: BiP specific antibodies have been seen in patients with rheumatoid arthritis and mouse model of Sjogren's syndrome. This suggests that UPR-specific genes may act as autoantigens. UPR in the epithelium leads to development of Colitis, atherosclerosis. These variable roles of UPR can promote autoimmunity.

- Developing resistance to UPR-mediated apoptosis and leading to enhanced ERAD.

Humans and rodents with autoimmune diseases have been shown to elicit autoreactive B- and T-cell response due to HSP's and BiP. It was seen that patients with rheumatoid arthritis have 80% more antibodies for BiP than patients with other rheumatic conditions [13]. Stress proteins act as an immune adjuvant and elicit immune response [12].

Pathogenesis of atherosclerosis involves inflammatory pathways with a critical role of UPR [59]. Elevation of IL-6 can be attributed to activation of p38 MAPK and is CHOP dependent [107]. In inflammatory atherosclerosis lesions, oxidized phosphorylcholine induces the ATF4 and XBP1 UPR pathways along with IL-6 by aortic endothelial cells [50].

The vast links of UPR with several diseases provide us with unique opportunities to extend the study of the model. We shall aim to formulate the individual models of these diseases and prioritize experiments targeted to these systems. We hope to be able to identify targets for drug discovery for these systems, using sensitivity and coupling studies. The scale of these models also provide us opportunity to create new tools to aid in the analysis of these models.

Table 5.3: ER stress and drug discovery

Compound	Pathway targeted	Role
Valporate, lithium	ER chaperone inducers	Used as mood stabilizers to induce ER chaperones in case of Neuroprotection [15, 70, 172]
BIX	ER Chaperone Inducers	Used as a small-molecule inducer of GRP78 in case of Celebral ischemia, stroke [94]
Salubrinal	PERK-eIF2α pathway	Used as an agonist of PERK-eIF2α pathway in case of Parkinson's disease and stroke [168, 16, 161, 95, 61, 3]
p38 MAPK antagonists	p38 MAPK (CHOP activity)	Used to prevent p38 dependent CHOP phosphorylation in case of stroke, diabetes [225, 210, 122, 150, 186]
Versipelostatin	GRP78	Used in case of Cancer [148]
Bortezomib, nelfavir, atazanavir	Proteasome	Used to kill auto-antibody-producing plasma cells and multiple myeloma cells in case of cancer and autoimmune disorders [99, 155, 51, 130]
Brefeldin A, breflate	ADP-ribosylation factor	Used in case of leukaemia [152, 18]

APPENDIX A

TABLE OF THE REACTIONS IN THE MODEL

In the following table, we have provided all the reactions that have been modeled with the corresponding rate constants for the nominal set. This nominal set was obtained by hand-fitting the model to the experimental observations made in the literature.

Table A.1: Reactions in UPR with their corresponding reaction rates

Reaction	K_f	K_b	K_{cat}
[] ⇋ PROT	–	–	0.1
HSP_40+PROT ⇋ PROT_HSP_40	2.0	5.0	–
PERK+BiP ⇋ PERK_BiP	5.0	10.0	–
PERK_BiP+PROT_HSP_40+ATP ⇋ BiP_ATP_PROT_HSP_40+PERK_f	2.0	0.2	–
2*PERK_f ⇋ PERK_d	1.0	0.8	–
eIF2a+PERK_d ⇋ eIF2a_comp	0.5	0.8	–
eIF2a_comp ⇋ eIF2a_p+PERK_d	1.0	1.2	–
eIF2a_p ⇋ ATF4_prod	–	–	0.8
ATF4_prod ⇋ ATF4+eIF2a_p	–	–	0.8
ATF4+ATF3 ⇋ ATF3_act_ATF4	–	–	0.7
ATF3_act_ATF4 ⇋ ATF3_act+ATF4	–	–	0.8
ATF3_act ⇋ GADD34_complex	–	–	0.6
GADD34_complex ⇋ GADD34+ATF3_act	–	–	0.7
GADD34+PP1a ⇋ GADD34_PP1a	0.7	0.3	–
GADD34_PP1a+eIF2a_p ⇋ GADD34_PP1a_eIF2a_p	0.6	0.3	–
GADD34_PP1a_eIF2a_p ⇋ eIF2a+GADD34_PP1a	0.7	0.3	–
IRE1_TITPKE+BiP ⇋ IRE1_TITPKE_BiP	5.0	12.0	–
IRE1_TITPKE_BiP+PROT_HSP_40+ATP ⇋ BiP_ATP_PROT_HSP_40+IRE1_TITPKE_f	1.8	0.2	–
2*IRE1_TITPKE_f ⇋ IRE1_dimer	2.5	0.4	–
IRE1_dimer ⇋ IRE1_act	0.5	2.0	–
IRE1_dimer+Bak ⇋ IRE1_act	0.3	1.0	–
mRNA_XBP1+IRE1_act ⇋ mRNA_XBP1_spliced_complex	–	–	0.8
mRNA_XBP1_spliced_complex ⇋ mRNA_XBP1_spliced+IRE1_act	–	–	0.8
XBP1+NFY ⇋ XBP1_NFY	0.6	1.1	–
XBP1_NFY+UPRE ⇋ XBP1_NFY_UPRE	0.4	1.1	–
XBP1_NFY+ERSE ⇋ XBP1_NFY_ERSE	0.4	1.1	–
IRE1_act+TRAF2 ⇋ IRE1_act_TRAF2	0.2	1.0	–
IRE1_act_TRAF2+ASK1 ⇋ IRE1_act_TRAF2_ASK1	0.5	1.0	–

continued on next page

continued from previous page

Reaction	K_f	K_b	K_{cat}
IRE1_act_TRAF2_ASK1 ⇋ IRE1_act_TRAF2+ASK1_act	0.4	1.0	–
JNK+ASK1_act ⇋ JNK_ASK1_act	1.0	2.0	–
JNK_ASK1_act ⇋ JNK_act+ASK1_act	0.5	0.5	–
p38MAPK+ASK1_act ⇋ p38MAPK_ASK1_act	1.0	2.0	–
p38MAPK_ASK1_act ⇋ p38MAPK_act+ASK1_act	0.5	0.5	–
Bim+JNK_act ⇋ Bim_JNK_act	1.0	0.3	–
Bim_JNK_act ⇋ JNK_act+Bim_p	–	–	2.0
JNK_act+Bcl2 ⇋ JNK_Bcl2	–	–	0.5
ERSE ⇋ []	–	–	0.3
TRAF2 ⇋ []	–	–	0.3
JNK ⇋ []	–	–	0.3
ASK1 ⇋ []	–	–	0.3
p38MAPK ⇋ []	–	–	0.3
[] ⇋ mRNA_ERSE	–	–	0.2
mRNA_ERSE+Ribosome ⇋ Rm_ERSE	0.2	0.1	–
Rm_ERSE ⇋ Ar_ERSE	–	–	0.2
Ar_ERSE ⇋ ERSE+Ribosome	–	–	0.2
[] ⇋ mRNA_TRAF2	–	–	0.2
mRNA_TRAF2+Ribosome ⇋ Rm_TRAF2	0.2	0.1	–
Rm_TRAF2 ⇋ Ar_TRAF2	–	–	0.2
Ar_TRAF2 ⇋ TRAF2+Ribosome	–	–	0.2
[] ⇋ mRNA_JNK	–	–	0.4
mRNA_JNK+Ribosome ⇋ Rm_JNK	0.4	0.2	–
Rm_JNK ⇋ Ar_JNK	–	–	0.4
Ar_JNK ⇋ JNK+Ribosome	–	–	0.4
[] ⇋ mRNA_ASK1	–	–	0.4
mRNA_ASK1+Ribosome ⇋ Rm_ASK1	0.4	0.2	–
Rm_ASK1 ⇋ Ar_ASK1	–	–	0.4
Ar_ASK1 ⇋ ASK1+Ribosome	–	–	0.4

continued on next page

continued from previous page

Reaction	K_f	K_b	K_{cat}
[] ⇋ mRNA_p38MAPK	–	–	0.2
mRNA_p38MAPK+Ribosome ⇋ Rm_p38MAPK	0.2	0.1	–
Rm_p38MAPK ⇋ Ar_p38MAPK	–	–	0.2
Ar_p38MAPK ⇋ p38MAPK+Ribosome	–	–	0.2
ATF6a+BiP ⇋ ATF6a_BiP	5.0	15.0	–
ATF6a_BiP+PROT_HSP_40+ATP ⇋ BiP_ATP_PROT_HSP_40+ATF6a_f	1.5	0.4	–
ATF6a_f ⇋ ATF6a_g	2.0	0.1	–
ATF6a_g+S1P ⇋ ATF6a_S1P	2.0	0.3	–
ATF6a_S1P+S2P ⇋ ATF6_CNTP	1.0	0.2	–
ATF6_CNTP ⇋ ATF6_c_n	0.8	0.1	–
ATF6_c_n+ATF ⇋ ATF6_ATF	1.0	0.4	–
ATF6_ATF+NFY ⇋ ATF6_ATF_NFY	0.5	1.4	–
ATF6_ATF_NFY+ERSE1 ⇋ ATF6_ATF_NFY_ERSE1	0.5	2.4	–
ATF6_ATF+ERSE2 ⇋ ATF6_ATF_ERSE2	1.3	3.5	–
[] ⇋ ATP	–	–	10.0
[] ⇋ mRNA_BiP	–	–	10.0
mRNA_BiP+Ribosome ⇋ Rm_BiP	10.0	0.5	–
Rm_BiP ⇋ Ar_BiP	–	–	10.0
Ar_BiP ⇋ BiP+Ribosome	–	–	10.0
[] ⇋ mRNA_HSP_40	–	–	20.0
mRNA_HSP_40+Ribosome ⇋ Rm_HSP_40	20.0	0.5	–
Rm_HSP_40 ⇋ Ar_HSP_40	–	–	20.0
Ar_HSP_40 ⇋ HSP_40+Ribosome	–	–	20.0
[] ⇋ mRNA_NEF	–	–	0.0
mRNA_NEF+Ribosome ⇋ Rm_NEF	0.0	0.0	–
Rm_NEF ⇋ Ar_NEF	–	–	0.0
Ar_NEF ⇋ NEF+Ribosome	–	–	0.0
[] ⇋ mRNA_PERK	–	–	10.0
mRNA_PERK+Ribosome ⇋ Rm_PERK	10.0	0.1	–

continued on next page

continued from previous page

Reaction	K_f	K_b	K_{cat}
Rm_PERK ⇋ Ar_PERK	–	–	10.0
Ar_PERK ⇋ PERK+Ribosome	–	–	10.0
[] ⇋ mRNA_eIF2a	–	–	10.0
mRNA_eIF2a+Ribosome ⇋ Rm_eIF2a	10.0	0.1	–
Rm_eIF2a ⇋ Ar_eIF2a	–	–	10.0
Ar_eIF2a ⇋ eIF2a+Ribosome	–	–	10.0
[] ⇋ mRNA_ATF3	–	–	0.5
mRNA_ATF3+Ribosome ⇋ Rm_ATF3	0.5	0.1	–
Rm_ATF3 ⇋ Ar_ATF3	–	–	0.5
Ar_ATF3 ⇋ ATF3+Ribosome	–	–	0.5
[] ⇋ mRNA_PP1a	–	–	0.3
mRNA_PP1a+Ribosome ⇋ Rm_PP1a	0.3	0.1	–
Rm_PP1a ⇋ Ar_PP1a	–	–	0.3
Ar_PP1a ⇋ PP1a+Ribosome	–	–	0.3
[] ⇋ mRNA_Nrf2	–	–	0.3
mRNA_Nrf2+Ribosome ⇋ Rm_Nrf2	0.3	0.1	–
Rm_Nrf2 ⇋ Ar_Nrf2	–	–	0.3
Ar_Nrf2 ⇋ Nrf2+Ribosome	–	–	0.3
[] ⇋ mRNA_Keap1	–	–	0.3
mRNA_Keap1+Ribosome ⇋ Rm_Keap1	0.3	0.1	–
Rm_Keap1 ⇋ Ar_Keap1	–	–	0.3
Ar_Keap1 ⇋ Keap1+Ribosome	–	–	0.3
[] ⇋ mRNA_P2CE	–	–	0.3
mRNA_P2CE+Ribosome ⇋ Rm_P2CE	0.3	0.1	–
Rm_P2CE ⇋ Ar_P2CE	–	–	0.3
Ar_P2CE ⇋ P2CE+Ribosome	–	–	0.3
[] ⇋ mRNA_IRE1_TITPKE	–	–	10.0
mRNA_IRE1_TITPKE+Ribosome ⇋ Rm_IRE1_TITPKE	10.0	0.1	–
Rm_IRE1_TITPKE ⇋ Ar_IRE1_TITPKE	–	–	10.0

continued on next page

continued from previous page

Reaction	K_f	K_b	K_{cat}
Ar_IRE1_TITPKE ⇋ IRE1_TITPKE+Ribosome	–	–	10.0
[] ⇋ mRNA_Bak	–	–	0.5
mRNA_Bak+Ribosome ⇋ Rm_Bak	0.5	0.1	–
Rm_Bak ⇋ Ar_Bak	–	–	0.5
Ar_Bak ⇋ Bak+Ribosome	–	–	0.5
[] ⇋ mRNA_XBP1	–	–	0.2
mRNA_XBP1+Ribosome ⇋ Rm_XBP1	0.2	0.1	–
mRNA_XBP1_spliced+Ribosome ⇋ Rm_XBP1	1.8	0.2	–
Rm_XBP1 ⇋ Ar_XBP1	–	–	0.2
Ar_XBP1 ⇋ XBP1+Ribosome	–	–	0.2
[] ⇋ mRNA_UPRE	–	–	0.2
mRNA_UPRE+Ribosome ⇋ Rm_UPRE	0.2	0.01	–
Rm_UPRE ⇋ Ar_UPRE	–	–	0.2
Ar_UPRE ⇋ UPRE+Ribosome	–	–	0.2
[] ⇋ mRNA_ATF6a	–	–	3.0
mRNA_ATF6a+Ribosome ⇋ Rm_ATF6a	3.0	0.1	–
Rm_ATF6a ⇋ Ar_ATF6a	–	–	3.0
Ar_ATF6a ⇋ ATF6a+Ribosome	–	–	3.0
[] ⇋ mRNA_S1P	–	–	0.2
mRNA_S1P+Ribosome ⇋ Rm_S1P	0.2	0.1	–
Rm_S1P ⇋ Ar_S1P	–	–	0.2
Ar_S1P ⇋ S1P+Ribosome	–	–	0.2
[] ⇋ mRNA_S2P	–	–	0.2
mRNA_S2P+Ribosome ⇋ Rm_S2P	0.2	0.1	–
Rm_S2P ⇋ Ar_S2P	–	–	0.2
Ar_S2P ⇋ S2P+Ribosome	–	–	0.2
[] ⇋ mRNA_ATF	–	–	0.2
mRNA_ATF+Ribosome ⇋ Rm_ATF	0.2	0.1	–
Rm_ATF ⇋ Ar_ATF	–	–	0.2

continued on next page

continued from previous page

Reaction	K_f	K_b	K_{cat}
Ar_ATF ⇋ ATF+Ribosome	–	–	0.2
[] ⇋ mRNA_NFY	–	–	0.2
mRNA_NFY+Ribosome ⇋ Rm_NFY	0.2	0.1	–
Rm_NFY ⇋ Ar_NFY	–	–	0.2
Ar_NFY ⇋ NFY+Ribosome	–	–	0.2
[] ⇋ mRNA_ERSE1	–	–	0.2
mRNA_ERSE1+Ribosome ⇋ Rm_ERSE1	0.2	0.1	–
Rm_ERSE1 ⇋ Ar_ERSE1	–	–	0.2
Ar_ERSE1 ⇋ ERSE1+Ribosome	–	–	0.2
[] ⇋ mRNA_ERSE2	–	–	0.2
mRNA_ERSE2+Ribosome ⇋ Rm_ERSE2	0.2	0.1	–
Rm_ERSE2 ⇋ Ar_ERSE2	–	–	0.2
Ar_ERSE2 ⇋ ERSE2+Ribosome	–	–	0.2
ATP ⇋ []	–	–	0.3
BiP ⇋ []	–	–	0.5
HSP_40 ⇋ []	–	–	0.3
NEF ⇋ []	–	–	0.3
PERK ⇋ []	–	–	0.6
eIF2a ⇋ []	–	–	0.5
ATF4 ⇋ []	–	–	0.5
ATF3 ⇋ []	–	–	0.3
GADD34 ⇋ []	–	–	0.6
PP1a ⇋ []	–	–	0.3
Nrf2 ⇋ []	–	–	0.3
Keap1 ⇋ []	–	–	0.3
P2CE ⇋ []	–	–	0.3
IRE1_TITPKE ⇋ []	–	–	0.4
Bax ⇋ []	–	–	0.0
Bak ⇋ []	–	–	0.3

continued on next page

continued from previous page

Reaction	K_f	K_b	K_{cat}
XBP1 ⇋ []	–	–	0.7
UPRE ⇋ []	–	–	0.3
SAGA ⇋ []	–	–	0.3
KAR2 ⇋ []	–	–	0.3
PDII ⇋ []	–	–	0.3
ATF6a ⇋ []	–	–	0.4
S1P ⇋ []	–	–	0.2
S2P ⇋ []	–	–	0.2
ATF ⇋ []	–	–	0.2
NFY ⇋ []	–	–	0.2
ERSE1 ⇋ []	–	–	0.3
ERSE2 ⇋ []	–	–	0.3
Dol ⇋ []	–	–	0.2
PROT ⇋ []	–	–	0.1
[] ⇋ Ribosome	–	–	10.0
eIF2a_p ⇋ []	–	–	0.5
ATF3_act ⇋ []	–	–	0.2
IRE1_act_TRAF2+CASP12 ⇋ IRE1_act_TRAF2_CASP12	0.8	1.0	–
IRE1_act_TRAF2_CASP12 ⇋ CASP12_act+IRE1_act_TRAF2	0.8	1.0	–
2*ATF4+CEBP ⇋ ATF4_hdimer	0.4	4.0	–
[] ⇋ mRNA_CEBP	–	–	0.2
mRNA_CEBP+Ribosome ⇋ Rm_CEBP	–	–	0.2
Rm_CEBP ⇋ Ar_CEBP	–	–	0.2
Ar_CEBP ⇋ CEBP+Ribosome	–	–	0.2
CEBP ⇋ []	–	–	0.4
ATF4_hdimer+mRNA_GADD153 ⇋ mRNA_GADD153_act_comp	–	–	0.6
mRNA_GADD153_act_comp ⇋ mRNA_GADD153_act+ATF4_hdimer	–	–	0.8
GADD153+CREB ⇋ GADD153_CREB	–	–	0.4
mRNA_Bcl2+GADD153_CREB ⇋ mRNA_Bcl2_weak	0.4	0.2	–

continued on next page

continued from previous page

Reaction	K_f	K_b	K_{cat}
[] ⇋ mRNA_CREB	–	–	0.2
mRNA_CREB+Ribosome ⇋ Rm_CREB	–	–	0.3
Rm_CREB ⇋ Ar_CREB	–	–	0.3
Ar_CREB ⇋ CREB+Ribosome	–	–	0.3
CREB ⇋ []	–	–	0.2
[] ⇋ mRNA_Bcl2	–	–	2.0
mRNA_Bcl2+Ribosome ⇋ Rm_Bcl2	2.0	0.1	–
mRNA_Bcl2_weak+Ribosome ⇋ Rm_Bcl2	0.5	0.1	–
Rm_Bcl2 ⇋ Ar_Bcl2	–	–	2.0
Ar_Bcl2 ⇋ Bcl2+Ribosome	–	–	2.0
[] ⇋ mRNA_GADD153	–	–	0.2
mRNA_GADD153+Ribosome ⇋ Rm_GADD153	–	–	0.2
mRNA_GADD153_act+Ribosome ⇋ Rm_GADD153	–	–	1.0
Rm_GADD153 ⇋ Ar_GADD153	–	–	0.2
Ar_GADD153 ⇋ GADD153+Ribosome	–	–	0.2
ASK1_act+Bcl2 ⇋ ASK_comp	0.2	0.1	–
ASK_comp ⇋ ASK1_act	–	–	0.1
JNK_act+Bcl2 ⇋ JNK_comp	0.3	0.2	–
JNK_comp ⇋ JNK_act	–	–	0.1
XBP1_NFY_ERSE+bZIP ⇋ XBP1_NFY_ERSE_comp	0.4	0.2	–
XBP1_NFY_ERSE_comp ⇋ XBP1_NFY_ERSE+bZIP_act	0.3	0.1	–
bZIP_act+mRNA_BiP ⇋ mRNA_BiP_act	–	–	0.3
mRNA_BiP_act+Ribosome ⇋ Rm_BiP	2.0	0.5	–
CASP12_act+ProCASP9 ⇋ ProCASP9_casp12_comp	0.8	1.0	–
ProCASP9_casp12_comp ⇋ CASP9+CASP12_act	0.8	1.0	–
[] ⇋ mRNA_ProCASP8	–	–	0.5
mRNA_ProCASP8+Ribosome ⇋ Rm_ProCASP8	0.5	0.1	–
Rm_ProCASP8 ⇋ Ar_ProCASP8	–	–	0.5
Ar_ProCASP8 ⇋ ProCASP8+Ribosome	–	–	0.5

continued on next page

continued from previous page

Reaction	K_f	K_b	K_{cat}
CASP8+ProCASP3 ⇋ CASP8_ProCASP3	0.5	1.0	–
CASP8_ProCASP3 ⇋ CASP8+CASP3	–	–	0.4
[] ⇋ mRNA_ProCASP3	–	–	0.5
mRNA_ProCASP3+Ribosome ⇋ Rm_ProCASP3	0.5	0.1	–
Rm_ProCASP3 ⇋ Ar_ProCASP3	–	–	0.5
Ar_ProCASP3 ⇋ ProCASP3+Ribosome	–	–	0.5
CASP8+ProCASP6 ⇋ CASP8_ProCASP6	0.5	1.0	–
CASP8_ProCASP6 ⇋ CASP8+CASP6	–	–	0.4
[] ⇋ mRNA_ProCASP6	–	–	0.5
mRNA_ProCASP6+Ribosome ⇋ Rm_ProCASP6	0.5	0.1	–
Rm_ProCASP6 ⇋ Ar_ProCASP6	–	–	0.5
Ar_ProCASP6 ⇋ ProCASP6+Ribosome	–	–	0.5
CASP8+ProCASP7 ⇋ CASP8_ProCASP7	0.5	1.0	–
CASP8_ProCASP7 ⇋ CASP8+CASP7	–	–	0.4
[] ⇋ mRNA_ProCASP7	–	–	0.5
mRNA_ProCASP7+Ribosome ⇋ Rm_ProCASP7	0.5	0.1	–
Rm_ProCASP7 ⇋ Ar_ProCASP7	–	–	0.5
Ar_ProCASP7 ⇋ ProCASP7+Ribosome	–	–	0.5
ProCASP8+CASP3 ⇋ ProCASP8_CASP3	0.6	1.0	–
ProCASP8_CASP3 ⇋ CASP8+CASP3	–	–	0.7
ProCASP8+CASP6 ⇋ ProCASP8_CASP6	0.6	1.0	–
ProCASP8_CASP6 ⇋ CASP8+CASP6	–	–	0.7
ProCASP8+CASP7 ⇋ ProCASP8_CASP7	0.6	1.0	–
ProCASP8_CASP7 ⇋ CASP8+CASP7	–	–	0.7
Bid_c+CKI ⇋ Bid_CKI	0.5	0.1	–
Bid_CKI ⇋ P_Bid_c+CKI	–	–	0.4
[] ⇋ mRNA_Bid	–	–	0.3
mRNA_Bid+Ribosome ⇋ Rm_Bid	0.3	0.1	–
Rm_Bid ⇋ Ar_Bid	–	–	0.3

continued on next page

continued from previous page

Reaction	K_f	K_b	K_{cat}
Ar_Bid ⇋ Bid_c+Ribosome	–	–	0.3
[] ⇋ mRNA_CKI	–	–	0.3
mRNA_CKI+Ribosome ⇋ Rm_CKI	0.3	0.1	–
Rm_CKI ⇋ Ar_CKI	–	–	0.3
Ar_CKI ⇋ CKI+Ribosome	–	–	0.3
[] ⇋ mRNA_CKII	–	–	0.2
mRNA_CKII+Ribosome ⇋ Rm_CKII	0.2	0.1	–
Rm_CKII ⇋ Ar_CKII	–	–	0.2
Ar_CKII ⇋ CKII+Ribosome	–	–	0.2
Bid_c+CKII ⇋ Bid_CKII	0.3	0.2	–
Bid_CKII ⇋ P_Bid_c+CKII	–	–	0.3
Bid_c+CASP8 ⇋ Bid_CASP8	0.4	1.5	–
Bid_CASP8 ⇋ t_Bid_c+CASP8	–	–	0.5
PTP ⇋ PTP_open	0.2	1.0	–
Bak+PTP_open ⇋ Bak_PTP_open	0.3	2.0	–
Bak_PTP_open ⇋ Bak+5*PTP_open	–	–	0.5
Bcl2+PTP_open ⇋ Bcl2_PTP_open	0.5	1.0	–
cytoc_m+PTP_open ⇋ cytoc_m_PTP_open	0.4	1.0	–
cytoc_m_PTP_open ⇋ PTP_open+cytochromeC_c	–	–	0.8
CAi+Bad_inactive ⇋ CAi_Bad_inactive	–	–	0.3
CAi_Bad_inactive ⇋ CAi+Bad	0.3	0.6	–
Bcl2+Bak ⇋ Bcl2_Bak	10.0	0.5	–
Bcl2_Bak+Bad ⇋ Bak+Bcl2_Bad	0.3	0.7	–
Bcl2+Bak_inactive ⇋ Bcl2_Bak	0.0	0.0	–
Bad+Bak_inactive ⇋ Bak_inactive_Bad	0.0	0.0	–
Bak_inactive_Bad ⇋ Bak+Bad	0.0	0.0	–
t_Bid_c+PTP_open ⇋ t_Bid_c_PTP_open	0.5	2.0	–
t_Bid_c_PTP_open ⇋ t_Bid_c+5*PTP_open	–	–	0.3
CrmA+Bid_CASP8 ⇋ CrmA_Bid_CASP8	0.8	0.4	–

continued on next page

continued from previous page

Reaction	K_f	K_b	K_{cat}
PTP_open+Diablo_m ⇋ Diablo_PTP_open	0.4	1.8	–
Diablo_PTP_open ⇋ Diablo_c+PTP_open	–	–	0.5
[] ⇋ mRNA_Diablo	–	–	0.2
mRNA_Diablo+Ribosome ⇋ Rm_Diablo	0.2	0.1	–
Rm_Diablo ⇋ Ar_Diablo	–	–	0.2
Ar_Diablo ⇋ Diablo_m+Ribosome	–	–	0.2
PTP_open+Omi_m ⇋ Omi_PTP_open	0.4	1.9	–
Omi_PTP_open ⇋ Omi_c+PTP_open	–	–	0.4
[] ⇋ mRNA_Omi	–	–	0.2
mRNA_Omi+Ribosome ⇋ Rm_Omi	0.2	0.1	–
Rm_Omi ⇋ Ar_Omi	–	–	0.2
Ar_Omi ⇋ Omi_m+Ribosome	–	–	0.2
PTP_open+AIF_m ⇋ AIF_PTP_open	0.3	1.8	–
AIF_PTP_open ⇋ AIF_c+PTP_open	–	–	0.4
[] ⇋ mRNA_AIF	–	–	0.2
mRNA_AIF+Ribosome ⇋ Rm_AIF	0.2	0.1	–
Rm_AIF ⇋ Ar_AIF	–	–	0.2
Ar_AIF ⇋ AIF_m+Ribosome	–	–	0.2
PTP_open+endoG_m ⇋ endoG_PTP_open	–	–	0.4
endoG_PTP_open ⇋ endoG_c+PTP_open	–	–	0.4
[] ⇋ mRNA_endoG	–	–	0.1
mRNA_endoG+Ribosome ⇋ Rm_endoG	0.1	0.01	–
Rm_endoG ⇋ Ar_endoG	–	–	0.1
Ar_endoG ⇋ endoG_m+Ribosome	–	–	0.1
Diablo_c+IAP1 ⇋ Diablo_IAP1	0.3	0.1	–
Omi_c+IAP1 ⇋ Omi_IAP1	0.4	0.1	–
AIF_c ⇋ AIF_n	0.5	0.1	–
endoG_c ⇋ endoG_n	0.5	0.1	–
AIF_n+DNA_intact ⇋ AIF_DNA_intact	0.8	1.9	–

continued on next page

continued from previous page

Reaction	K_f	K_b	K_{cat}
AIF_DNA_intact ⇋ AIF_n+DNA_degraded	–	–	0.6
endoG_n+DNA_intact ⇋ endoG_DNA_intact	0.7	1.9	–
endoG_DNA_intact ⇋ endoG_n+DNA_degraded	–	–	0.5
IAP1+CASP3 ⇋ IAP1_CASP3	1.5	0.6	–
[] ⇋ mRNA_IAP1	–	–	0.3
mRNA_IAP1+Ribosome ⇋ Rm_IAP1	0.3	0.1	–
Rm_IAP1 ⇋ Ar_IAP1	–	–	0.3
Ar_IAP1 ⇋ IAP1+Ribosome	–	–	0.3
IAP1+CASP6 ⇋ IAP1_CASP6	1.5	0.6	–
IAP1+CASP7 ⇋ IAP1_CASP7	1.5	0.6	–
IAP2+CASP3 ⇋ IAP2_CASP3	1.5	0.5	–
[] ⇋ mRNA_IAP2	–	–	0.3
mRNA_IAP2+Ribosome ⇋ Rm_IAP2	0.3	0.1	–
Rm_IAP2 ⇋ Ar_IAP2	–	–	0.3
Ar_IAP2 ⇋ IAP2+Ribosome	–	–	0.3
IAP2+CASP6 ⇋ IAP2_CASP6	1.5	0.5	–
IAP2+CASP7 ⇋ IAP2_CASP7	1.5	0.5	–
XIAP+CASP3 ⇋ XIAP_CASP3	1.5	0.4	–
[] ⇋ mRNA_XIAP	–	–	0.3
mRNA_XIAP+Ribosome ⇋ Rm_XIAP	0.3	0.1	–
Rm_XIAP ⇋ Ar_XIAP	–	–	0.3
Ar_XIAP ⇋ XIAP+Ribosome	–	–	0.3
XIAP+CASP6 ⇋ XIAP_CASP6	1.5	0.4	–
XIAP+CASP7 ⇋ XIAP_CASP7	1.5	0.4	–
XIAP+Omi_c ⇋ XIAP_Omi_c	0.5	0.1	–
Apaf1 ⇋ Apaf1_p	0.0	0.0	–
7*cytochromeC_c+7*Apaf1_p+7*ProCASP9 ⇋ Apoptosome	0.0	0.0	–
7*cytochromeC_c+7*Apaf1+7*ProCASP9 ⇋ Apoptosome	0.9	1.5	–
[] ⇋ mRNA_Apaf1	–	–	0.3

continued on next page

continued from previous page

Reaction	K_f	K_b	K_{cat}
mRNA_Apaf1+Ribosome ⇋ Rm_Apaf1	0.3	0.1	–
Rm_Apaf1 ⇋ Ar_Apaf1	–	–	0.3
Ar_Apaf1 ⇋ Apaf1+Ribosome	–	–	0.3
[] ⇋ mRNA_ProCASP9	–	–	0.5
mRNA_ProCASP9+Ribosome ⇋ Rm_ProCASP9	0.5	0.1	–
Rm_ProCASP9 ⇋ Ar_ProCASP9	–	–	0.5
Ar_ProCASP9 ⇋ ProCASP9+Ribosome	–	–	0.7
Apoptosome ⇋ 7*CASP9+7*cytochromeC_c+7*Apaf1	–	–	0.9
ProCASP3+CASP9 ⇋ ProCASP3_CASP9	0.6	1.0	–
ProCASP3_CASP9 ⇋ CASP9+CASP3	–	–	0.7
ProCASP6+CASP9 ⇋ ProCASP6_CASP9	0.6	1.0	–
ProCASP6_CASP9 ⇋ CASP9+CASP6	–	–	0.7
ProCASP7+CASP9 ⇋ ProCASP7_CASP9	0.6	1.0	–
ProCASP7_CASP9 ⇋ CASP9+CASP7	–	–	0.7
ProCASP9+CASP3 ⇋ ProCASP9_CASP3	0.5	1.0	–
ProCASP9_CASP3 ⇋ CASP9+CASP3	–	–	0.8
ProCASP9+CASP6 ⇋ ProCASP9_CASP3	0.5	1.0	–
ProCASP9_CASP3 ⇋ CASP9+CASP6	–	–	0.8
ProCASP9+CASP7 ⇋ ProCASP9_CASP7	0.5	1.0	–
ProCASP9_CASP7 ⇋ CASP9+CASP7	–	–	0.8
ProCASP8 ⇋ []	–	–	0.9
CASP8 ⇋ []	–	–	0.4
ProCASP3 ⇋ []	–	–	0.9
CASP3 ⇋ []	–	–	0.6
ProCASP6 ⇋ []	–	–	0.9
CASP6 ⇋ []	–	–	0.6
ProCASP7 ⇋ []	–	–	0.9
CASP7 ⇋ []	–	–	0.6
Bid_c ⇋ []	–	–	0.4

continued on next page

continued from previous page

Reaction	K_f	K_b	K_{cat}
CKI ⇋ []	–	–	0.3
CKII ⇋ []	–	–	0.3
CrmA ⇋ []	–	–	0.2
Diablo_m ⇋ []	–	–	0.2
Diablo_c ⇋ []	–	–	0.4
Omi_m ⇋ []	–	–	0.2
Omi_c ⇋ []	–	–	0.4
AIF_m ⇋ []	–	–	0.2
AIF_c ⇋ []	–	–	0.4
endoG_m ⇋ []	–	–	0.2
endoG_c ⇋ []	–	–	0.4
IAP1 ⇋ []	–	–	0.2
AIF_n ⇋ []	–	–	0.2
endoG_n ⇋ []	–	–	0.2
DNA_intact ⇋ []	–	–	0.3
IAP2 ⇋ []	–	–	0.2
XIAP ⇋ []	–	–	0.2
Apaf1 ⇋ []	–	–	0.3
ProCASP9 ⇋ []	–	–	0.9
CASP9 ⇋ []	–	–	0.5
[] ⇋ mRNA_Casper	–	–	0.2
mRNA_Casper+Ribosome ⇋ Rm_Casper	0.2	0.1	–
Rm_Casper ⇋ Ar_Casper	–	–	0.2
Ar_Casper ⇋ Casper+Ribosome	–	–	0.2
[] ⇋ mRNA_I_FLICE	–	–	0.2
mRNA_I_FLICE+Ribosome ⇋ Rm_I_FLICE	0.2	0.1	–
Rm_I_FLICE ⇋ Ar_I_FLICE	–	–	0.2
Ar_I_FLICE ⇋ I_FLICE+Ribosome	–	–	0.2
[] ⇋ DNA_intact	–	–	0.5

continued on next page

continued from previous page

Reaction	K_f	K_b	K_{cat}
[] ⇋ mRNA_CrmA	–	–	0.3
mRNA_CrmA+Ribosome ⇋ Rm_CrmA	0.3	0.1	–
Rm_CrmA ⇋ Ar_CrmA	–	–	0.3
Ar_CrmA ⇋ CrmA+Ribosome	–	–	0.3
[] ⇋ mRNA_cytoc_m	–	–	0.3
mRNA_cytoc_m+Ribosome ⇋ Rm_cytoc_m	0.3	0.1	–
Rm_cytoc_m ⇋ Ar_cytoc_m	–	–	0.3
Ar_cytoc_m ⇋ cytoc_m+Ribosome	–	–	0.3
[] ⇋ mRNA_Bad_inactive	–	–	0.2
mRNA_Bad_inactive+Ribosome ⇋ Rm_Bad_inactive	0.2	0.1	–
Rm_Bad_inactive ⇋ Ar_Bad_inactive	–	–	0.2
Ar_Bad_inactive ⇋ Bad_inactive+Ribosome	–	–	0.2
[] ⇋ PTP	–	–	0.5
[] ⇋ mRNA_VDAC	–	–	0.2
mRNA_VDAC+Ribosome ⇋ Rm_VDAC	0.2	0.1	–
Rm_VDAC ⇋ Ar_VDAC	–	–	0.2
Ar_VDAC ⇋ VDAC+Ribosome	–	–	0.2
[] ⇋ mRNA_UP	–	–	0.2
mRNA_UP+Ribosome ⇋ Rm_UP	0.2	0.1	–
Rm_UP ⇋ Ar_UP	–	–	0.2
Ar_UP ⇋ UP+Ribosome	–	–	0.2
[] ⇋ mRNA_cyclophilin_D	–	–	0.2
mRNA_cyclophilin_D+Ribosome ⇋ Rm_cyclophilin_D	0.2	0.1	–
Rm_cyclophilin_D ⇋ Ar_cyclophilin_D	–	–	0.2
Ar_cyclophilin_D ⇋ cyclophilin_D+Ribosome	–	–	0.2
CA_cytosol ⇋ []	–	–	0.2
VDAC ⇋ []	–	–	0.2
UP ⇋ []	–	–	0.2
cyclophilin_D ⇋ []	–	–	0.2

continued on next page

continued from previous page

Reaction	K_f	K_b	K_{cat}
PTP $\leftrightharpoons$ []	–	–	0.2
Bak $\leftrightharpoons$ []	–	–	0.0
Bcl2 $\leftrightharpoons$ []	–	–	0.1
cytoc_m $\leftrightharpoons$ []	–	–	0.2
Bad_inactive $\leftrightharpoons$ []	–	–	0.0
[] $\leftrightharpoons$ CA_cytosol	–	–	0.2
CA_external $\leftrightharpoons$ CAi	–	–	0.0
CASP8+BAP31 $\leftrightharpoons$ CASP8_BAP31	–	–	0.4
CASP8_BAP31 $\leftrightharpoons$ BAP20+CASP8	–	–	0.8
BAP20+CAs $\leftrightharpoons$ BAP20_CAs	–	–	0.3
BAP20_CAs $\leftrightharpoons$ BAP20+CAi	–	–	0.6
CAi $\leftrightharpoons$ CA_external	–	–	0.0
[] $\leftrightharpoons$ mRNA_CASP12	–	–	1.0
mRNA_CASP12+Ribosome $\leftrightharpoons$ Rm_CASP12	1.0	0.1	–
Rm_CASP12 $\leftrightharpoons$ Ar_CASP12	–	–	1.0
Ar_CASP12 $\leftrightharpoons$ CASP12+Ribosome	–	–	1.0
CASP12_act $\leftrightharpoons$ []	–	–	0.3
CASP12 $\leftrightharpoons$ []	–	–	0.5
JNK_act $\leftrightharpoons$ []	–	–	0.3
ASK1_act $\leftrightharpoons$ []	–	–	0.3
PTP_open $\leftrightharpoons$ []	–	–	0.4
cytochromeC_c $\leftrightharpoons$ []	–	–	0.4
CASP8+CASP3 $\leftrightharpoons$ CASP8_ProCASP3	–	–	1.1
CASP8+CASP6 $\leftrightharpoons$ CASP8_ProCASP6	–	–	1.1
CASP8+CASP7 $\leftrightharpoons$ CASP8_ProCASP7	–	–	1.1
CASP8+CASP3 $\leftrightharpoons$ ProCASP8_CASP3	–	–	1.1
CASP8+CASP6 $\leftrightharpoons$ ProCASP8_CASP6	–	–	1.1
CASP8+CASP7 $\leftrightharpoons$ ProCASP8_CASP7	–	–	1.1
P_Bid_c+CKI $\leftrightharpoons$ Bid_CKI	–	–	1.5

continued on next page

continued from previous page

Reaction	K_f	K_b	K_{cat}
P_Bid_c+CKII ⇋ Bid_CKII	–	–	1.5
t_Bid_c+CASP8 ⇋ Bid_CASP8	–	–	1.5
7*CASP9+7*cytochromeC_c+7*Apaf1 ⇋ Apoptosome	–	–	1.5
CASP9+CASP3 ⇋ ProCASP3_CASP9	–	–	1.0
CASP9+CASP6 ⇋ ProCASP6_CASP9	–	–	1.0
CASP9+CASP7 ⇋ ProCASP7_CASP9	–	–	1.0
CASP9+CASP3 ⇋ ProCASP9_CASP3	–	–	1.0
CASP9+CASP6 ⇋ ProCASP9_CASP3	–	–	1.0
CASP9+CASP7 ⇋ ProCASP9_CASP7	–	–	1.0
CASP3+GAS2 ⇋ CASP3_GAS2	0.5	1.0	–
CASP3_GAS2 ⇋ CASP3+t_GAS2	0.4	1.0	–
[] ⇋ mRNA_GAS2	–	–	0.2
mRNA_GAS2+Ribosome ⇋ Rm_GAS2	0.2	0.1	–
Rm_GAS2 ⇋ Ar_GAS2	–	–	0.2
Ar_GAS2 ⇋ GAS2+Ribosome	–	–	0.2
GAS2 ⇋ []	–	–	0.2
CASP3+Fodrin ⇋ CASP3_Fodrin	0.5	1.0	–
CASP3_Fodrin ⇋ CASP3+t_Fodrin	0.8	1.0	–
[] ⇋ mRNA_Fodrin	–	–	0.2
mRNA_Fodrin+Ribosome ⇋ Rm_Fodrin	0.2	0.1	–
Rm_Fodrin ⇋ Ar_Fodrin	–	–	0.2
Ar_Fodrin ⇋ Fodrin+Ribosome	–	–	0.2
Fodrin ⇋ []	–	–	0.2
CASP3+Gelsolin ⇋ CASP3_Gelsolin	0.5	1.0	–
CASP3_Gelsolin ⇋ CASP3+t_Gelsolin	0.8	1.0	–
[] ⇋ mRNA_Gelsolin	–	–	0.2
mRNA_Gelsolin+Ribosome ⇋ Rm_Gelsolin	0.2	0.1	–
Rm_Gelsolin ⇋ Ar_Gelsolin	–	–	0.2
Ar_Gelsolin ⇋ Gelsolin+Ribosome	–	–	0.2

continued on next page

continued from previous page

Reaction	K_f	K_b	K_{cat}
Gelsolin $\leftrightharpoons$ []	–	–	0.2
CASP6+LaminA $\leftrightharpoons$ CASP6_LaminA	0.7	1.0	–
CASP6_LaminA $\leftrightharpoons$ CASP6+t_LaminA	0.8	1.0	–
[] $\leftrightharpoons$ mRNA_LaminA	–	–	0.2
mRNA_LaminA+Ribosome $\leftrightharpoons$ Rm_LaminA	0.2	0.1	–
Rm_LaminA $\leftrightharpoons$ Ar_LaminA	–	–	0.2
Ar_LaminA $\leftrightharpoons$ LaminA+Ribosome	–	–	0.2
LaminA $\leftrightharpoons$ []	–	–	0.2
CASP3+LaminB1 $\leftrightharpoons$ CASP3_LaminB1	0.0	0.0	–
CASP3_LaminB1 $\leftrightharpoons$ CASP3+t_LaminB1	0.0	0.0	–
[] $\leftrightharpoons$ mRNA_LaminB1	–	–	0.0
mRNA_LaminB1+Ribosome $\leftrightharpoons$ Rm_LaminB1	0.0	0.0	–
Rm_LaminB1 $\leftrightharpoons$ Ar_LaminB1	–	–	0.0
Ar_LaminB1 $\leftrightharpoons$ LaminB1+Ribosome	–	–	0.0
LaminB1 $\leftrightharpoons$ []	–	–	0.0
CASP6+LaminC $\leftrightharpoons$ CASP6_LaminC	0.4	1.0	–
CASP6_LaminC $\leftrightharpoons$ CASP6+t_LaminC	0.8	1.0	–
[] $\leftrightharpoons$ mRNA_LaminC	–	–	0.2
mRNA_LaminC+Ribosome $\leftrightharpoons$ Rm_LaminC	0.2	0.1	–
Rm_LaminC $\leftrightharpoons$ Ar_LaminC	–	–	0.2
Ar_LaminC $\leftrightharpoons$ LaminC+Ribosome	–	–	0.2
LaminC $\leftrightharpoons$ []	–	–	0.2
CASP3+Nup153 $\leftrightharpoons$ CASP3_Nup153	0.5	1.0	–
CASP3_Nup153 $\leftrightharpoons$ CASP3+t_Nup153	0.8	1.0	–
[] $\leftrightharpoons$ mRNA_Nup153	–	–	0.2
mRNA_Nup153+Ribosome $\leftrightharpoons$ Rm_Nup153	0.2	0.1	–
Rm_Nup153 $\leftrightharpoons$ Ar_Nup153	–	–	0.2
Ar_Nup153 $\leftrightharpoons$ Nup153+Ribosome	–	–	0.2
Nup153 $\leftrightharpoons$ []	–	–	0.2

continued on next page

continued from previous page

Reaction	K_f	K_b	K_{cat}
CASP3+PARP ⇋ CASP3_PARP	0.5	1.0	–
CASP3_PARP ⇋ CASP3+t_PARP	1.0	1.0	–
[] ⇋ mRNA_PARP	–	–	0.3
mRNA_PARP+Ribosome ⇋ Rm_PARP	0.3	0.1	–
Rm_PARP ⇋ Ar_PARP	–	–	0.3
Ar_PARP ⇋ PARP+Ribosome	–	–	0.3
PARP ⇋ []	–	–	0.6
CASP7+PARP ⇋ CASP7_PARP	0.5	1.0	–
CASP7_PARP ⇋ CASP7+t_PARP	1.0	1.0	–
CASP9+PARP ⇋ CASP9_PARP	0.5	1.0	–
CASP9_PARP ⇋ CASP9+t_PARP	1.0	1.0	–
CASP3+TopoI ⇋ CASP3_TopoI	0.5	1.0	–
CASP3_TopoI ⇋ CASP3+t_TopoI	0.8	1.0	–
[] ⇋ mRNA_TopoI	–	–	0.2
mRNA_TopoI+Ribosome ⇋ Rm_TopoI	0.2	0.1	–
Rm_TopoI ⇋ Ar_TopoI	–	–	0.2
Ar_TopoI ⇋ TopoI+Ribosome	–	–	0.2
TopoI ⇋ []	–	–	0.2
CASP3+PolE ⇋ CASP3_PolE	0.5	1.0	–
CASP3_PolE ⇋ CASP3+t_PolE	0.8	1.0	–
[] ⇋ mRNA_PolE	–	–	0.2
mRNA_PolE+Ribosome ⇋ Rm_PolE	0.2	0.1	–
Rm_PolE ⇋ Ar_PolE	–	–	0.2
Ar_PolE ⇋ PolE+Ribosome	–	–	0.2
PolE ⇋ []	–	–	0.2
CASP9+ICAD ⇋ CASP9_ICAD	0.5	1.0	–
CASP9_ICAD ⇋ CASP9+CAD	0.8	1.0	–
[] ⇋ mRNA_ICAD	–	–	0.3
mRNA_ICAD+Ribosome ⇋ Rm_ICAD	0.2	0.1	–

continued on next page

continued from previous page

Reaction	K_f	K_b	K_{cat}
Rm_ICAD ⇋ Ar_ICAD	–	–	0.2
Ar_ICAD ⇋ ICAD+Ribosome	–	–	0.2
ICAD ⇋ []	–	–	0.2
CAD+DNA_intact ⇋ CAD_DNA_intact	0.5	1.0	–
CAD_DNA_intact ⇋ CAD+DNA_degraded	–	–	0.5
t_Fodrin ⇋ []	–	–	0.3
t_GAS2 ⇋ []	–	–	0.3
t_Gelsolin ⇋ []	–	–	0.3
t_LaminA ⇋ []	–	–	0.3
t_LaminB1 ⇋ []	–	–	0.3
t_LaminC ⇋ []	–	–	0.3
t_Nup153 ⇋ []	–	–	0.3
t_PARP ⇋ []	–	–	0.3
t_TopoI ⇋ []	–	–	0.3
t_PolE ⇋ []	–	–	0.3
CAD ⇋ []	–	–	0.2
UB+ATP ⇋ UB_ATP	1.0	0.5	–
UB_ATP+E1_SH ⇋ E1_S_UB+AMP+PPi	0.8	0.4	–
E1_S_UB ⇋ E2_S_UB	0.7	0.3	–
E2_S_UB+E3 ⇋ E3_E2_S_UB	0.7	0.2	–
PROT+E3_E2_S_UB ⇋ Prot_degrad_target	0.5	0.1	–
Prot_degrad_target ⇋ []	–	–	0.0
AMP ⇋ []	–	–	0.2
PPi ⇋ []	–	–	0.2
UB ⇋ []	–	–	0.3
E1_SH ⇋ []	–	–	0.2
E3 ⇋ []	–	–	0.2
[] ⇋ mRNA_UB	–	–	0.3
mRNA_UB+Ribosome ⇋ Rm_UB	0.3	0.1	–

continued on next page

continued from previous page

Reaction	K_f	K_b	K_{cat}
Rm_UB ⇋ Ar_UB	–	–	0.3
Ar_UB ⇋ UB+Ribosome	–	–	0.3
[] ⇋ mRNA_E1_SH	–	–	0.2
mRNA_E1_SH+Ribosome ⇋ Rm_E1_SH	0.3	0.1	–
Rm_E1_SH ⇋ Ar_E1_SH	–	–	0.2
Ar_E1_SH ⇋ E1_SH+Ribosome	–	–	0.2
[] ⇋ mRNA_E3	–	–	0.3
mRNA_E3+Ribosome ⇋ Rm_E3	0.3	0.1	–
Rm_E3 ⇋ Ar_E3	–	–	0.3
Ar_E3 ⇋ E3+Ribosome	–	–	0.3
ATF6_ATF_NFY_ERSE1+mRNA_GADD153 ⇋ mRNA_GADD153_act	1.0	1.5	–
ATF6_ATF_ERSE2+mRNA_GADD153 ⇋ mRNA_GADD153_act	0.8	1.2	–
XBP1_NFY_ERSE+mRNA_GADD153 ⇋ mRNA_GADD153_act	0.9	1.8	–
[] ⇋ mRNA_bZIP	–	–	0.2
mRNA_bZIP+Ribosome ⇋ Rm_bZIP	0.2	0.1	–
Rm_bZIP ⇋ Ar_bZIP	–	–	0.2
Ar_bZIP ⇋ bZIP+Ribosome	–	–	0.2
GADD153 ⇋ []	–	–	0.8
p38MAPK_act ⇋ []	–	–	0.6
GADD153+p38MAPK_act ⇋ GADD153_p38MAPK_act	0.9	1.4	–
GADD153_p38MAPK_act ⇋ GADD153_p+p38MAPK_act	0.8	1.4	–
GADD153_p ⇋ []	–	–	0.6
CA_cytosol+t_Bid_c ⇋ CA_BID_complex	–	–	0.3
CA_BID_complex ⇋ CAi+t_Bid_c	–	–	0.3
CAi+VDAC ⇋ CA_VDAC	0.3	0.6	–
CA_VDAC ⇋ CA_OMM+VDAC	0.4	0.8	–
CA_OMM+UP ⇋ CA_OMM_UP	0.5	1.0	–
CA_OMM_UP ⇋ CAm+UP	0.4	0.8	–
CAm ⇋ CSMDH_1	0.3	0.6	–

continued on next page

continued from previous page

Reaction	K_f	K_b	K_{cat}
CSMDH_1 ⇋ CSMDH+CAm	0.4	0.8	–
CAm+cyclophilin_D ⇋ CAm_cyclophilin_D	0.5	1.0	–
CAm ⇋ ROS_1	0.4	0.6	–
ROS_1 ⇋ ROS+CAm	0.5	0.8	–
CAm ⇋ FFA_1	0.3	0.6	–
FFA_1 ⇋ FFA+CAm	0.4	0.8	–
CAm_cyclophilin_D+PTP ⇋ CAm_cyclophilin_D_PTP	0.4	0.8	–
CAm_cyclophilin_D_PTP ⇋ CAm_cyclophilin_D+PTP_open	0.8	1.5	–
IP3Ri+cytochromeC_c ⇋ IP3R_comp	0.5	1.0	–
IP3R_comp ⇋ IP3R_act+cytochromeC_c	0.4	0.8	–
IP3Ri+Bak ⇋ IP3R_act	0.3	0.6	–
IP3R_act+Bcl2 ⇋ IP3Ri_Bcl2	1.0	0.5	–
IP3R+IP3 ⇋ IP3R_IP3	0.3	0.3	–
IP3R_IP3 ⇋ IP3R_IP3a	0.3	0.3	–
IP3R_IP3a+CAi ⇋ IP3R_act	0.3	0.8	–
IP3R_act+CAs ⇋ IP3R_CAs	0.4	0.8	–
IP3R_CAs ⇋ IP3R_act+CAi	0.4	0.8	–
Bap31+Bcl2 ⇋ Bap31_Bcl2	0.8	0.4	–
[] ⇋ mRNA_Bap31	–	–	0.2
mRNA_Bap31+Ribosome ⇋ Rm_Bap31	0.2	0.1	–
Rm_Bap31 ⇋ Ar_Bap31	–	–	0.2
Ar_Bap31 ⇋ Bap31+Ribosome	–	–	0.2
Bap31 ⇋ []	–	–	0.2
DRP1+CAi ⇋ DRP1_CAi	0.3	0.3	–
DRP1_CAi ⇋ DRP1_act+CAi	0.3	0.3	–
[] ⇋ mRNA_DRP1	–	–	0.2
mRNA_DRP1+Ribosome ⇋ Rm_DRP1	0.2	0.1	–
Rm_DRP1 ⇋ Ar_DRP1	–	–	0.2
Ar_DRP1 ⇋ DRP1+Ribosome	–	–	0.2

continued on next page

continued from previous page

Reaction	K_f	K_b	K_{cat}
DRP1 ⇋ []	–	–	0.7
DRP1_act ⇋ []	–	–	0.8
CAi+Plases_inact ⇋ CAi_Plases	0.3	0.3	–
[] ⇋ mRNA_Plases_inact	–	–	0.3
mRNA_Plases_inact+Ribosome ⇋ Rm_Plases_inact	0.2	0.1	–
Rm_Plases_inact ⇋ Ar_Plases_inact	–	–	0.3
Ar_Plases_inact ⇋ Plases_inact+Ribosome	–	–	0.2
Plases_inact ⇋ []	–	–	0.4
CAi_Plases_m ⇋ []	–	–	0.3
CAi_Plases ⇋ CAi_Plases_m	0.3	0.3	–
Card_in+CAi_Plases_m ⇋ Card_Plases	0.4	0.4	–
Card_Plases ⇋ Card_out+CAi_Plases_m	0.5	0.5	–
[] ⇋ mRNA_Card_in	–	–	0.3
mRNA_Card_in+Ribosome ⇋ Rm_Card_in	0.3	0.2	–
Rm_Card_in ⇋ Ar_Card_in	–	–	0.3
Ar_Card_in ⇋ Card_in+Ribosome	–	–	0.3
Card_in ⇋ []	–	–	0.7
Card_out ⇋ []	–	–	0.4
Bak+PTP_open+Card_out ⇋ Bak_PTP_open_Card_out	–	–	0.3
Bak_PTP_open_Card_out ⇋ Bak+5*PTP_open+Card_out	–	–	0.5
t_Bid_c+PTP_open+Card_out ⇋ t_Bid_c_PTP_open_Card_out	–	–	0.3
t_Bid_c_PTP_open_Card_out ⇋ t_Bid_c+5*PTP_open+Card_out	–	–	0.5
CAi+NOS ⇋ CAi_RNS	0.3	0.3	–
CAi_RNS ⇋ CAi+RNS	0.3	0.3	–
[] ⇋ NOS	0.2	0.4	–
CAi+PTP_open ⇋ CAi_PTP	0.6	0.8	–
CAi_PTP ⇋ CAi+5*PTP_open	0.3	0.7	–
CAi+DAPK1 ⇋ CA_DAPK	0.3	0.3	–
CA_DAPK ⇋ CAi+DAPK_act	0.4	0.4	–

continued on next page

continued from previous page

Reaction	K_f	K_b	K_{cat}
[] ⇋ mRNA_DAPK1	–	–	0.2
mRNA_DAPK1+Ribosome ⇋ Rm_DAPK1	0.2	0.1	–
Rm_DAPK1 ⇋ Ar_DAPK1	–	–	0.2
Ar_DAPK1 ⇋ DAPK1+Ribosome	–	–	0.2
DAPK1 ⇋ []	–	–	0.6
DAPK_act ⇋ []	–	–	0.8
CAi+Calpain_inact ⇋ Calpain_CA_comp	0.3	0.3	–
Calpain_CA_comp ⇋ Calpain_act+CAi	0.3	0.4	–
[] ⇋ mRNA_Calpain_inact	–	–	0.2
mRNA_Calpain_inact+Ribosome ⇋ Rm_Calpain_inact	0.2	0.1	–
Rm_Calpain_inact ⇋ Ar_Calpain_inact	–	–	0.2
Ar_Calpain_inact ⇋ Calpain_inact+Ribosome	–	–	0.2
Calpain_inact ⇋ []	–	–	0.7
Calpain_act ⇋ []	–	–	0.8
CAm ⇋ []	–	–	0.2
CAi ⇋ []	–	–	0.2
CAs ⇋ []	–	–	0.2
RNS ⇋ []	–	–	0.5
[] ⇋ mRNA_IP3R	–	–	0.3
mRNA_IP3R+Ribosome ⇋ Rm_IP3R	0.3	0.1	–
Rm_IP3R ⇋ Ar_IP3R	–	–	0.3
Ar_IP3R ⇋ IP3R+Ribosome	–	–	0.3
[] ⇋ mRNA_IP3	–	–	0.2
mRNA_IP3+Ribosome ⇋ Rm_IP3	0.2	0.1	–
Rm_IP3 ⇋ Ar_IP3	–	–	0.2
Ar_IP3 ⇋ IP3+Ribosome	–	–	0.2
IP3R_act ⇋ []	–	–	0.7
IP3Ri ⇋ []	–	–	0.7
IP3R ⇋ []	–	–	0.7

continued on next page

continued from previous page

Reaction	K_f	K_b	K_{cat}
IP3 ⇋ []	–	–	0.8
CA_BID_complex ⇋ CA_cytosol+t_Bid_c	–	–	0.6
CAi+t_Bid_c ⇋ CA_BID_complex	–	–	0.6
P_Bid_c+CKI ⇋ Bid_CKI	–	–	0.8
P_Bid_c+CKII ⇋ Bid_CKII	–	–	0.8
t_Bid_c+CASP8 ⇋ Bid_CASP8	–	–	0.8
[] ⇋ CAs	–	–	0.2
ATF4_prod ⇋ eIF2a_p	–	–	1.4
ATF4+eIF2a_p ⇋ ATF4_prod	–	–	1.0
ATF3_act_ATF4 ⇋ ATF4+ATF3	–	–	1.0
ATF3_act+ATF4 ⇋ ATF3_act_ATF4	–	–	1.0
GADD34_complex ⇋ ATF3_act	–	–	1.0
GADD34+ATF3_act ⇋ GADD34_complex	–	–	1.0
mRNA_XBP1_spliced_complex ⇋ mRNA_XBP1+IRE1_act	–	–	1.0
mRNA_XBP1_spliced+IRE1_act ⇋ mRNA_XBP1_spliced_complex	–	–	1.4
JNK_act+Bim_p ⇋ Bim_JNK_act	–	–	2.0
JNK_Bcl2 ⇋ JNK_act+Bcl2	–	–	0.5
PTP+Bim_JNK_act ⇋ PTP_Bim_JNK_act	0.5	0.8	–
PTP_Bim_JNK_act ⇋ Bim_JNK_act+3*PTP_open	0.4	0.8	–
[] ⇋ CAs	–	–	0.2

BIBLIOGRAPHY

[1] J.M. Adams. Ways of dying: multiple pathways to apoptosis. *Genes & Development*, 17(20):2481–2495, 2003.

[2] E.S. Alnemri, D.J. Livingston, D.W. Nicholson, G. Salvesen, N.A. Thornberry, W.W. Wong, and J. Yuan. Human ICE/CED-3 Protease Nomenclature. *CELL-CAMBRIDGE MA-*, 87:171–172, 1996.

[3] E. ARAKI, S. OYADOMARI, and M. MORI. Endoplasmic reticulum stress and diabetes mellitus. *Internal Medicine*, 42(1):7–14, 2003.

[4] S. Arnaudeau, M. Frieden, K. Nakamura, C. Castelbou, M. Michalak, and N. Demaurex. Calreticulin Differentially Modulates Calcium Uptake and Release in the Endoplasmic Reticulum and Mitochondria. *Journal of Biological Chemistry*, 277(48):46696–46705, 2002.

[5] A. Ashkenazi and V.M. Dixit. Death Receptors: Signaling and Modulation. *Science*, 281(5381):1305, 1998.

[6] P.J. Belmont, A. Tadimalla, W.J. Chen, J.J. Martindale, D.J. Thuerauf, M. Marcinko, N. Gude, M.A. Sussman, and C.C. Glembotski. Coordination of Growth and Endoplasmic Reticulum Stress Signaling by Regulator of Calcineurin 1 (RCAN1), a Novel ATF6-inducible Gene. *Journal of Biological Chemistry*, 283(20):14012, 2008.

[7] S. Bernales, K.L. McDonald, and P. Walter. Autophagy counterbalances endoplasmic reticulum expansion during the unfolded protein response. *PLoS Biol*, 4(12):e423, 2006.

[8] P. Bernardi. Mitochondrial transport of cations: channels, exchangers, and permeability transition. *Physiological reviews*, 79(4):1127–1155, 1999.

[9] A. Bertolotti, Y. Zhang, L.M. Hendershot, H.P. Harding, and D. Ron. Dynamic interaction of BiP and ER stress transducers in the unfolded-protein response. *Nature cell biology*, 2(6):326–332, 2000.

[10] M. Bi, C. Naczki, M. Koritzinsky, D. Fels, J. Blais, N. Hu, H. Harding, I. Novoa, M. Varia, J. Raleigh, et al. ER stress-regulated translation increases tolerance to extreme hypoxia and promotes tumor growth. *The EMBO Journal*, 24(19):3470, 2005.

[11] M. Bi, C. Naczki, M. Koritzinsky, D. Fels, J. Blais, N. Hu, H. Harding, I. Novoa, M. Varia, J. Raleigh, et al. ER stress-regulated translation increases tolerance to extreme hypoxia and promotes tumor growth. *The EMBO Journal*, 24:3470–3481, 2005.

[12] N.E. Blachere, Z. Li, R.Y. Chandawarkar, R. Suto, N.S. Jaikaria, S. Basu, H. Udono, and P.K. Srivastava. Heat shock protein-peptide complexes, reconstituted in vitro, elicit peptide-specific cytotoxic T lymphocyte response and tumor immunity. *Journal of Experimental Medicine*, 186(8):1315–1322, 1997.

[13] S. Blass, A. Union, J. Raymackers, F. Schumann, U. Ungethum, S. Muller-Steinbach, F. De Keyser, J.M. Engel, and G.R. Burmester. The stress protein BiP is overexpressed and is a major B and T cell target in rheumatoid arthritis. *Arthritis & Rheumatism*, 44(4), 2001.

[14] M.P. Boldin, T.M. Goncharov, Y.V. Goltseve, and D. Wallach. Involvement of MACH, a Novel MORT1/FADD-Interacting Protease, in Fas/APO-1- and TNF Receptor–Induced Cell Death. *Cell*, 85(6):803–815, 1996.

[15] C.D. Bown, J.F. Wang, B. Chen, and L.T. Young. Regulation of ER stress proteins by valproate: therapeutic implications. *Bipolar Disorders*, 4(2):145–151, 2002.

[16] M. Boyce, K.F. Bryant, C. Jousse, K. Long, H.P. Harding, D. Scheuner, R.J. Kaufman, D. Ma, D.M. Coen, D. Ron, et al. A selective inhibitor of eIF2α dephosphorylation protects cells from ER stress, 2005.

[17] A. Bruhat, C. Jousse, V. Carraro, A.M. Reimold, M. Ferrara, and P. Fafournoux. Amino acids control mammalian gene transcription: activating transcription factor 2 is essential for the amino acid responsiveness of the CHOP promoter. *Molecular and Cellular Biology*, 20(19):7192–7204, 2000.

[18] J.S. Carew, S.T. Nawrocki, Y.V. Krupnik, K. Dunner, D.J. McConkey, M.J. Keating, and P. Huang. Targeting endoplasmic reticulum protein transport: a novel strategy to kill malignant B cells and overcome fludarabine resistance in CLL. *Blood*, 107(1):222–231, 2006.

[19] F. Cecconi, G. Alvarez-Bolado, BI Meyer, KA Roth, and P. Gruss. Apaf1 (CED-4 homolog) regulates programmed cell death in mammalian development. *Cell*, 94(6):727, 1998.

[20] X. Chen, J. Shen, and R. Prywes. The luminal domain of ATF6 senses endoplasmic reticulum (ER) stress and causes translocation of ATF6 from the ER to the Golgi. *Journal of Biological Chemistry*, 277(15):13045–13052, 2002.

[21] S. Cichon, S. Buervenich, G. Kirov, N. Akula, A. Dimitrova, E. Green, J. Schumacher, N. Klopp, T. Becker, S. Ohlraun, et al. Lack of support for a genetic association of the XBP1 promoter polymorphism with bipolar disorder in probands of European origin. *Nature genetics*, 36(8):783–783, 2004.

[22] P. Codogno and AJ Meijer. Autophagy and signaling: their role in cell survival and cell death. *Cell Death & Differentiation*, 12:1509–1518, 2005.

[23] MN Corradetti and KL Guan. Upstream of the mammalian target of rapamycin: do all roads pass through mTOR? *Oncogene*, 25(48):6347–6360, 2006.

[24] V.M. Corrigall, M.D. Bodman-Smith, M.S. Fife, B. Canas, L.K. Myers, P.H. Wooley, C. Soh, N.A. Staines, D.J.C. Pappin, S.E. Berlo, et al. The Human Endoplasmic Reticulum Molecular Chaperone BiP Is an Autoantigen for Rheumatoid Arthritis and Prevents the Induction of Experimental Arthritis 1. *The Journal of Immunology*, 166(3):1492–1498, 2001.

[25] J.S. Cox, C.E. Shamu, and P. Walter. Transcriptional induction of genes encoding endoplasmic reticulum resident proteins requires a transmembrane protein kinase. *CELL-CAMBRIDGE MA-*, 73:1197–1197, 1993.

[26] E. Craig, J.D. Oliver, H.L. Roderick, D.H. Llewellyn, and S. High. ERp57 functions as a subunit of specific complexes formed with the ER lectins calreticulin and calnexin. *Molecular biology of the cell*, 10(8):2573–2582, 1999.

[27] S.B. Cullinan and J.A. Diehl. PERK-dependent activation of Nrf2 contributes to redox homeostasis and cell survival following endoplasmic reticulum stress. *Journal of Biological Chemistry*, 279(19):20108, 2004.

[28] S.B. Cullinan, D. Zhang, M. Hannink, E. Arvisais, R.J. Kaufman, and J.A. Diehl. Nrf2 is a direct PERK substrate and effector of PERK-dependent cell survival. *Molecular and Cellular Biology*, 23(20):7198–7209, 2003.

[29] D.J. Davidson, C. Haskell, S. Majest, A. Kherzai, D.A. Egan, K.A. Walter, A. Schneider, E.F. Gubbins, L. Solomon, Z. Chen, et al. Kringle 5 of human

plasminogen induces apoptosis of endothelial and tumor cells through surface-expressed glucose-regulated protein 78, 2005.

[30] R.J. Davis. Signal transduction by the JNK group of MAP kinases. *Cell*, 103(2):239–252, 2000.

[31] T.M. Dawson and V.L. Dawson. Rare genetic mutations shed light on the pathogenesis of Parkinson disease, 2003.

[32] D. Decaudin, S. Geley, T. Hirsch, M. Castedo, P. Marchetti, A. Macho, R. Kofler, and G. Kroemer. Bcl-2 and Bcl-XL antagonize the mitochondrial dysfunction preceding nuclear apoptosis induced by chemotherapeutic agents. *Cancer Research*, 57(1):62–67, 1997.

[33] N. Demaurex and C. Distelhorst. CELL BIOLOGY: Apoptosis–the Calcium Connection, 2003.

[34] J. Deng, P.D. Lu, Y. Zhang, D. Scheuner, R.J. Kaufman, N. Sonenberg, H.P. Harding, and D. Ron. Translational repression mediates activation of nuclear factor kappa B by phosphorylated translation initiation factor 2. *Molecular and Cellular Biology*, 24(23):10161–10168, 2004.

[35] A. Deniaud et al. Endoplasmic reticulum stress induces calcium-dependent permeability transition, mitochondrial outer membrane permeabilization and apoptosis. *Oncogene*, 27(3):285–299, 2007.

[36] P. Dent, A. Yacoub, S. Grant, D.T. Curiel, and P.B. Fisher. MDA-7/IL-24 regulates proliferation, invasion and tumor cell radiosensitivity: A new cancer therapy? *Journal of cellular biochemistry*, 95(4), 2005.

[37] R.P. Dickinson and R.J. Gelinas. Sensitivity analysis of ordinary differential equation systems—a direct method. *J. Comput. Phys*, 21(2), 1976.

[38] C.W. Distelhorst and G.C. Shore. Bcl-2 and calcium: controversy beneath the surface. *Oncogene*, 23:2875–2880, 2004.

[39] D. Dong, L. Dubeau, J. Bading, K. Nguyen, M. Luna, H. Yu, G. Gazit-Bornstein, E.M. Gordon, C. Gomer, F.L. Hall, et al. Spontaneous and controllable activation of suicide gene expression driven by the stress-inducible grp78 promoter resulting in eradication of sizable human tumors. *Human gene therapy*, 15(6):553–561, 2004.

[40] L. Egger, J. Schneider, C. Rheme, M. Tapernoux, J. Häcki, and C. Borner. Serine proteases mediate apoptosis-like cell death and phagocytosis under caspase-inhibiting conditions. *Cell Death & Differentiation*, 10(10):1188–1203, 2003.

[41] L. Ellgaard and A. Helenius. Quality control in the endoplasmic reticulum. *Nature Reviews Molecular Cell Biology*, 4(3):181–191, 2003.

[42] L. Ellgaard, M. Molinari, and A. Helenius. Setting the standards: quality control in the secretory pathway. *Science*, 286(5446):1882, 1999.

[43] T.W. Fawcett, J.L. Martindale, K.Z. Guyton, T. Hai, and N.J. Holbrook. Complexes containing activating transcription factor (ATF)/cAMP-responsive-element-binding protein (CREB) interact with the CCAAT enhancer-binding protein (C/EBP)-ATF composite site to regulate Gadd153 expression during the stress response. *BIOCHEMICAL JOURNAL-LONDON-*, 339:135–141, 1999.

[44] C.M. Fonseca, P.J. Fleming, et al. Genetic algorithms for multiobjective optimization: Formulation, discussion and generalization. In *Proceedings of the fifth international conference on genetic algorithms*, volume 423. Citeseer, 1993.

[45] S.G. Fonseca, M. Fukuma, K.L. Lipson, L.X. Nguyen, J.R. Allen, Y. Oka, and F. Urano. WFS1 is a novel component of the unfolded protein response and maintains homeostasis of the endoplasmic reticulum in pancreatic {beta}-cells. *Journal of Biological Chemistry*, 280(47):39609, 2005.

[46] AM Fra, C. Fagioli, D. Finazzi, R. Sitia, and CM Alberini. Quality control of ER synthesized proteins: an exposed thiol group as a three-way switch mediating assembly, retention and degradation. *The EMBO Journal*, 12(12):4755, 1993.

[47] Y. Fu, J. Li, and A.S. Lee. GRP78/BiP inhibits endoplasmic reticulum BIK and protects human breast cancer cells against estrogen starvation-induced apoptosis. *Cancer Research*, 67(8):3734, 2007.

[48] T. Fujimoto, M. Onda, H. Nagai, T. Nagahata, K. Ogawa, and M. Emi. Up-regulation and overexpression of human X-box binding protein 1 (hXBP-1) gene in primary breast cancers. *Breast cancer*, 10(4):301–306, 2003.

[49] E. Fujita, Y. Kouroku, A. Isoai, H. Kumagai, A. Misutani, C. Matsuda, Y.K.

Hayashi, and T. Momoi. Two endoplasmic reticulum-associated degradation(ERAD) systems for the novel variant of the mutant dysferlin: ubiquitin/proteasome ERAD (I) and autophagy/lysosome ERAD (II). *Human Molecular Genetics*, 16(6):618, 2007.

[50] P.S. Gargalovic, N.M. Gharavi, M.J. Clark, J. Pagnon, W.P. Yang, A. He, A. Truong, T. Baruch-Oren, J.A. Berliner, T.G. Kirchgessner, et al. The unfolded protein response is an important regulator of inflammatory genes in endothelial cells. *Arteriosclerosis, thrombosis, and vascular biology*, 26(11):2490, 2006.

[51] J.J. Gills, J. LoPiccolo, J. Tsurutani, R.H. Shoemaker, C.J.M. Best, M.S. Abu-Asab, J. Borojerdi, N.A. Warfel, E.R. Gardner, M. Danish, et al. Nelfinavir, A lead HIV protease inhibitor, is a broad-spectrum, anticancer agent that induces endoplasmic reticulum stress, autophagy, and apoptosis in vitro and in vivo. *Clinical Cancer Research*, 13(17):5183, 2007.

[52] C.C. Glembotski. Endoplasmic reticulum stress in the heart. *Circulation Research*, 101(10):975, 2007.

[53] C.C. Glembotski. The role of the unfolded protein response in the heart. *Journal of Molecular and Cellular Cardiology*, 44(3):453–459, 2008.

[54] T. Gotoh, K. Terada, and M. Mori. hsp70-DnaJ chaperone pairs prevent nitric oxide-mediated apoptosis in RAW 264.7 macrophages.

[55] G. Guidotti, J.K. VanSlyke, S.M. Deschenes, and L.S. Musil. Intracellular transport, assembly, and degradation of wild-type and disease-linked mutant gap junction proteins. *Molecular Biology of the Cell*, 11(6):1933–1946, 2000.

[56] TW Hai, F. Liu, WJ Coukos, and MR Green. Transcription factor ATF cDNA clones: an extensive family of leucine zipper proteins able to selectively form DNA-binding heterodimers. *Genes & Development*, 3(12b):2083, 1989.

[57] R. HAKEM, A. HAKEM, GS DUNCAN, JT HENDERSON, M. WOO, MS SOENGAS, A. ELIA, JL DE LA POMPA, D. KAGI, W. KHOO, et al. DIFFERENTIAL REQUIREMENT FOR CASPASE 9 IN APOPTOTIC PATHWAYS IN VIVO. *Cell(Cambridge)*, 94(3):339–352, 1998.

[58] RB Hamanaka, E. Bobrovnikova-Marjon, X. Ji, SA Liebhaber, and

JA Diehl. PERK-dependent regulation of IAP translation during ER stress. *Oncogene*, 2008.

[59] G.K. Hansson. Inflammation, atherosclerosis, and coronary artery disease. *New England Journal of Medicine*, 352(16):1685–1695, 2005.

[60] H.P. Harding, I. Novoa, Y. Zhang, H. Zeng, R. Wek, M. Schapira, and D. Ron. Regulated translation initiation controls stress-induced gene expression in mammalian cells. *Molecular Cell*, 6(5):1099–1108, 2000.

[61] H.P. Harding, H. Zeng, Y. Zhang, R. Jungries, P. Chung, H. Plesken, D.D. Sabatini, and D. Ron. Diabetes mellitus and exocrine pancreatic dysfunction in perk-/- mice reveals a role for translational control in secretory cell survival. *Molecular Cell*, 7(6):1153–1163, 2001.

[62] H.P. Harding, Y. Zhang, A. Bertolotti, H. Zeng, and D. Ron. Perk is essential for translational regulation and cell survival during the unfolded protein response. *Molecular cell*, 5(5):897–904, 2000.

[63] H.P. Harding, Y. Zhang, and D. Ron. Protein translation and folding are coupled by an endoplasmic-reticulum-resident kinase. *Nature*, 397:271–274, 1999.

[64] H.P. Harding, Y. Zhang, H. Zeng, I. Novoa, P.D. Lu, M. Calfon, N. Sadri, C. Yun, B. Popko, R. Paules, et al. An integrated stress response regulates amino acid metabolism and resistance to oxidative stress. *Molecular cell*, 11(3):619–633, 2003.

[65] D.N. Hebert, B. Foellmer, and A. Helenius. Glucose trimming and reglucosylation determine glycoprotein association with calnexin in the endoplasmic reticulum. *Cell*, 81(3):425–434, 1995.

[66] A. Helenius, ES Trombetta, DN Hebert, and JF Simons. Calnexin, calreticulin and the folding of glycoproteins. *Trends in Cell Biology*, 7(5):193–200, 1997.

[67] R. Hellman, M. Vanhove, A. Lejeune, F.J. Stevens, and L.M. Hendershot. The in vivo association of BiP with newly synthesized proteins is dependent on the rate and stability of folding and not simply on the presence of sequences that can bind to BiP. *Journal of Cell Biology*, 144(1):21–30, 1999.

[68] LM Hendershot. The ER function BiP is a master regulator of ER function. *The Mount Sinai journal of medicine, New York*, 71(5):289, 2004.

[69] C. Hetz, P. Bernasconi, J. Fisher, A.H. Lee, M.C. Bassik, B. Antonsson, G.S. Brandt, N.N. Iwakoshi, A. Schinzel, L.H. Glimcher, et al. Proapoptotic BAX and BAK modulate the unfolded protein response by a direct interaction with IRE1α, 2006.

[70] T. Hiroi, H. Wei, C. Hough, P. Leeds, and DM Chuang. Protracted lithium treatment protects against the ER stress elicited by thapsigargin in rat PC12 cells: roles of intracellular calcium, GRP78 and Bcl-2. *The Pharmacogenomics Journal*, 5(2):102–111, 2005.

[71] J. Hitomi, T. Katayama, Y. Eguchi, T. Kudo, M. Taniguchi, Y. Koyama, T. Manabe, S. Yamagishi, Y. Bando, K. Imaizumi, et al. Involvement of caspase-4 in endoplasmic reticulum stress-induced apoptosis and A {beta}-induced cell death. *Journal of Cell Biology*, 2004.

[72] J. Hollien and J.S. Weissman. Decay of endoplasmic reticulum-localized mRNAs during the unfolded protein response, 2006.

[73] M. Hong, S. Luo, P. Baumeister, J.M. Huang, R.K. Gogia, M. Li, and A.S. Lee. Underglycosylation of ATF 6 as a Novel Sensing Mechanism for Activation of the Unfolded Protein Response. *Journal of Biological Chemistry*, 279(12):11354–11363, 2004.

[74] M. Høyer-Hansen, L. Bastholm, P. Szyniarowski, M. Campanella, G. Szabadkai, T. Farkas, K. Bianchi, N. Fehrenbacher, F. Elling, R. Rizzuto, et al. Control of macroautophagy by calcium, calmodulin-dependent kinase kinase-β, and Bcl-2. *Molecular cell*, 25(2):193–205, 2007.

[75] P. Hu, Z. Han, A.D. Couvillon, R.J. Kaufman, and J.H. Exton. Autocrine tumor necrosis factor alpha links endoplasmic reticulum stress to the membrane death receptor pathway through IRE1α-mediated NF-κB activation and down-regulation of TRAF2 expression. *Molecular and Cellular Biology*, 26(8):3071–3084, 2006.

[76] Y. Imai, M. Soda, and R. Takahashi. Parkin suppresses unfolded protein stress-induced cell death through its E3 ubiquitin-protein ligase activity, 2000.

[77] H. Ishihara, S. Takeda, A. Tamura, R. Takahashi, S. Yamaguchi, D. Takei, T. Yamada, H. Inoue, H. Soga, H. Katagiri, et al. Disruption of

the WFS1 gene in mice causes progressive β-cell loss and impaired stimulus-secretion coupling in insulin secretion. *Human Molecular Genetics*, 13(11):1159–1170, 2004.

[78] N.N. Iwakoshi, M. Pypaert, and L.H. Glimcher. The transcription factor XBP-1 is essential for the development and survival of dendritic cells. *Journal of Experimental Medicine*, 2007.

[79] C. Jamora, G. Dennert, and AS Lee. Inhibition of tumor progression by suppression of stress protein GRP78/BiP induction in fibrosarcoma B/C10ME. *Proceedings of the National Academy of Sciences of the United States of America*, 93(15):7690, 1996.

[80] C. Kakiuchi, M. Ishiwata, S. Nanko, H. Kunugi, Y. Minabe, K. Nakamura, N. Mori, K. Fujii, T. Umekage, M. Tochigi, et al. Functional polymorphisms of HSPA5: possible association with bipolar disorder. *Biochemical and Biophysical Research Communications*, 336(4):1136–1143, 2005.

[81] C. Kakiuchi, K. Iwamoto, M. Ishiwata, M. Bundo, T. Kasahara, I. Kusumi, T. Tsujita, Y. Okazaki, S. Nanko, H. Kunugi, et al. Impaired feedback regulation of XBP1 as a genetic risk factor for bipolar disorder. *Nature genetics*, 35(2):171–175, 2003.

[82] T. Kamimoto, S. Shoji, T. Hidvegi, N. Mizushima, K. Umebayashi, D.H. Perlmutter, and T. Yoshimori. Intracellular inclusions containing mutant {alpha} 1-antitrypsin Z are propagated in the absence of autophagic activity. *Journal of Biological Chemistry*, 281(7):4467, 2006.

[83] T. Katayama, K. Imaizumi, N. Sato, K. Miyoshi, T. Kudo, J. Hitomi, T. Morihara, T. Yoneda, F. Gomi, Y. Mori, et al. Presenilin-1 mutations downregulate the signalling pathway of the unfolded-protein response. *Nature Cell Biology*, 1:479–485, 1999.

[84] JF Kerr, AH Wyllie, and AR Currie. Apoptosis: a basic biological phenomenon with wide-ranging implications in tissue kinetics. *Br J Cancer*, 26(4):239–57, 1972.

[85] A. Khanna and R. Campbell. The gene G13 in the class III region of the human MHC encodes a potential DNA-binding protein. *Biochem. J*, 319:81–89, 1996.

[86] D.G. Kim, K.R. You, M.J. Liu, Y.K. Choi, and Y.S. Won. GADD153-mediated Anticancer Effects of N-(4-Hydroxyphenyl) retinamide on Hu-

man Hepatoma Cells. *Journal of Biological Chemistry*, 277(41):38930–38938, 2002.

[87] Y. Kimata, Y.I. Kimata, Y. Shimizu, H. Abe, I.C. Farcasanu, M. Takeuchi, M.D. Rose, and K. Kohno. Genetic evidence for a role of BiP/Kar2 that regulates Ire1 in response to accumulation of unfolded proteins. *Molecular biology of the cell*, 14(6):2559–2569, 2003.

[88] K. Kohno, K. Normington, J. Sambrook, MJ Gething, and K. Mori. The promoter region of the yeast KAR2 (BiP) gene contains a regulatory domain that responds to the presence of unfolded proteins in the endoplasmic reticulum. *Molecular and Cellular Biology*, 13(2):877–890, 1993.

[89] K. Kokame, H. Kato, and T. Miyata. Identification of ERSE-II, a new cis-acting element responsible for the ATF6-dependent mammalian unfolded protein response. *Journal of Biological Chemistry*, 276(12):9199–9205, 2001.

[90] M. Koritzinsky, M.G. Magagnin, T. van den Beucken, R. Seigneuric, K. Savelkouls, J. Dostie, S. Pyronnet, R.J. Kaufman, S.A. Weppler, J.W. Voncken, et al. Gene expression during acute and prolonged hypoxia is regulated by distinct mechanisms of translational control. *The EMBO Journal*, 25(5):1114, 2006.

[91] C. Koumenis, C. Naczki, M. Koritzinsky, S. Rastani, A. Diehl, N. Sonenberg, A. Koromilas, and B.G. Wouters. Regulation of protein synthesis by hypoxia via activation of the endoplasmic reticulum kinase PERK and phosphorylation of the translation initiation factor eIF2α. *Molecular and Cellular Biology*, 22(21):7405–7416, 2002.

[92] Y. Kouroku, E. Fujita, I. Tanida, T. Ueno, A. Isoai, H. Kumagai, S. Ogawa, RJ Kaufman, E. Kominami, and T. Momoi. ER stress (PERK/eIF2α phosphorylation) mediates the polyglutamine-induced LC3 conversion, an essential step for autophagy formation. *Cell Death & Differentiation*, 14(2):230–239, 2006.

[93] G. Kroemer and M. Jäättelä. Lysosomes and autophagy in cell death control. *Nature Reviews Cancer*, 5(11):886–897, 2005.

[94] T. Kudo, S. Kanemoto, H. Hara, N. Morimoto, T. Morihara, R. Kimura, T. Tabira, K. Imaizumi, and M. Takeda. A molecular chaperone inducer protects neurons from ER stress. *Cell Death & Differentiation*, 15(2):364–375, 2007.

[95] R. Kumar, S. Azam, J.M. Sullivan, C. Owen, D.R. Cavener, P. Zhang, D. Ron, H.P. Harding, J.J. Chen, A. Han, et al. Brain ischemia and reperfusion activates the eukaryotic initiation factor 2 [alpha] kinase, PERK. *Journal of neurochemistry*, 77(5):1418, 2001.

[96] H. Kyosuke, T. OKADA, H. YOSHIDA, H. YANAGI, T. YURA, M. NEGISHI, and M. Kazutoshi. Identification of the G13 (cAMP-response-element-binding protein-related protein) gene product related to activating transcription factor 6 as a transcriptional activator of the mammalian unfolded protein response. *Biochem. j*, 355:19–28, 2001.

[97] M. Lam, G. Dubyak, L. Chen, G. Nunez, RL Miesfeld, and CW Distelhorst. Evidence that BCL-2 represses apoptosis by regulating endoplasmic reticulum-associated Ca2+ fluxes. *Proceedings of the National Academy of Sciences*, 91(14):6569–6573, 1994.

[98] I.N. Lavrik, A. Golks, and P.H. Krammer. Caspases: pharmacological manipulation of cell death. *J. Clin. Invest*, 115(10):2665–2672, 2005.

[99] A.H. Lee, N.N. Iwakoshi, K.C. Anderson, and L.H. Glimcher. Proteasome inhibitors disrupt the unfolded protein response in myeloma cells. *Proceedings of the National Academy of Sciences*, 100(17):9946–9951, 2003.

[100] A.H. Lee, E.F. Scapa, D.E. Cohen, and L.H. Glimcher. Regulation of hepatic lipogenesis by the transcription factor XBP1. *Science*, 320(5882):1492, 2008.

[101] A.S. Lee. The glucose-regulated proteins: stress induction and clinical applications. *Trends in Biochemical Sciences*, 26(8):504–510, 2001.

[102] K. Lee, W. Tirasophon, X. Shen, M. Michalak, R. Prywes, T. Okada, H. Yoshida, K. Mori, and R.J. Kaufman. IRE1-mediated unconventional mRNA splicing and S2P-mediated ATF6 cleavage merge to regulate XBP1 in signaling the unfolded protein response. *Genes & development*, 16(4):452–466, 2002.

[103] K. Lei and R.J. Davis. JNK phosphorylation of Bim-related members of the Bcl2 family induces Bax-dependent apoptosis. *Proceedings of the National Academy of Sciences*, 100(5):2432–2437, 2003.

[104] B. Levine and D.J. Klionsky. Development by self-digestion molecular mechanisms and biological functions of autophagy. *Developmental cell*, 6(4):463–477, 2004.

[105] J. Li and AS Lee. Stress induction of GRP78/BiP and its role in cancer. *Current molecular medicine*, 6(1):45, 2006.

[106] J. Li, B. Lee, and A.S. Lee. Endoplasmic reticulum stress-induced apoptosis: multiple pathways and activation of p53-up-regulated modulator of apoptosis (PUMA) and NOXA by p53. *Journal of Biological Chemistry*, 281(11):7260, 2006.

[107] Y. Li, R.F. Schwabe, T. DeVries-Seimon, P.M. Yao, M.C. Gerbod-Giannone, A.R. Tall, R.J. Davis, R. Flavell, D.A. Brenner, and I. Tabas. Free cholesterol-loaded macrophages are an abundant source of tumor necrosis factor-{alpha} and interleukin-6: model of NF-{kappa} B-and MAP kinase-dependent inflammation in advanced atherosclerosis. *Journal of Biological Chemistry*, 280(23):21763, 2005.

[108] C.Y. Liu, H.N. Wong, J.A. Schauerte, and R.J. Kaufman. The protein kinase/endoribonuclease IRE1α that signals the unfolded protein response has a luminal N-terminal ligand-independent dimerization domain. *Journal of Biological Chemistry*, 277(21):18346–18356, 2002.

[109] C.Y. Liu, Z. Xu, and R.J. Kaufman. Structure and intermolecular interactions of the luminal dimerization domain of human IRE1α. *Journal of Biological Chemistry*, 278(20):17680–17687, 2003.

[110] Y. Liu, P. Choudhury, C.M. Cabral, and R.N. Sifers. Oligosaccharide modification in the early secretory pathway directs the selection of a misfolded glycoprotein for degradation by the proteasome. *Journal of Biological Chemistry*, 274(9):5861–5867, 1999.

[111] P.D. Lu, H.P. Harding, and D. Ron. Translation reinitiation at alternative open reading frames regulates gene expression in an integrated stress response. *The Journal of cell biology*, 167(1):27, 2004.

[112] Y. Ma and L.M. Hendershot. Delineation of a Negative Feedback Regulatory Loop That Controls Protein Translation during Endoplasmic Reticulum Stress*. *Journal of Biological Chemistry*, 278(37):34864–34873, 2003.

[113] J.D. Malhotra and R.J. Kaufman. The endoplasmic reticulum and the unfolded protein response. In *Seminars in Cell and Developmental Biology*, volume 18, pages 716–731. Elsevier, 2007.

[114] J.J. Martindale, R. Fernandez, D. Thuerauf, R. Whittaker, N. Gude, M.A.

Sussman, and C.C. Glembotski. Endoplasmic reticulum stress gene induction and protection from ischemia/reperfusion injury in the hearts of transgenic mice with a tamoxifen-regulated form of ATF6, 2006.

[115] J. Mathers, JA Fraser, M. McMahon, RD Saunders, JD Hayes, and LI McLellan. Antioxidant and cytoprotective responses to redox stress. In *Biochemical Society symposium*, number 71, page 157, 2004.

[116] J. Matsukawa, A. Matsuzawa, K. Takeda, and H. Ichijo. The ASK1-MAP kinase cascades in mammalian stress response. *Journal of Biochemistry*, 136(3):261, 2004.

[117] M. Matsumoto, M. Minami, K. Takeda, Y. Sakao, and S. Akira. Ectopic expression of CHOP (GADD153) induces apoptosis in M1 myeloblastic leukemia cells. *FEBS letters*, 395(2-3):143–147, 1996.

[118] E.V. Maytin, M. Ubeda, J.C. Lin, and J.F. Habener. Stress-inducible transcription factor CHOP/gadd153 induces apoptosis in mammalian cells via p38 kinase-dependent and-independent mechanisms. *Experimental Cell Research*, 267(2):193–204, 2001.

[119] AA McCracken and JL Brodsky. Assembly of ER-associated protein degradation in vitro: dependence on cytosol, calnexin, and ATP. *Journal of Cell Biology*, 132(3):291–298, 1996.

[120] K.D. McCullough, J.L. Martindale, L.O. Klotz, T.Y. Aw, and N.J. Holbrook. Gadd153 sensitizes cells to endoplasmic reticulum stress by down-regulating Bcl2 and perturbing the cellular redox state. *Molecular and Cellular Biology*, 21(4):1249–1259, 2001.

[121] A.J. Meijer and P. Codogno. Signalling and autophagy regulation in health, aging and disease. *Molecular Aspects of Medicine*, 27(5-6):411–425, 2006.

[122] O. Milhavet, J.L. Martindale, S. Camandola, S.L. Chan, D.S. Gary, A. Cheng, N.J. Holbrook, and M.P. Mattson. Involvement of Gadd153 in the pathogenic action of presenilin-1 mutations. *Journal of neurochemistry*, 83(3):673, 2002.

[123] J. Min, H. Shukla, H. Kozono, S.K. Bronson, S.M. Weissman, and D.D. Chaplin. A novel Creb family gene telomeric of HLA-DRA in the HLA complex. *Genomics*, 30(2):149–156, 1995.

[124] Y. Minami, A.M. Weissman, L.E. Samelson, and R.D. Klausner. Building a multichain receptor: synthesis, degradation, and assembly of the T-cell antigen receptor. *Proceedings of the National Academy of Sciences*, 84(9):2688–2692, 1987.

[125] U.K. Misra, R. Deedwania, and S.V. Pizzo. Activation and cross-talk between Akt, NF-{kappa} B, and unfolded protein response signaling in 1-LN prostate cancer cells consequent to ligation of cell surface-associated GRP78. *Journal of Biological Chemistry*, 281(19):13694, 2006.

[126] M. Muzio, B.R. Stockwell, H.R. Stennicke, G.S. Salvesen, and V.M. Dixit. An Induced Proximity Model for Caspase-8 Activation. *Journal of Biological Chemistry*, 273(5):2926–2930, 1998.

[127] S. NAGATA. APOPTOSIS BY DEATH FACTOR. *Cell(Cambridge)*, 88(3):355–365, 1997.

[128] K. Nakamura, E. Bossy-Wetzel, K. Burns, M.P. Fadel, M. Lozyk, I.S. Goping, M. Opas, R.C. Bleackley, D.R. Green, and M. Michalak. Changes in Endoplasmic Reticulum Luminal Environment Affect Cell Sensitivity to Apoptosis. *The Journal of Cell Biology*, 150(4):731–740, 2000.

[129] S.T. Nawrocki, J.S. Carew, K. Dunner, L.H. Boise, P.J. Chiao, P. Huang, J.L. Abbruzzese, and D.J. McConkey. Bortezomib inhibits PKR-like endoplasmic reticulum (ER) kinase and induces apoptosis via ER stress in human pancreatic cancer cells, 2005.

[130] K. Neubert, S. Meister, K. Moser, F. Weisel, D. Maseda, K. Amann, C. Wiethe, T.H. Winkler, J.R. Kalden, R.A. Manz, et al. The proteasome inhibitor bortezomib depletes plasma cells and protects mice with lupus-like disease from nephritis. 2008.

[131] P. Nickson, A. Toth, and P. Erhardt. PUMA is critical for neonatal cardiomyocyte apoptosis induced by endoplasmic reticulum stress. *Cardiovascular research*, 73(1):48, 2007.

[132] P. Nicotera and S. Orrenius. The role of calcium in apoptosis. *Cell Calcium*, 23(2-3):173–180, 1998.

[133] H. Nishitoh, H. Kadowaki, A. Nagai, T. Maruyama, T. Yokota, H. Fukutomi, T. Noguchi, A. Matsuzawa, K. Takeda, and H. Ichijo. ALS-linked mutant SOD1 induces ER stress-and ASK1-dependent motor neuron death by targeting Derlin-1. *Genes & Development*, 22(11):1451, 2008.

[134] H. Nishitoh, A. Matsuzawa, K. Tobiume, K. Saegusa, K. Takeda, K. Inoue, S. Hori, A. Kakizuka, and H. Ichijo. ASK1 is essential for endoplasmic reticulum stress-induced neuronal cell death triggered by expanded polyglutamine repeats. *Genes & development*, 16(11):1345–1355, 2002.

[135] M. Niwa, C. Sidrauski, R.J. Kaufman, and P. Walter. A role for presenilin-1 in nuclear accumulation of Ire 1 fragments and induction of the mammalian unfolded protein response. *CELL-CAMBRIDGE MA-*, 99(7):691–702, 1999.

[136] T. Noda and Y. Ohsumi. Tor, a phosphatidylinositol kinase homologue, controls autophagy in yeast. *Journal of Biological Chemistry*, 273(7):3963–3966, 1998.

[137] M. Ogata, S. Hino, A. Saito, K. Morikawa, S. Kondo, S. Kanemoto, T. Murakami, M. Taniguchi, I. Tanii, K. Yoshinaga, et al. Autophagy Is Activated for Cell Survival after Endoplasmic Reticulum Stress. *Molecular and Cellular Biology*, 26(24):9220, 2006.

[138] K. Okada, T. Minamino, Y. Tsukamoto, Y. Liao, O. Tsukamoto, S. Takashima, A. Hirata, M. Fujita, Y. Nagamachi, T. Nakatani, et al. Prolonged Endoplasmic Reticulum Stress in Hypertrophic and Failing Heart After Aortic Constriction Possible Contribution of Endoplasmic Reticulum Stress to Cardiac Myocyte Apoptosis, 2004.

[139] K. Okamura, Y. Kimata, H. Higashio, A. Tsuru, and K. Kohno. Dissociation of Kar2p/BiP from an ER sensory molecule, Ire1p, triggers the unfolded protein response in yeast. *Biochemical and biophysical research communications*, 279(2):445–450, 2000.

[140] J.D. Oliver, F.J. van der Wal, N.J. Bulleid, and S. High. Interaction of the thiol-dependent reductase ERp57 with nascent glycoproteins. *Science*, 275(5296):86, 1997.

[141] Y. Omori, J. Imai, M. Watanabe, T. Komatsu, Y. Suzuki, K. Kataoka, S. Watanabe, A. Tanigami, and S. Sugano. CREB-H: a novel mammalian transcription factor belonging to the CREB/ATF family and functioning via the box-B element with a liver-specific expression. *Nucleic Acids Research*, 29(10):2154, 2001.

[142] S. Oyadomari, A. Koizumi, K. Takeda, T. Gotoh, S. Akira, E. Araki, and M. Mori. Targeted disruption of the Chop gene delays endoplasmic retic-

ulum stress-mediated diabetes. *Journal of Clinical Investigation*, 109(4):525–532, 2002.

[143] S. Oyadomari, K. Takeda, M. Takiguchi, T. Gotoh, M. Matsumoto, I. Wada, S. Akira, E. Araki, and M. Mori. Nitric oxide-induced apoptosis in pancreatic β cells is mediated by the endoplasmic reticulum stress pathway. *Proceedings of the National Academy of Sciences*, 98(19):10845, 2001.

[144] U. Ozcan, Q. Cao, E. Yilmaz, A.H. Lee, N.N. Iwakoshi, E. Ozdelen, G. Tuncman, C. Gorgun, L.H. Glimcher, and G.S. Hotamisligil. Endoplasmic reticulum stress links obesity, insulin action, and type 2 diabetes. *Science*, 306(5695):457–461, 2004.

[145] Y.X. Pan, L. Lin, A.J. Ren, X.J. Pan, H. Chen, C.S. Tang, and W.J. Yuan. HSP70 and GRP78 Induced by Endothelin-1 Pretreatment Enhance Tolerance to Hypoxia in Cultured Neonatal Rat Cardiomyocytes. *Journal of Cardiovascular Pharmacology*, 44:S117, 2004.

[146] F.R. Papa, C. Zhang, K. Shokat, and P. Walter. Bypassing a kinase activity with an ATP-competitive drug. *Science*, 302(5650):1533–1537, 2003.

[147] D.N.C.H. Park. Multiobjective simulated annealing: a comparative study to evolutionary algorithms, 2002.

[148] H.R. Park, A. Tomida, S. Sato, Y. Tsukumo, J. Yun, T. Yamori, Y. Hayakawa, T. Tsuruo, and K. Shin-ya. Effect on tumor cells of blocking survival response to glucose deprivation. *jnci*, 96(17):1300–1310, 2004.

[149] A.J. Parodi. P ROTEIN G LUCOSYLATION AND I TS R OLE IN P ROTEIN F OLDING. *Annual Review of Biochemistry*, 69(1):69–93, 2000.

[150] W. Paschen, C. Gissel, T. Linden, S. Althausen, and J. Doutheil. Activation of gadd153 expression through transient cerebral ischemia: evidence that ischemia causes endoplasmic reticulum dysfunction. *Molecular Brain Research*, 60(1):115–122, 1998.

[151] L. Petrucelli, C. O'Farrell, P.J. Lockhart, M. Baptista, K. Kehoe, L. Vink, P. Choi, B. Wolozin, M. Farrer, J. Hardy, et al. Parkin protects against the toxicity associated with mutant α-synuclein proteasome dysfunction selectively affects catecholaminergic neurons. *Neuron*, 36(6):1007–1019, 2002.

[152] LR Phillips, TL Wolfe, L. Malspeis, and JG Supko. Analysis of brefeldin A and the prodrug breflate in plasma by gas chromatography with mass selective detection. *Journal of pharmaceutical and biomedical analysis*, 16(8):1301–1309, 1998.

[153] P. Pinton, D. Ferrari, E. Rapizzi, F. Di Virgilio, T. Pozzan, and R. Rizzuto. The Ca 2 concentration of the endoplasmic reticulum is a key determinant of ceramide-induced apoptosis: significance for the molecular mechanism of Bcl-2 action. *The EMBO Journal*, 20:2690–2701, 2001.

[154] G.V. Putcha, S. Le, S. Frank, C.G. Besirli, K. Clark, B. Chu, S. Alix, R.J. Youle, A. LaMarche, A.C. Maroney, et al. JNK-mediated BIM phosphorylation potentiates BAX-dependent apoptosis. *Neuron*, 38(6):899–914, 2003.

[155] P. Pyrko, A. Kardosh, W. Wang, W. Xiong, A.H. Schonthal, and T.C. Chen. HIV-1 protease inhibitors nelfinavir and atazanavir induce malignant glioma death by triggering endoplasmic reticulum stress. *Cancer Research*, 67(22):10920, 2007.

[156] S. Raha and B.H. Robinson. Mitochondria, oxygen free radicals, disease and ageing. *Trends in Biochemical Sciences*, 25(10):502–508, 2000.

[157] A.C. Ranganathan, L. Zhang, A.P. Adam, and J.A. Aguirre-Ghiso. Functional coupling of p38-induced up-regulation of BiP and activation of RNA-dependent protein kinase-like endoplasmic reticulum kinase to drug resistance of dormant carcinoma cells, 2006.

[158] R.V. Rao and D.E. Bredesen. Misfolded proteins, endoplasmic reticulum stress and neurodegeneration. *Current opinion in cell biology*, 16(6):653–662, 2004.

[159] R.V. Rao, S. Castro-Obregon, H. Frankowski, M. Schuler, V. Stoka, G. del Rio, D.E. Bredesen, and H.M. Ellerby. Coupling Endoplasmic Reticulum Stress to the Cell Death Program AN Apaf-1-INDEPENDENT INTRINSIC PATHWAY. *Journal of Biological Chemistry*, 277(24):21836–21842, 2002.

[160] R.K. Reddy, C. Mao, P. Baumeister, R.C. Austin, R.J. Kaufman, and A.S. Lee. Endoplasmic Reticulum Chaperone Protein GRP78 Protects Cells from Apoptosis Induced by Topoisomerase Inhibitors ROLE OF ATP BINDING SITE IN SUPPRESSION OF CASPASE-7 ACTIVATION*. *Journal of Biological Chemistry*, 278(23):20915–20924, 2003.

[161] S. Reijonen, N. Putkonen, A. Nørremølle, D. Lindholm, and L. Korhonen. Inhibition of endoplasmic reticulum stress counteracts neuronal cell death and protein aggregation caused by N-terminal mutant huntingtin proteins. *Experimental Cell Research*, 2008.

[162] A.M. Reimold, N.N. Iwakoshi, J. Manis, P. Vallabhajosyula, E. Szomolanyi-Tsuda, E.M. Gravallese, D. Friend, M.J. Grusby, F. Alt, and L.H. Glimcher. Plasma cell differentiation requires the transcription factor XBP-1. *Nature*, 412:300–307, 2001.

[163] J. Rius, M. Guma, C. Schachtrup, K. Akassoglou, A.S. Zinkernagel, V. Nizet, R.S. Johnson, G.G. Haddad, and M. Karin. NF-&kgr; B links innate immunity to the hypoxic response through transcriptional regulation of HIF-1&agr. *Nature*, 453(7196):807–811, 2008.

[164] L. Romero-Ramirez, H. Cao, D. Nelson, E. Hammond, A.H. Lee, H. Yoshida, K. Mori, L.H. Glimcher, N.C. Denko, A.J. Giaccia, et al. XBP1 is essential for survival under hypoxic conditions and is required for tumor growth, 2004.

[165] D. Ron and JF Habener. CHOP, a novel developmentally regulated nuclear protein that dimerizes with transcription factors C/EBP and LAP and functions as a dominant-negative inhibitor of gene transcription. *Genes & Development*, 6(3):439–453, 1992.

[166] E.J. Ryu, H.P. Harding, J.M. Angelastro, O.V. Vitolo, D. Ron, and L.A. Greene. Endoplasmic reticulum stress and the unfolded protein response in cellular models of Parkinson's disease. *Journal of Neuroscience*, 22(24):10690, 2002.

[167] D.M. Sabatini. mTOR and cancer: insights into a complex relationship. *Nature Reviews Cancer*, 6(9):729–734, 2006.

[168] D. Scheuner, B. Song, E. McEwen, C. Liu, R. Laybutt, P. Gillespie, T. Saunders, S. Bonner-Weir, and R.J. Kaufman. Translational control is required for the unfolded protein response and in vivo glucose homeostasis. *Molecular Cell*, 7(6):1165–1176, 2001.

[169] J.D. Schrag, J.J.M. Bergeron, Y. Li, S. Borisova, M. Hahn, D.Y. Thomas, and M. Cygler. The structure of calnexin, an ER chaperone involved in quality control of protein folding. *Molecular Cell*, 8(3):633–644, 2001.

[170] L. Scorrano, S.A. Oakes, J.T. Opferman, E.H. Cheng, M.D. Sorcinelli, T. Pozzan, and S.J. Korsmeyer. BAX and BAK regulation of endoplasmic reticulum Ca2+: a control point for apoptosis, 2003.

[171] CE Shamu and P. Walter. Oligomerization and phosphorylation of the Ire1p kinase during intracellular signaling from the endoplasmic reticulum to the nucleus. *The EMBO Journal*, 15(12):3028, 1996.

[172] L. Shao, X. Sun, L. Xu, L.T. Young, and J.F. Wang. Mood stabilizing drug lithium increases expression of endoplasmic reticulum stress proteins in primary cultured rat cerebral cortical cells. *Life Sciences*, 78(12):1317–1323, 2006.

[173] J. Shen, X. Chen, L. Hendershot, and R. Prywes. ER stress regulation of ATF6 localization by dissociation of BiP/GRP78 binding and unmasking of Golgi localization signals. *Developmental Cell*, 3(1):99–111, 2002.

[174] J. Shen and R. Prywes. Dependence of site-2 protease cleavage of ATF6 on prior site-1 protease digestion is determined by the size of the luminal domain of ATF6. *Journal of Biological Chemistry*, 279(41):43046, 2004.

[175] J. Shen, E.L. Snapp, J. Lippincott-Schwartz, and R. Prywes. Stable binding of ATF6 to BiP in the endoplasmic reticulum stress response. *Molecular and Cellular Biology*, 25(3):921–932, 2005.

[176] X. Shen, R.E. Ellis, K. Lee, C.Y. Liu, K. Yang, A. Solomon, H. Yoshida, R. Morimoto, D.M. Kurnit, K. Mori, et al. Complementary signaling pathways regulate the unfolded protein response and are required for C. elegans development. *Cell*, 107(7):893–903, 2001.

[177] PR Shepherd, G. Salvesen, T. Xu-Beijing, A. Toker, RA Anderson, J. Arino, J. Backer, J. Blank, M. Bogoyevitch, B. Brune, et al. Distinct roles of activating transcription factor 6 (ATF6) and double-stranded RNA-activated protein kinase-like endoplasmic reticulum kinase (PERK) in transcription during the mammalian unfolded protein response. *Biochem. J*, 366:585–594, 2002.

[178] Y. Shi, J. An, J. Liang, S.E. Hayes, G.E. Sandusky, L.E. Stramm, and N.N. Yang. Characterization of a mutant pancreatic eIF-2α kinase, PEK, and co-localization with somatostatin in islet delta cells. *Journal of Biological Chemistry*, 274(9):5723–5730, 1999.

[179] Y. Shi, K.M. Vattem, R. Sood, J. An, J. Liang, L. Stramm, and R.C. Wek. Identification and characterization of pancreatic eukaryotic initiation factor 2 α-subunit kinase, PEK, involved in translational control. *Molecular and Cellular Biology*, 18(12):7499–7509, 1998.

[180] K. Shintani-Ishida, M. Nakajima, K. Uemura, and K. Yoshida. Ischemic preconditioning protects cardiomyocytes against ischemic injury by inducing GRP78. *Biochemical and Biophysical Research Communications*, 345(4):1600–1605, 2006.

[181] M. Shuda, N. Kondoh, N. Imazeki, K. Tanaka, T. Okada, K. Mori, A. Hada, M. Arai, T. Wakatsuki, O. Matsubara, et al. Activation of the ATF 6, XBP 1 and grp 78 genes in human hepatocellular carcinoma: a possible involvement of the ER stress pathway in hepatocarcinogenesis. *Journal of hepatology*, 38(5):605–614, 2003.

[182] C. Sidrauski and P. Walter. The transmembrane kinase Ire1p is a site-specific endonuclease that initiates mRNA splicing in the unfolded protein response. *Cell*, 90(6):1031–1040, 1997.

[183] P. Silver, K. Haze, H. Yoshida, H. Yanagi, T. Yura, and K. Mori. Mammalian transcription factor ATF6 is synthesized as a transmembrane protein and activated by proteolysis in response to endoplasmic reticulum stress. *Molecular Biology of the Cell*, 10(11):3787–3799, 1999.

[184] KI Smith, RM Everson, and JE Fieldsend. Dominance measures for multi-objective simulated annealing. In *Evolutionary Computation, 2004. CEC2004. Congress on*, volume 1, 2004.

[185] J. Stelling, U. Sauer, Z. Szallasi, F.J. Doyle, and J. Doyle. Robustness of cellular functions. *Cell*, 118(6):675–685, 2004.

[186] S. Tajiri, S. Oyadomari, S. Yano, M. Morioka, T. Gotoh, JI Hamada, Y. Ushio, and M. Mori. Ischemia-induced neuronal cell death is mediated by the endoplasmic reticulum stress pathway involving CHOP. *Cell Death & Differentiation*, 11(4):403–415, 2004.

[187] R. TAKAHASHI, Y. IMAI, N. HATTORI, and Y. MIZUNO. Parkin and endoplasmic reticulum stress. *Annals of the New York Academy of Sciences*, 991(1 PARKINSON'S DISEASE The Life Cycle of the Dopamine Neuron):101–106, 2003.

[188] S. Tanaka, T. Uehara, and Y. Nomura. Up-regulation of protein-disulfide isomerase in response to hypoxia/brain ischemia and its protective effect against apoptotic cell death. *Journal of Biological Chemistry*, 275(14):10388–10393, 2000.

[189] F. Terro, C. Czech, F. Esclaire, W. Elyaman, C. Yardin, M.C. Baclet, N. Touchet, G. Tremp, L. Pradier, and J. Hugon. Neurons overexpressing mutant presenilin-1 are more sensitive to apoptosis induced by endoplasmic reticulum-Golgi stress. *Journal of neuroscience research*, 69(4), 2002.

[190] M.J. Thomenius and C.W. Distelhorst. Bcl-2 on the endoplasmic reticulum: protecting the mitochondria from a distance, 2003.

[191] N.A. Thornberry and Y. Lazebnik. Caspases: enemies within. *Science*, 281(5381):1312, 1998.

[192] D.J. Thuerauf, M. Marcinko, P.J. Belmont, and C.C. Glembotski. Effects of the Isoform-specific Characteristics of ATF6 {alpha} and ATF6beta on Endoplasmic Reticulum Stress Response Gene Expression and Cell Viability. *Journal of Biological Chemistry*, 282(31):22865, 2007.

[193] D.J. Thuerauf, M. Marcinko, N. Gude, M. Rubio, M.A. Sussman, and C.C. Glembotski. Activation of the unfolded protein response in infarcted mouse heart and hypoxic cultured cardiac myocytes. *Circulation research*, 99(3):275, 2006.

[194] D.J. Thuerauf, L. Morrison, and C.C. Glembotski. Opposing Roles for ATF 6 {alpha} and ATF 6 {beta} in Endoplasmic Reticulum Stress Response Gene Induction. *Journal of Biological Chemistry*, 279(20):21078–21084, 2004.

[195] W. Tirasophon, A.A. Welihinda, and R.J. Kaufman. A stress response pathway from the endoplasmic reticulum to the nucleus requires a novel bifunctional protein kinase/endoribonuclease (Ire1p) in mammalian cells. *Genes & development*, 12(12):1812–1824, 1998.

[196] K. Tobiume, A. Matsuzawa, T. Takahashi, H. Nishitoh, K. Morita, K. Takeda, O. Minowa, K. Miyazono, T. Noda, and H. Ichijo. ASK1 is required for sustained activations of JNK/p38 MAP kinases and apoptosis. *EMBO reports*, 2(3):222, 2001.

[197] D.J. Todd, A.H. Lee, and L.H. Glimcher. The endoplasmic reticulum stress response in immunity and autoimmunity. *Nature Reviews Immunology*, 8(9):663–674, 2008.

[198] A. Toth, J.R. Jeffers, P. Nickson, J.Y. Min, J.P. Morgan, G.P. Zambetti, and P. Erhardt. Targeted deletion of Puma attenuates cardiomyocyte death and improves cardiac function during ischemia-reperfusion. *AJP-Heart and Circulatory Physiology*, 291(1):H52, 2006.

[199] B.P. Tu and J.S. Weissman. The FAD-and O2-dependent reaction cycle of Ero1-mediated oxidative protein folding in the endoplasmic reticulum. *Molecular cell*, 10(5):983–994, 2002.

[200] B.P. Tu and J.S. Weissman. Oxidative protein folding in eukaryotes: mechanisms and consequences. *Journal of Cell Biology*, 164(3):341, 2004.

[201] M. Ubeda and J.F. Habener. CHOP gene expression in response to endoplasmic-reticular stress requires NFY interaction with different domains of a conserved DNA-binding element. *Nucleic Acids Research*, 28(24):4987, 2000.

[202] U. Unterberger, R. Höftberger, E. Gelpi, H. Flicker, H. Budka, and T. Voigtländer. Endoplasmic reticulum stress features are prominent in Alzheimer disease but not in prion diseases in vivo. *Journal of neuropathology and experimental neurology*, 65(4):348, 2006.

[203] F. Urano, X.Z. Wang, A. Bertolotti, Y. Zhang, P. Chung, H.P. Harding, and D. Ron. Coupling of stress in the ER to activation of JNK protein kinases by transmembrane protein kinase IRE1. *Science's STKE*, 287(5453):664, 2000.

[204] K.M. Vattem and R.C. Wek. Reinitiation involving upstream ORFs regulates ATF4 mRNA translation in mammalian cells. *Proceedings of the National Academy of Sciences*, 101(31):11269–11274, 2004.

[205] S.S. Vembar and J.L. Brodsky. One step at a time: endoplasmic reticulum-associated degradation. *Nature Reviews Molecular Cell Biology*, 9(12):944–957, 2008.

[206] RI Viner, DA Ferrington, TD Williams, DJ Bigelow, and C. Schöneich. Protein modification during biological aging: selective tyrosine nitration of the SERCA2a isoform of the sarcoplasmic reticulum Ca2+-ATPase in skeletal muscle. *Biochemical Journal*, 340(Pt 3):657, 1999.

[207] M. Vitadello, D. Penzo, V. Petronilli, G. Michieli, S. Gomirato, R. MENABO', F. Di Lisa, and L. Gorza. Overexpression of the stress pro-

tein Grp94 reduces cardiomyocyte necrosis due to calcium overload and simulated ischemia 1, 2003.

[208] H.G. Wang, N. Pathan, I.M. Ethell, S. Krajewski, Y. Yamaguchi, F. Shibasaki, F. McKeon, T. Bobo, T.F. Franke, and J.C. Reed. Ca2+-induced apoptosis through calcineurin dephosphorylation of BAD. *Science*, 284(5412):339, 1999.

[209] XZ Wang, HP Harding, Y. Zhang, EM Jolicoeur, M. Kuroda, and D. Ron. Cloning of mammalian Ire1 reveals diversity in the ER stress responses. *The EMBO Journal*, 17(19):5708, 1998.

[210] X.Z. Wang and D. Ron. Stress-induced phosphorylation and activation of the transcription factor CHOP (GADD153) by p38 MAP kinase. *Science*, 272(5266):1347.

[211] Y. Wang, J. Shen, N. Arenzana, W. Tirasophon, R.J. Kaufman, and R. Prywes. Activation of ATF6 and an ATF6 DNA binding site by the endoplasmic reticulum stress response. *Journal of Biological Chemistry*, 275(35):27013–27020, 2000.

[212] F.E. Ware, A. Vassilakos, P.A. Peterson, M.R. Jackson, M.A. Lehrman, and D.B. Williams. The molecular chaperone calnexin binds Glc (1) Man (9) GlcNAc (2) oligosaccharide as an initial step in recognizing unfolded glycoproteins. *Journal of Biological Chemistry*, 270(9):4697, 1995.

[213] A. Weiss, J. Schlessinger, R.J. Salmond, and D.R. Alexander. Switching signals on or off by receptor dimerization. *Biophysical Journal*, 94(3):277–280, 1998.

[214] A.A. Welihinda and R.J. Kaufman. The unfolded protein response pathway in Saccharomyces cerevisiae. Oligomerization and transphosphorylation of Ire1p (Ern1p) are required for kinase activation. *Journal of Biological Chemistry*, 271(30):18181, 1996.

[215] J. Wu, D.T. Rutkowski, M. Dubois, J. Swathirajan, T. Saunders, J. Wang, B. Song, G.D.Y. Yau, and R.J. Kaufman. ATF6α optimizes long-term endoplasmic reticulum function to protect cells from chronic stress. *Developmental Cell*, 13(3):351–364, 2007.

[216] K.Y. Xu, D.L. Huso, T.M. Dawson, D.S. Bredt, and L.C. Becker. Nitric oxide synthase in cardiac sarcoplasmic reticulum, 1999.

[217] L. Xu, J.P. Eu, G. Meissner, and J.S. Stamler. Activation of the cardiac calcium release channel (ryanodine receptor) by poly-S-nitrosylation. *Science*, 279(5348):234, 1998.

[218] T. Yamada, H. Ishihara, A. Tamura, R. Takahashi, S. Yamaguchi, D. Takei, A. Tokita, C. Satake, F. Tashiro, H. Katagiri, et al. WFS1-deficiency increases endoplasmic reticulum stress, impairs cell cycle progression and triggers the apoptotic pathway specifically in pancreatic β-cells. *Human Molecular Genetics*, 15(10):1600–1609, 2006.

[219] O. Yamaguchi, Y. Higuchi, S. Hirotani, K. Kashiwase, H. Nakayama, S. Hikoso, T. Takeda, T. Watanabe, M. Asahi, M. Taniike, et al. Targeted deletion of apoptosis signal-regulating kinase 1 attenuates left ventricular remodeling. *Proceedings of the National Academy of Sciences*, 100(26):15883–15888, 2003.

[220] K. Yamamoto, H. Ichijo, and S.J. Korsmeyer. BCL-2 is phosphorylated and inactivated by an ASK1/Jun N-terminal protein kinase pathway normally activated at G2/M. *Molecular and Cellular Biology*, 19(12):8469–8478, 1999.

[221] K. Yamamoto, T. Sato, T. Matsui, M. Sato, T. Okada, H. Yoshida, A. Harada, and K. Mori. Transcriptional Induction of Mammalian ER Quality Control Proteins Is Mediated by Single or Combined Action of ATF6α and XBP1. *Developmental Cell*, 13(3):365–376, 2007.

[222] J. Ye, R.B. Rawson, R. Komuro, X. Chen, U.P. Davé, R. Prywes, M.S. Brown, and J.L. Goldstein. ER stress induces cleavage of membrane-bound ATF6 by the same proteases that process SREBPs. *Molecular cell*, 6(6):1355–1364, 2000.

[223] T. Yoneda, K. Imaizumi, K. Oono, D. Yui, F. Gomi, T. Katayama, and M. Tohyama. Activation of caspase-12, an endoplastic reticulum (ER) resident caspase, through tumor necrosis factor receptor-associated factor 2-dependent mechanism in response to the ER stress. *Journal of Biological Chemistry*, 276(17):13935–13940, 2001.

[224] T. Yorimitsu, U. Nair, Z. Yang, and D.J. Klionsky. Endoplasmic reticulum stress triggers autophagy. *Journal of Biological Chemistry*, 281(40):30299, 2006.

[225] H. Yoshida. ER stress and diseases. *FEBS Journal*, 274(3):630–658, 2007.

[226] H. Yoshida, K. Haze, H. Yanagi, T. Yura, and K. Mori. Identification of the cis-acting endoplasmic reticulum stress response element responsible for transcriptional induction of mammalian glucose-regulated proteins involvement of basic leucine zipper transcription factors. *Journal of Biological Chemistry*, 273(50):33741–33749, 1998.

[227] H. Yoshida, T. Matsui, A. Yamamoto, T. Okada, and K. Mori. XBP1 mRNA is induced by ATF6 and spliced by IRE1 in response to ER stress to produce a highly active transcription factor. *Cell*, 107(7):881–891, 2001.

[228] H. Yoshida, T. Okada, K. Haze, H. Yanagi, T. Yura, M. Negishi, and K. Mori. ATF6 activated by proteolysis binds in the presence of NF-Y (CBF) directly to the cis-acting element responsible for the mammalian unfolded protein response. *Molecular and Cellular Biology*, 20(18):6755–6767, 2000.

[229] H. Yoshida, M. Oku, M. Suzuki, and K. Mori. pXBP1 (U) encoded in XBP1 pre-mRNA negatively regulates unfolded protein response activator pXBP1 (S) in mammalian ER stress response. *Journal of Cell Biology*, 172(4):565, 2006.

[230] C. Zhang, J. Kawauchi, M.T. Adachi, Y. Hashimoto, S. Oshiro, T. Aso, and S. Kitajima. Activation of JNK and transcriptional repressor ATF3/LRF1 through the IRE1/TRAF2 pathway is implicated in human vascular endothelial cell death by homocysteine. *Biochemical and Biophysical Research Communications*, 289(3):718–724, 2001.

[231] D.D. Zhang. Mechanistic Studies of the Nrf2-Keap1 Signaling Pathway*. *Drug Metabolism Reviews*, 38(4):769–789, 2006.

[232] K. Zhang and RJ Kaufman. Protein folding in the endoplasmic reticulum and the unfolded protein response. *Molecular chaperones in health and disease*, page 69, 2006.

[233] K. Zhang and R.J. Kaufman. From endoplasmic-reticulum stress to the inflammatory response. *Nature*, 454(7203):455–462, 2008.

[234] K. Zhang, X. Shen, J. Wu, K. Sakaki, T. Saunders, D.T. Rutkowski, S.H. Back, and R.J. Kaufman. Endoplasmic reticulum stress activates cleavage of CREBH to induce a systemic inflammatory response. *Cell*, 124(3):587–599, 2006.

[235] H. Zou, Y. Li, X. Liu, and X. Wang. An APAF-1? Cytochrome c Multimeric Complex Is a Functional Apoptosome That Activates Procaspase-9. *Journal of Biological Chemistry*, 274(17):11549–11556, 1999.